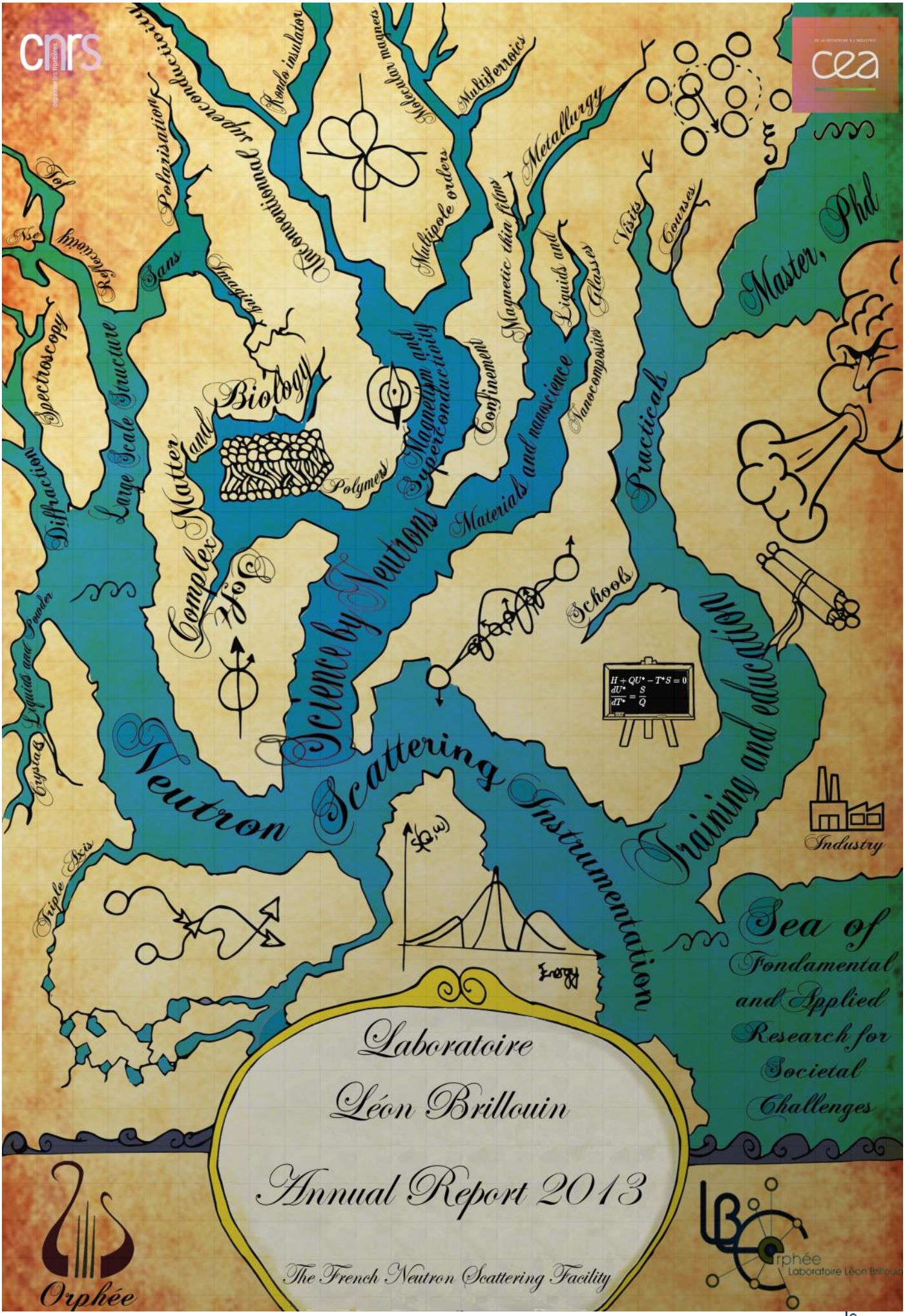
cnrs
cea
Unconventional superconductivity
Fondo insulator
Molecular magnets
Multiferroics
Metallurgy
Multipole orders
Magnetic thin films
Liquids and Glasses
Nanocomposites
Visits
Courses
Master, Phd
Practicals
Schools
Training and education
Industry
Sea of Fondamental and Applied Research for Societal Challenges
Instrumentation
Science by Neutrons
Neutron Scattering
Materials and nanoscience
Magnetism and Superconductivity
Confinement
Complex Matter and Biology
Polymers
Soft
Diffraction
Spectroscopy
Large Scale Structure
Reflectometry
Imaging
Tof
Triple Axis
Crystal
Liquids and Powder
Laboratoire
Léon Brillouin
Annual Report 2013
The French Neutron Scattering Facility
Orphée
Orphée
Laboratoire Léon Brillouin

Laboratoire Léon Brillouin

ANNUAL REPORT 2013

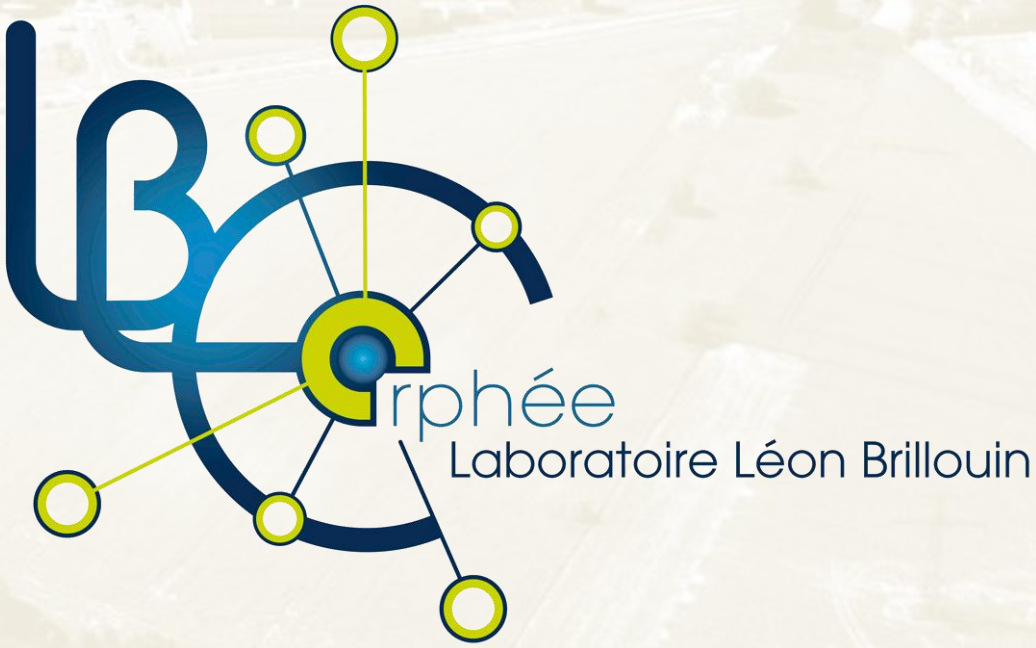

Director's word

THE LABORATOIRE LÉON BRILLOUIN (LLB)-ORPHÉE REACTOR IS THE FRENCH NEUTRON SCATTERING FACILITY. It is a research infrastructure supported jointly by the Commissariat à l'Energie Atomique et aux Energies Alternatives (CEA/DSM) and the Centre National de la Recherche Scientifique (CNRS/INP) The objectives of the LLB/ Orphée, as defined in the French roadmap for large scale-infrastructures (LSI), are to perform research on its own scientific programs, to promote the use of neutron diffraction and spectroscopy, to welcome and assist experimentalists. The LLB constructs and operates spectrometers that exploit the neutron beams delivered by the 14MW research reactor Orphée.

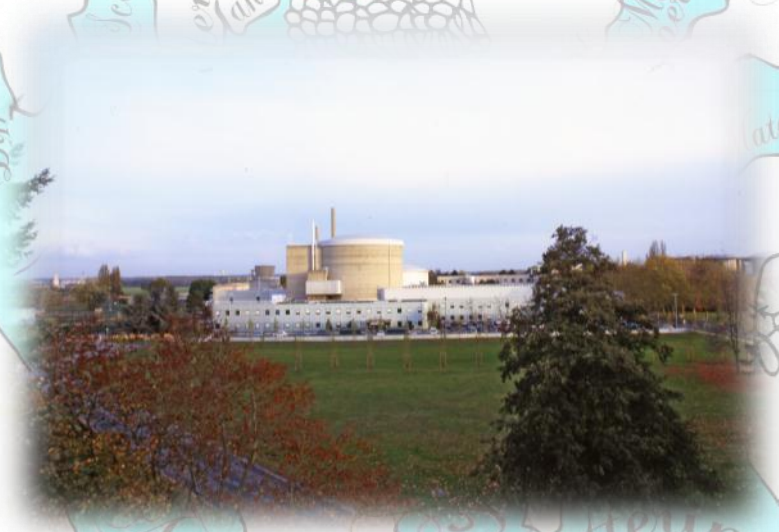

Over these last years, the LLB has conducted, on one hand, as a LSI, a renewal program of the instrumental suite and several international programs, and, on the other hand, as an Unité Mixte de Recherche (UMR 12), the implementation of specific scientific axis in close relation with the French academic and industrial communities. The directorate reports yearly to a Steering Committee and to an International Council for Science and Instrumentation. The LLB benefits from the exceptional scientific environment provided by the 'Plateau of Saclay', which includes the synchrotron source SOLEIL and many renowned Universities, research centers and engineering schools, while respecting its national missions and links with other universities in France. It is one of the leading hubs for neutron scattering at the international level and a part of the European network of national facilities, (MLZ in Germany, ISIS in UK, PSI in Switzerland…) in the NMI3 project under the Seventh Framework Program of the European Union Commission.

As a national facility, beyond access to neutron users, the LLB provide

(i) training and education (including maintaining links with universities);

(ii) access for industrial partner;

(iii) exploratory studies and experiment preparation including development of instrumentation and methodology;

(iv) provision of complementary capabilities, unique instruments and increased flexibility,

(v) ensuring the transfer of expertise and supporting the emergence of innovative research programs taking full advantages of neutron scattering.

These are enduring and complementary roles alongside international centers such as the Institute Laue-Langevin and other European facilities.

Recently the LLB was invited to define and coordinate the instrumental and scientific actions of the French community in the construction of new instruments at the future European Spallation Source (ESS) at Lund (Sweden).

ORPHEE reactor is the French source of neutron scattering

In fall 2013, 19 instruments are distributed among three Instrumental Groups responsible for their operation and for providing expertise in data analysis, 2 are for tests and 4 under construction; all neutron scattering methods are or will be represented: *Spectroscopy (Triple–Axis, Time-of-Flight, Spin Echo), Diffraction (Powder and Liquid, Single Crystal) and Large Scale Structures (SANS and VSANS, Reflectivity, Stress and Strain, neutron Imaging).* The experimental support for running experiments and developing instruments is provided by four Technical Groups: *Instrument Development, Sample Environment, Electronics, and Information Technology*. *Common Platforms* have been implemented to ensure and support specific research activities (Chemistry, Biology and Modeling).

Several years ago, the LLB adopted an ambitious policy for instrumentation improvements and upgrades never undertaken previously: the first step was done via the CAP2010 program, whose financing was mainly taken without specific support. It was a modest phase before a more complete renewal with the CAP2015 program extended with new projects until 2017. With a limited financial support, in a few years, more than a half of the instruments were (or are going to be) put into service after rejuvenation or creation, insuring an average gain in flux of a factor 15 by instrument up to 27 with the current improvements until 2017.

The research activities are cross-cutting the operational groups and are organized in three different areas covering a broad scope of science addressed by neutron scattering: - *Magnetism and Superconductivity*, - *Materials and Nanosciences: Fundamental studies and Applications*, - *Soft Complex Matter*. This distinction follows the obvious specific scientific areas, but it also accounts for the different ways to work in terms of collaborations, contracts and publications, and their expertise in specific neutron scattering techniques. One should note that research at the LLB has a dual character as it encompasses both the own research programs carried out by the LLB members as well as the collaborations with visitors associated with the activities of local contacts and with instrument development.

Organization of Training sessions is a part of the main assignments of the LLB in addition to its own training activity through research programs for PhD students. It consists in Summer schools and lectures, but also implies to offer beam time access to students. The LLB proposes PhD and post-doc training sessions, such as "les FANS du LLB" (**F**ormation **à** la **N**eutronique), each year in autumn; the purpose is to offer a wide spectrum of the instruments used in a specific scientific domain. They are completed by practical experience for students at bachelor or Master Levels, or from engineering schools. The LLB also organizes visit tours for everybody interested. Recently we have created a new group in charge of the Training and Education; it illustrates the strong involvement of the personnel (2/3 are involved in various teaching activities) and the recognized importance of this mission. Thanks to this group, the LLB increased its actions toward education and training by welcoming more students in master classes and by setting up a series of training for young researchers and industrial engineers.

C. Alba-Simionesco and J.-P. Visticot

2013 EVENTS IN PICTURES

LLB Scientific
& Instrumental Committe
October, 2013

Journées du LLB
January, 2013

Visit of the Swedish
Research council
May, 2013

COMING IN 2014…

Neutrons and Food 3

Paris, Maison du Lait, July 9-11, 2014

http://neutronsandfood.com/

Magnetic Diffraction from Single Crystals at the ESS

Paris, May 26- 27, 2014

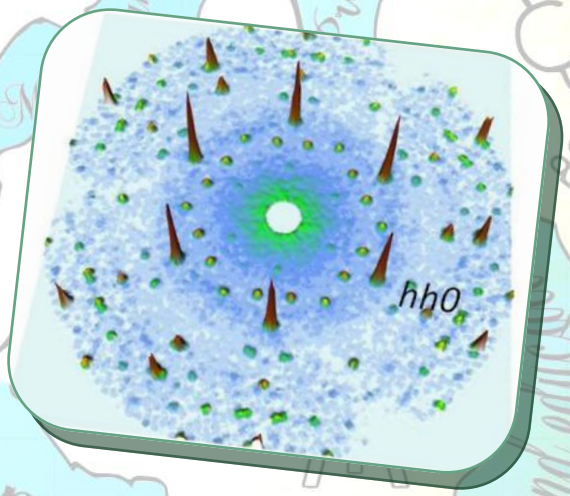

22èmes Journées de la Diffusion Neutronique (JDN22)

Ile d'Oléron, September 21-26, 2014

http://www-llb.cea.fr/JDN22/

Cristallographie et Grands Équipements 2013

Gif-sur-Yvette, October 13-17, 2014

http://www-llb.cea.fr/JDN22/

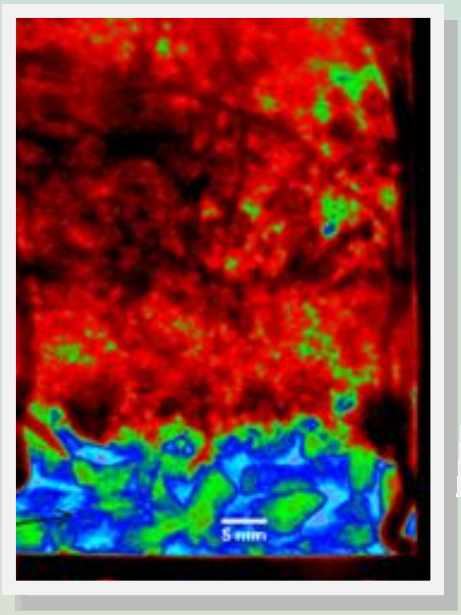
5 mm

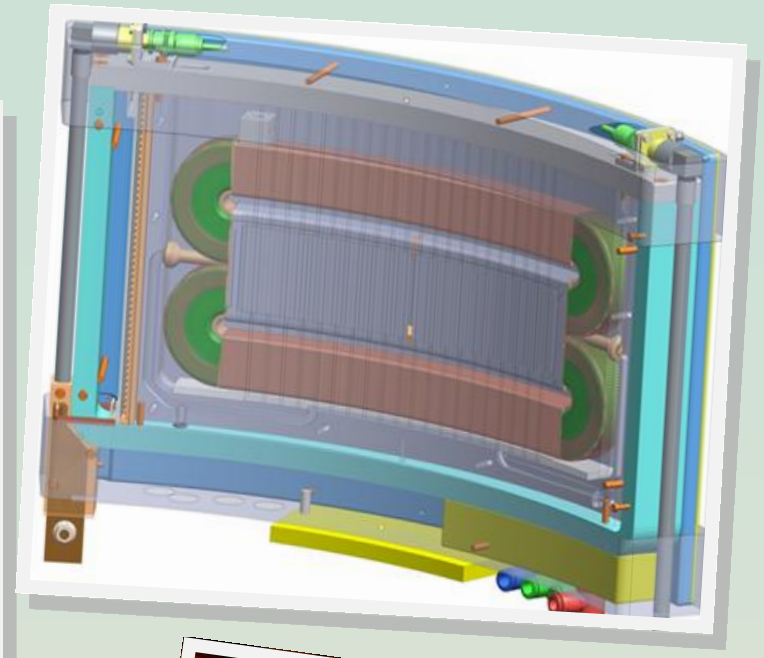

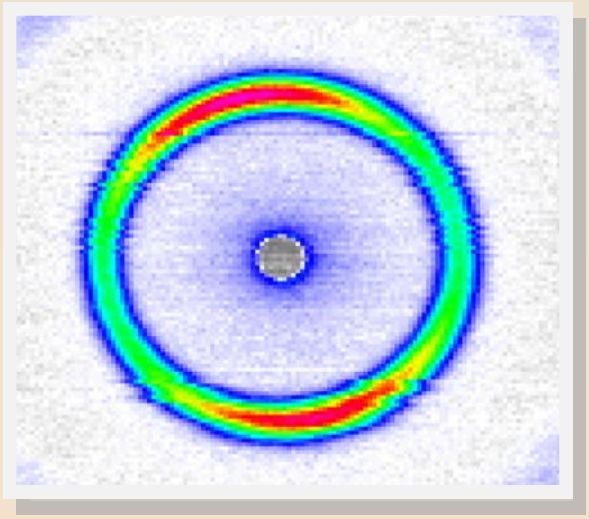

SCIENTIFIC HIGHLIGHTS

AXE 1:
Strongly Correlated Quantum Materials and Magnetism.

AXE 2:
Materials & Nanosciences: Fundamental Studies and Applications.

AXE 3:
Soft Matter & Biophysics.

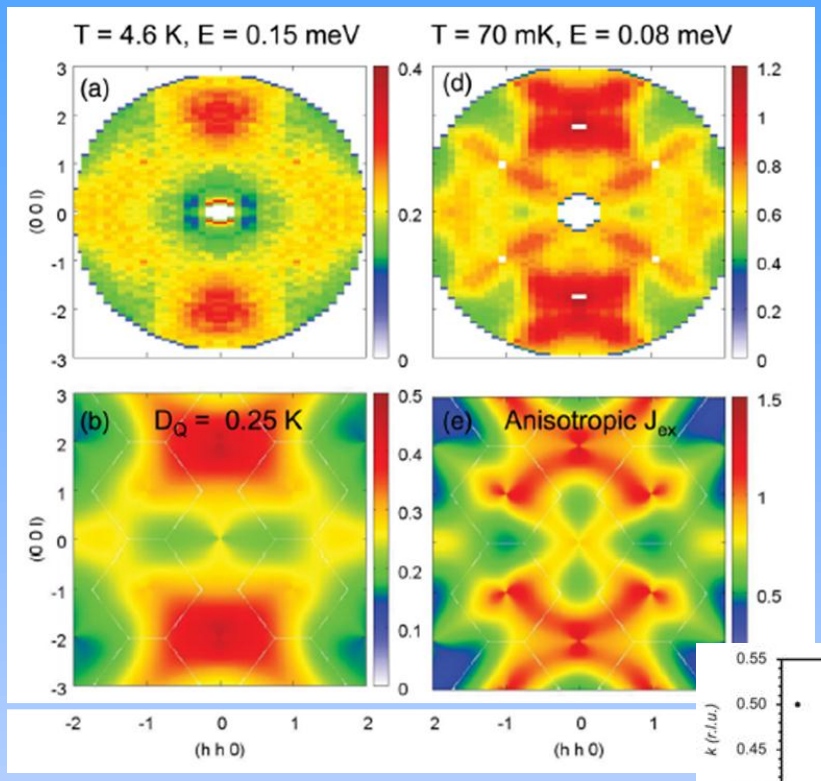
T = 4.6 K, E = 0.15 meV
T = 70 mK, E = 0.08 meV
(a)
(d)
(b) D_Q = 0.25 K
(e) Anisotropic J_{ex}
(0 0 l)
(h h 0)

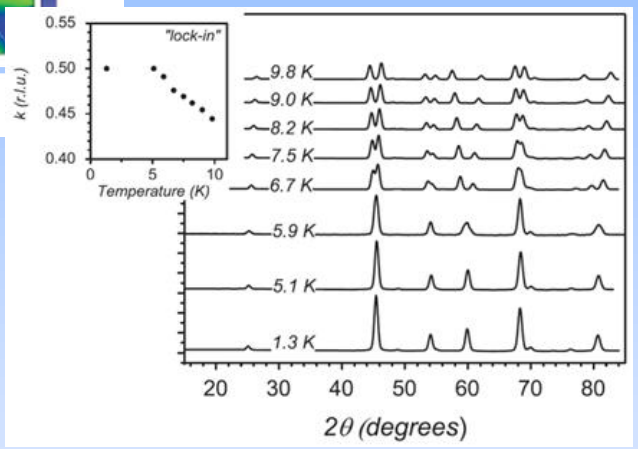
"lock-in"
k (r.l.u.)
Temperature (K)
9.8 K
9.0 K
8.2 K
7.5 K
6.7 K
5.9 K
5.1 K
1.3 K
2θ (degrees)

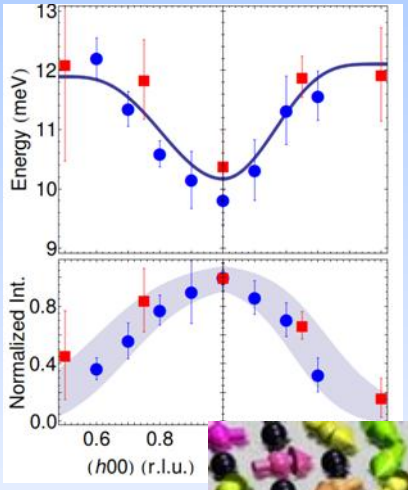
Energy (meV)
Normalized Int.
(h00) (r.l.u.)

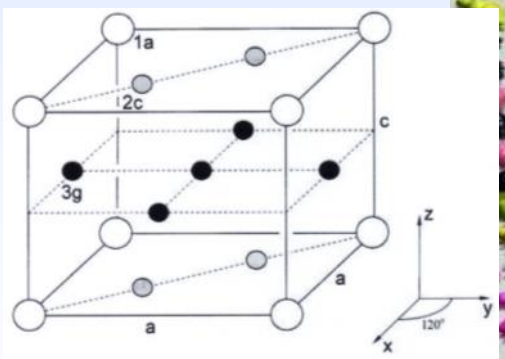
1a
2c
3g
c
a
a
z
y
x
120°

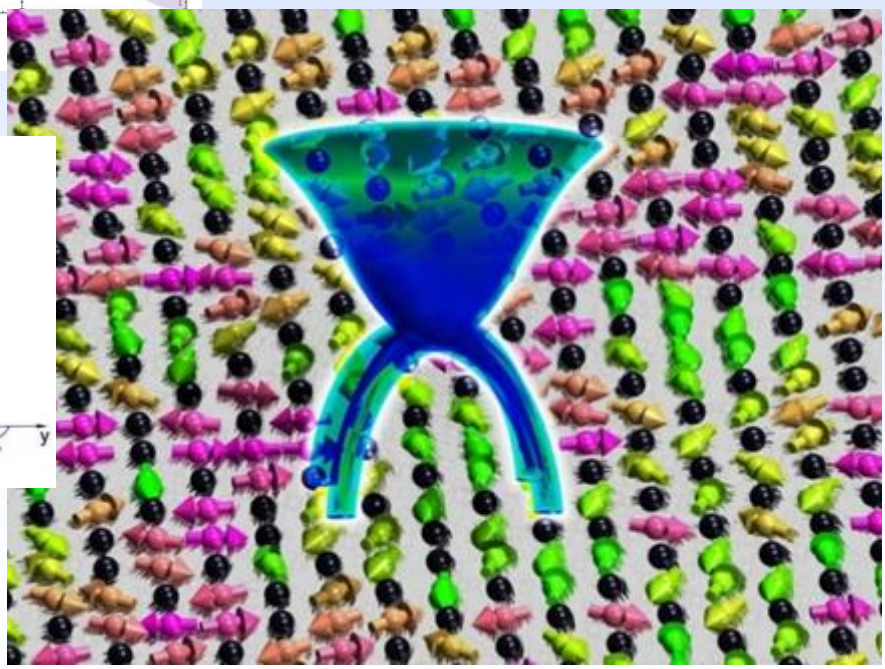

AXE 1:

Strongly Correlated Quantum Materials and Magnetism.

The "strongly correlated electron systems" denote a class of materials and physical phenomena which cannot be described in terms of the standard theory for a Fermi gas of non-interacting electrons. Such situations mainly occur in compounds containing transition-metal or rare-earth elements, because *d* and *f* orbitals have a more pronounced localized character. One common feature in many of these materials is the coexistence of several degrees of freedom associated with the electron- (charge, spin, orbital) or lattice subsystems, whose interplay is responsible for a large variety of ground states and excitation spectra. Well-known examples studied at LLB, both experimentally and theoretically, include cuprate or ferropnictide high-T_c superconductors, "giant magneto-resistance" manganites, compounds with short-range magnetic interactions subject to geometrical frustration (multiferroics, spin-ices, etc.), lanthanide-based heavy-fermion systems and "Kondo insulators", as well as a number of materials in which unconventional orders occur, such as the "magnetic blue phase" of MnSi, or the multipole-order states found in rare-earth hexaborides. Because neutrons interact with both the atom nuclei and their electron shells, neutron scattering is one of the best tools to study this type of physics involving interplay of lattice and magnetic properties. Polarized neutron beams, implemented on several spectrometers at LLB, further enhance the potential of neutron experiments for studying strong correlation phenomena in condensed matter.

- **Magnetic structure and phase transitions in the "green phase" $^{160}Gd_2BaCuO_5$: Neutron diffraction study.**
  A. Ovsyanikov, I. Golosovsky, I. Zobkalo & I. Mirebeau

- **Dispersive magnetic resonance mode in the Kondo semiconductor $CeFe_2Al_{10}$**
  J.-M. Mignot, P.A. Alekseev, J. Robert, S. Petit, T. Nishioka, M. Matsumura, R. Kobayashi, H. Tanida, H. Nohara, & M. Sera

- **Hour-glass spectrum in an insulating stripeless transition metal oxide**
  A. C. Komarek, Y. Drees, D. Lamago, & A. Piovano.

- **Magnetic structure determination of $TbCo_2Ni_3$ using polarized and non-polarized neutron powder diffraction**
  O. Rivin, E. N. Caspi, H. Ettedgui, H. Shaked & A. Gukasov

- **A spin liquid that does not freeze at 0.07K : $Tb_2Ti_2O_7$**
  S. Petit, J. Robert, S. Guitteny, P. Bonville, A. Gukasov, C. Decorse, I. Mirebeau

Magnetic structure and phase transitions in the "green phase" $^{160}Gd_2BaCuO_5$: Neutron diffraction study

A. OVSYANIKOV[A], I. GOLOSOVSKY[A], I. ZOBKALO[A], I. MIREBEAU[B]

a Petersburg Nuclear Physics Institute, National Research Centre "Kurchatov Institute", 188300 Gatchina, St.-Petersburg district, Russia

b Laboratoire Léon Brillouin, CEA-CNRS, CE Saclay, 91191 Gif sur Yvette, France

golosov@pnpi.spb.ru

By powder neutron diffraction on a $^{160}Gd_2BaCuO_5$ sample we observed an incommensurate magnetic structure with a propagation vector k = [0 0 1/2-δ] below 12 K.

A "lock-in" to a commensurate structure with k = [0 0 1/2] propagation vector occurs at 5 K accompanied with a spin re-orientation in the Gd subsystem and a magnetostructural transition. The temperature dependence of the Gd moments suggests a low dimensional behaviour similar to that found in other rare-earth cuprates.

(Published in Journal of Magnetism and Magnetic Materials, 353, 71, 2014)

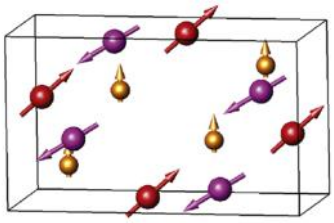

The green-coloured cuprates R_2BaCuO_5 known as "green phase" attracted attention, when they were observed as impurities in the synthesis of high-temperature superconducting oxides [1]. Later it was realized that these compounds are also excellent objects to study magnetic interactions between 3d- and 4f-sublattices. The magnetic structures derived by neutron diffraction for Dy, Ho, Er, Tm, Yb and Y compounds [2,3] show a large diversity. Gd_2BaCuO_5 is considered as the exception in this family. In contrast with other "green phases" heat and magnetic susceptibility show a single magnetic transition around 11.8–12.1 K [4].

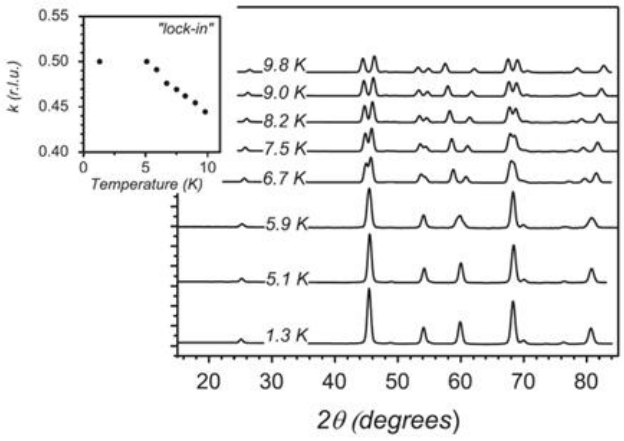

Figure 1 : Temperature evolution of the magnetic contribution. In inset – the temperature dependence of the z-component of the wave vector .

In order to increase the diffraction signal, measurements at the diffractometer G6.1 with a neutron wavelength of 4.76 Å in the Laboratory Léon Brillouin were performed. The large neutron wavelength yields a better resolution at small momentum transfers, which is important to measure magnetic scattering and especially to study incommensurate structures.

Gd_2BaCuO_5 crystallizes in the orthorhombic space group *Pnma*. A unit cell contains four formula units with magnetic atoms in the position 4*c*. The complex crystal structure induces many competing interactions and strong magnetic frustration in the system

The analysis of the neutron diffraction patterns shows that below 12 K an incommensurate magnetic order settles described by the wave vector k = [0 0 1/2-δ], where δ is a small value (Fig. 1). When temperature decreases the wave vector "locks-in" to the wave vector k = [0 0 1/2] at about 5 K, i.e. the magnetic order becomes commensurate with a doubling of the magnetic cell along the *c* axis (Inset in Fig. 1) .

There are three sets of magnetic atoms: two sets of Gd (Gd1 and Gd2) and a set of Cu located in the same four-fold crystallographic positions. The magnetic representation consists of two two-dimensional irreducible representations. In each representation the basic functions relate a pair of magnetic moments. Any mutual orientations of the magnetic moments within a pair are allowed. One representation links the y-projections of the moments, whereas other representation links the x- and z-projections.

The best fit at all temperatures corresponds to a configuration where all moment components are present and which must be described by combining the two different representations. This magnetic structure is shown as "logo". The magnetic order below and above the "lock-in" (~ 5 K) differs by the absence of the y-projection in the Gd1 moments below the "lock-in" point, that is consistent with the symmetry analysis.

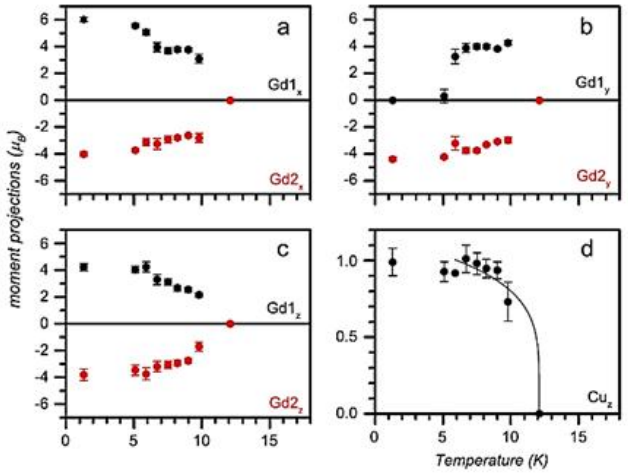

Figure 2: Temperature dependences of the magnetic moment projections. The x-, y- and z-projections of the Gd1 moments (in black) and Gd2 moments (in red) are displayed in panels (a), (b) and (c) respectively. Panel (d) corresponds to z-projection for the Cu moment

The temperature dependences of the magnetic moment components are shown in Fig.2. When the temperature decreases the y-component of the moments in the Gd1 site disappears abruptly at 5 K which means that the moment rotates towards the *a–c* plane. Nothing changes in the Gd2 or Cu sublattice.

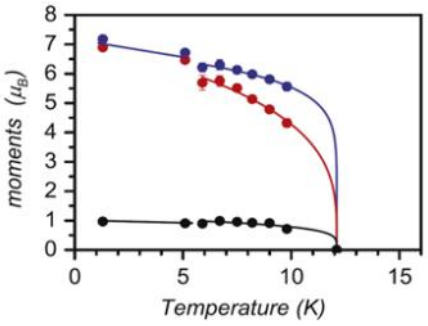

Figure 3: Temperature dependence of the magnetic moments : Gd1(Blue); Gd2(red); Cu (black).

The temperature dependences of the magnetic moments (Fig.3) give arguments in favour of a low dimensional magnetic behavior, deduced from Mössbauer spectroscopy [5] .

A possible reason for the spin re-orientation and the associated "lock-in" of the wave vector is a violation of a fine balance of the exchange integrals owing to the change of atomic distances with temperature. Indeed, the temperature dependences of the Gd-atoms position clearly show a magnetostriction effect at the "lock-in" temperature (Fig. 4). So the structural distortion lifts the frustration in the Gd-subsystem. The largest distortions are observed in the Gd1 sublattice, whose magnetic moment undergoes a re-orientation. No anomalies were detected in the temperature dependences of the unit cell parameters, that suggest the possibility of an isostructural transition.

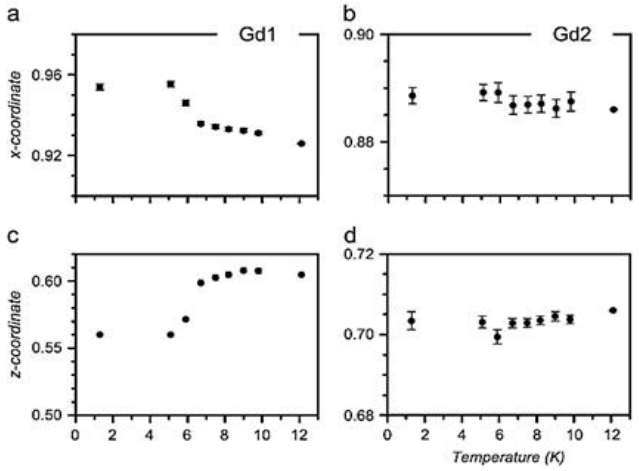

Figure 4: Temperature dependence of the relative atomic coordinates of the Gd atoms.

In all "green phase" compounds the magnetic order in the Cu and in the rare earth sublattices appears simultaneously due to the strong R–Cu coupling. The magnetic behaviour in Gd_2BaCuO_5 obeys a similar scenario, where the high temperature transition, driven by the Cu sublattice, induces magnetic order in the Gd sublattice. When the temperature decreases further, the exchange interactions within the rare earth sublattice induce the "lock-in" and re-orientation of the Gd moments.

References

1. C. Michel, B. Raveau, Journal of Solid State Chemistry 43 (1982) 73.
2. I.V. Golosovsky, V.P. Plakhty, V.P. Harchenkov, J. Zoubkova, B.V. Mill, M. Bonnet, E. Roudeau, Fizika Tverdogo Tela, 34 (1992) 1483.
3. I. Golosovsky, P. Böni, P. Fischer, Solid State Communications, 87 (1993) 1473.
4. R.Z. Levitin, B.V. Mill, V.V. Moshchalkov, N.A. Samarin, V.V. Snegirev, J. Zoubkova, JMMM, 90–91 (1990) 53.
5. M. Strecker, P. Hettkamp, G. Wortmaim, G.A. Stewart, JMMM, 177–181 (1998) 1095.

Dispersive magnetic resonance mode in the Kondo semiconductor $CeFe_2Al_{10}$

J.-M. MIGNOT[A], P. A. ALEKSEEV[B,C], J. ROBERT[A], S. PETIT[A], T. NISHIOKA[D], M. MATSUMURA[D], R. KOBAYASHI[E], H. TANIDA[F], H. NOHARA[F], M. SERA[F]

a Laboratoire Léon Brillouin, CEA/Saclay, 91191 Gif sur Yvette, France

b National Research Centre 'Kurchatov Institute', 123182 Moscow, Russia

c National Research Nuclear University "MEPhI", Kashirskoe sh. 31, 115409, Moscow, Russia

d Graduate School of Integrated Arts and Science, Kochi University, Kochi 780-8520, Japan

e Neutron Science Laboratory, Institute for Solid State Physics, University of Tokyo, Tokai, 319-1106, Japan

f Department of Quantum Matter, ADSM, Hiroshima University, Higashi-Hiroshima, 739-8530, Japan

jean-michel.mignot@cea.fr

The CeT_2Al_{10} family of orthorhombic compounds provides a unique example of a gradual evolution from a Kondo-insulator (T: Fe) to an unconventional antiferromagnet (T: Ru, Os). Neutron scattering experiments performed on single-crystal $CeFe_2Al_{10}$ reveal that this material develops a spin-gap in its magnetic spectral response below ~ 50 K, with a magnetic excitation dispersing from E = 10.2 ± 0.5 meV, at the zone-boundary point q = (0, 1, 0), to ≈ 12 meV at the top of the branch. The anisotropic behavior of this excitation is contrasted with that of the magnon-like modes previously reported for $CeRu_2Al_{10}$, and tentatively interpreted in terms of the "magnetic exciton" model first proposed for YbB_{12} .

Kondo insulators (KI) form a unique class among strongly correlated electron systems, in which semiconducting properties develop on cooling as a result of the opening of a narrow gap in the electronic density of states at the Fermi energy [1]. In those materials, a nonmagnetic singlet ground state is formed at low temperature, but short-range, dynamical, antiferromagnetic (AF) correlations can also play a major role, as was demonstrated by our comprehensive inelastic neutron scattering (INS) study of the archetype KI YbB_{12} [2]. The low-energy magnetic response of YbB_{12} at liquid helium temperature is dominated by a sharp, resolution-limited peak, located at about 14 meV, just below the edge of a spin gap. This excitation disappears rapidly upon heating as the system crosses over to an incoherent spin-fluctuation regime. It has been interpreted [1b] as an exciton peak (a resonance mode in the spin response function) reflecting residual AF interactions between the renormalized 4f quasiparticles. This model is reminiscent of that proposed to explain the well-known "resonance mode" (RM) in high-Tc superconductors [3], and may apply to the "topological KI" SmB_6 as well [2c]. On the other hand, evidence was still lacking for a comparable RM-type excitation in the case of Ce-based KIs .

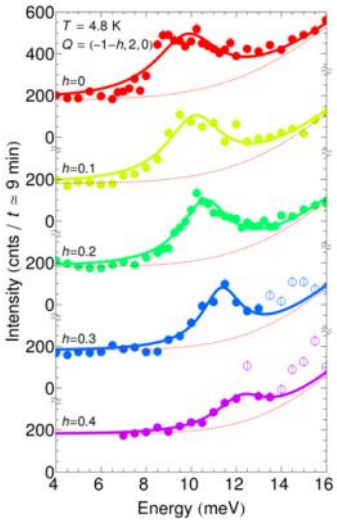

Figure 1 : Energy scans at constant neutron final energy Ef = 14.7 meV, measured at T = 4.8 K showing the dispersion of the magnetic excitation and the Q dependence of its intensity along the Q = (h, 0, 0) direction. Dashed lines: estimated background. Solid lines: fits assuming Lorentzian lineshapes .

$CeFe_2Al_{10}$ looked like a promising candidate because it exhibits a clear KI behavior in the temperature dependence of its resistivity and, unlike $CeRu_2Al_{10}$ studied previously [4] (LLB Annual Report 2010), does not undergo magnetic ordering at low temperature. Since large single crystals could not be obtained at this stage, 14 pieces (m ≈ 700 mg) were co-aligned on a specially designed, light-weight, Al sample holder, and fixed using low-background Cytop® glue. Magnetic excitation spectra were measured on 2T in the (***a****, ***b****) scattering plane [5].

Constant-**Q** scans recorded at about 5 K showed the existence of an inelastic peak at E = 9.5 meV for points in reciprocal space corresponding to the k vector (0, 1, 0), *i.e.* at positions (Y point) where AF Bragg satellites occurred in the Ru compound. The excitation disperses (Fig. 1) from this point, reaching approximately 12 meV at the top of the branch, but with a steep reduction in intensity, which makes its observation difficult in that region. The dispersion parameters plotted in Fig. 2 were obtained from a Lorentzian fit of the spectra. The main cause of uncertainty was the large sloping background, which was determined by comparing temperature dependences for different **Q** vectors. The dispersion was found to be rather isotropic along the high-symmetry directions accessible in the (***a****, ***b****) scattering plane .

With increasing temperature, the excitation peak

is gradually suppressed (Fig. 3, left), while a signal grows in the spin-gap region (Fig. 3, right), reflecting the appearance of quasielastic fluctuations. Interestingly, the peak is strongly suppressed at T = 40 K, without significant shift to lower energies, implying that the gap "fills" rather than

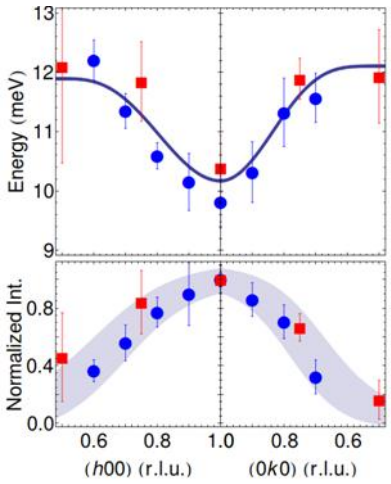

Figure 2 : Experimental dispersion curve and Q-dependent intensity of the magnetic excitation at T ≈ 4 K. Red squares [for Q = (h, 3, 0) and (0, 3 − k, 0)] and blue circles [for Q = (−1 − h, 2, 0) and (0, 2 + k, 0)] correspond to spectra measured along equivalent, yet distinct, (h, 0, 0) (left) and (0, k, 0) (frame) directions in reciprocal space.

"shrinks" upon heating. This behavior contrasts with the temperature softening of the magnon-like peaks observed in $CeRu_2Al_{10}$, while being reminiscent of that found in YbB_{12} .

The mode polarization was analyzed by comparing spectra measured at equivalent **Q** vectors oriented along (or close to) different crystallographic axes. The results imply that the signal mainly arises from correlations between magnetic components parallel to ***a***, the easy axis observed in susceptibility measure-ments. The quasielastic signal around 40 K exhibits a similar polarization but, since it is found to be rather uniform in **Q** space, the polarization along a likely reflects the single-ion anisotropy. This is again at variance with $CeRu_2Al_{10}$, where the quasielastic contribution was sizable in the vicinity of Q_{AF} and for temperatures close to the Néel point, pointing to a critical scattering regime.

The above-noted analogies with YbB_{12} lend support to the proposed interpretation of the $CeRu_2Al_{10}$ dispersive excitation as an exciton-type resonance mode. In this connection, it is worth recalling the early studies of CeNiSn, another anisotropic (orthorhombic) compound categorized as a KI (or a "Kondo semimetal"), in which one of the magnetic spectral components also exhibited a strong polarization and a temperature behavior analogous to that of the present system. The RM phenomenon in KI materials may thus be more widespread than previously thought, and deserves further investigations, both experimental and theoretical .

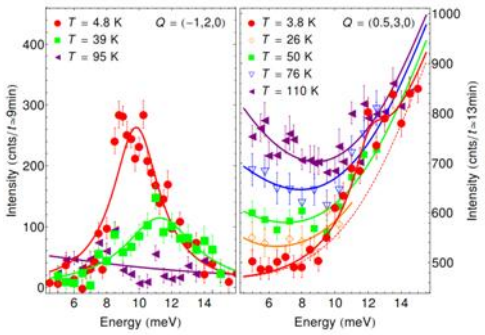

Figure 3 : Temperature evolution of the magnetic spectral response measured at constant neutron final energy Ef = 14.7 meV for Q = (−1, 2, 0) (left) and (0.5, 3, 0), showing the rapid suppression of the inelastic peak and the gradual appearance of the quasielastic signal as T increases .

References

1. P. Riseborough, Adv. Phys. 49, 257 (2000); P.S. Riseborough, J. Magn. Magn. Mater. 226, 127 (2001).

2. J.-M. Mignot, P. A. Alekseev, K. S. Nemkovski *et al.*, Phys. Rev. Lett. 94, 247204 (2005); K. S. Nemkovski, J.-M. Mignot, P. A. Alekseev *et al.*, Phys. Rev. Lett. 99, 137204 (2007); K. S. Nemkovski, P. A. Alekseev, J.-M. Mignot, and A.S. Ivanov, Physics Procedia 42, 18 (2013).

3. See *e.g.* M. Eschrig, Adv. Phys. 55, 47 (2006) and references therein.

4. J. Robert, J.-M. Mignot, S. Petit *et al.*, Phys. Rev. Lett. 109, 267208 (2012) ; J. Robert, J.-M. Mignot, G. André *et al.*, Phys. Rev. B 82, 100404(R) (2010).

5. J.-M. Mignot, P. A. Alekseev, J. Robert, S. Petit *et al.*, arXiv cond-mat.str-el, 1401.2892 (2014))

Hour-glass spectrum in an insulating stripeless transition metal oxide

A. C. KOMAREK[A], Y. DREES[A], D. LAMAGO[B], A. PIOVANO[C]

a Max-Planck-Institute for Chemical Physics of Solids, 01187 Dresden, Germany

b Laboratoire Léon Brillouin, CEA/CNRS, 91191 Gif-sur Yvette, France

c Institut Laue-Langevin, 6 Rue Jules Horowitz, 38043 Grenoble, France

Alexander.Komarek@cpfs.mpg.de

The magnetic excitations in high-temperature superconducting copper oxide superconductors are believed to be crucial for superconductivity. The most promising approaches that are able to describe their "hour-glass"-shaped magnetic excitation spectra are either based on models where the charges within the copper oxygen planes segregate into stripes or on purely itinerant models where Fermi surface effects are significant. By the recent observation of such a magnetic excitation spectrum in an insulating cobalt oxide it was shown that Fermi surface effects are not necessarily needed for an understanding of the hour-glass spectrum [1]. We were now able to synthesize an insulating cobalt oxide with such a spectral shape that additionally exhibits no charge stripes, thus, suggesting a different origin entirely [2].

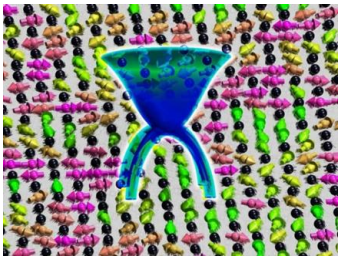

We studied a 40% hole-doped single layer perovskite cobaltate that is isostructural to the high-temperature superconducting cuprates. The 50% hole-doped "parent material" exhibits an extremely robust checkerboard charge ordering pattern with an antiferromagnetic structure that is shown in Fig. 1

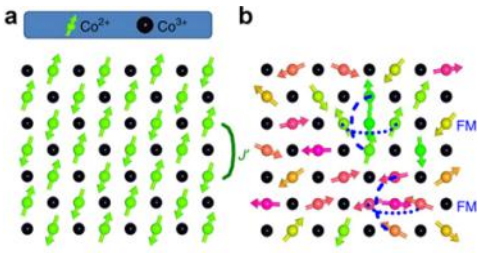

Figure 1: Taken from Ref. [2]. (a) Antiferromagnetic structure of the ideal checkerboard charge ordered half-doped cobaltate. Co^{3+} (black) ions are in the non-magnetic low-spin state whereas Co^{2+} ions (green).
(b) Our frustration scenario for our 40% Sr-doped cobaltate. The doping of one additional electron at a Co^{3+} site introduces strong nearest-neighbour exchange interactions J and turns originally antiferro-magnetic couplings ferro-magnetic as indicated by the blue dashed lines. This results in strong frustration

(a). Our studied 40% hole-doped cobalt oxide exhibits magnetic peaks in neutron scattering experiments that appear at positions that are distinctly away from any commensurate quarter-integer positions [2]. In the ideal half-doped "parent compound" the charges are known to order in an alternating Co^{2+}/Co^{3+} arrangement that looks like a checkerboard, see Fig. 1 (a). At variance, the incommensurate magnetic peak positions in our 40% hole-doped cobaltate in principle could be compatible with a diagonal stripe phase where charges arrange into stripes. Due to the comparably high sharpness of the magnetic peaks in our high-quality single crystals one would expect also quite sharp structural charge stripe ordering superstructure reflections. (Note, that magnetic stripe phases can not be easily decoupled from charge stripe phases in this insulating and localized system with non-magnetic Co^{3+} ions. The movement of one electron from a Co^{2+} to a Co^{3+} site would cost several 100 meV). But, in detailed neutron scattering experiments, we were not able to detect any indications for charge stripe ordering reflections in our 40% hole-doped cobaltate material [2], see Fig. 2. Instead, there appears to be still super-

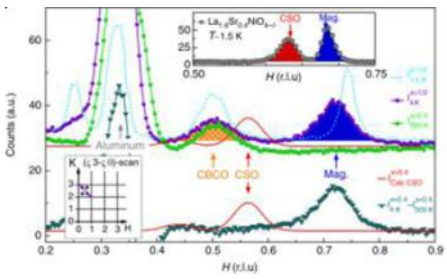

Figure 2: Taken from Ref. [2]. Scans across the charge stripe ordering positions reveal no indications for charge stripe ordering in $La_{1.6}Sr_{0.4}CoO_4$ (violet circles/cyan triangles: 4K/ 500K data). Instead, checkerboard charge ordering reflections are visible similar as in $La_{1.5}Sr_{0.5}CoO_4$ (dashed cyan line). The red line shows a simulation of an expected charge stripe ordering signal according to the observations in an isostructural nickelate with same hole-concentration, see inset .

structure reflection intensity at half- integer positions in reciprocal space that is indicative for checkerboard charge ordering like in the half-doped "parent compound". In fact, this is not fully surprising, because the half-doped compound exhibits a very robust checkerboard charge order that persists up to very high temperatures (above 800 K). For such a stable charge order it appears quite natural that it also persists in a certain doping regime around half-doping. Also at lower temperatures these stripes appear to be unlikely since the charges can not easily re-arrange themselves once they are frozen in an disordered checkerboard arrangement due to the strongly insulating properties triggered by the spin blockade mechanism. Also the study of high energy Cobalt-oxygen bond-stretching phonon modes in these cobaltates is consistent with our checkerboard charge ordering scenario and supports our elastic studies, see Fig. 3 (a). Such a kind of bond-stretching phonon modes can be expected to exhibit an anomalous softening at the charge ordering propagation vector of the underlying charge order in this system. Unlike an isostructural nickel oxide with the same hole-concentration, these phonon modes in our cobaltate indicate a behavior which is very similar to the behavior in a true checkerboard charge ordered material. Our study of the magnetic excitation spectrum in our 40% hole-doped cobaltate surprisingly revealed the presence of hour-glass shaped magnetic excitation spectra as can be seen in Fig. 3 (b,c). Therefore, the emergence of these hour-glass-shaped magnetic excitations in this insulating cobalt oxide is apparently neither connected to the existence of Fermi surface effects nor to the appearance of charge stripe phases in these layered insulators .

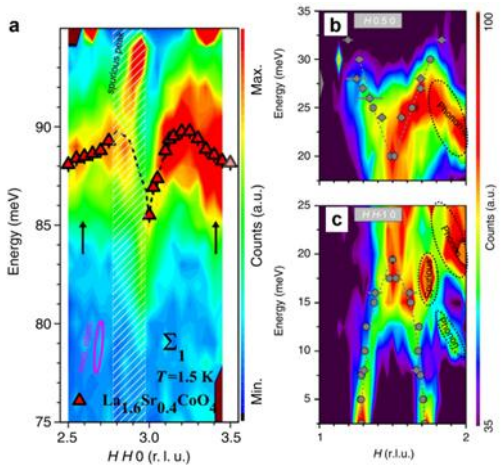

Figure 3: Taken from Ref. [2]. (a) Neutron scattering intensity as a function of energy and momentum transfer. Red triangles denote the high frequency Co-O bond-stretching phonon dispersion. A distinct softening at Q = (2.5 2.5 0) becomes apparent. (b,c) Inelastic neutron scattering intensities obtained from constant-energy scans across the planar antiferromagnetic wavevector in (b) [100]-direction and (c) [110]-direction. Measurement performed at the 2T spectrometer. All basic features of the so-called "hour-glass" dispersion are visible: the inwards dispersing branches that merge with increased intensity and the outwards dispersing branches at higher energies .

Hence, another third mechanism must trigger the onset of these hour-glass spectra (at least in these cobaltates). We propose a frustration scenario based on disordered checkerboard charge ordered structures which is shown in Fig. 1 (b). The doping of one additional electron in the originally undistorted checkerboard charge ordering pattern (Fig. 1 (a)) will turn two originally antiferro-magnetic exchange interactions ferromagnetic due to the strong nearest neighbor exchange interactions J compared to the weak exchange interactions J'. This high amount of frustration will most likely induce non-collinear magnetic structures as shown schematically in Fig. 1 (b) and indicates the high significance of frustration for "hour-glass" spectra. Concluding, we have shown that besides Fermi surface effects also charge stripes are not needed for the emergence of an "hour-glass" dispersion.

References

1. A. T.Boothroyd, P. Babkevich, D. Prabhakaran and P. G. Freeman, Nature 471, 341 (2011)
2. Y. Drees, D. Lamago, A. Piovano and A. C. Komarek, Nature Commun. 4, 2449 (2013)

Magnetic structure determination of $TbCo_2Ni_3$ using polarized and non-polarized neutron powder diffraction

O. RIVIN[A,B], E. N. CASPI[A], H. ETTEDGUI[A], H. SHAKED[B], A. GUKASOV[C]

a Department of Physics, Nuclear Research Centre-Negev, P.O. Box 9001, Beer Sheva 84190, Israel

b Department of Physics, Ben-Gurion University, P.O. Box 653, Beer Sheva 84105, Israel

c Laboratoire Léon Brillouin, CEA-CNRS, CE Saclay, 91191 Gif sur Yvette, France

lexoed@gmail.com

The structural (space group P6/mmm) and magnetic parameters of $TbCo_2Ni_3$ are investigated using neutron powder diffraction (NPD) and polarized neutron powder (PNPD) and a ferromagnetic structure is found below 315 K, with ferromagnetic Tb and Co/Ni sub-lattices.

The polarized powder diffraction technique is extended to the case of uni-axial, high anisotropy (hard) magnetic materials. The experimental applications of this technique are discussed and an appropriate analysis is developed.

The RCo_5 (R - Lanthanides) compounds have attracted great experimental and theoretical interest for many years for both technological importance and basic research [1]. They undergo magnetic ordering at high Curie temperatures (~1000 K) with very large magnetocrystalline anisotropy (MCA) [1]. The Co atoms occupy two non-equivalent crystallographic (Fig. 1) sites: '2c' (`6*m*2) and '3g' (*mmm*), which exhibit different MCAs. In particular, the very large MCA, along the unique hexagonal **c** axis, originates from the '2c' site, while that of the '3g' site is much smaller and favors the hexagonal plane.

The combined action of the magnetic exchange field (MEF), and the crystalline electric field (CEF), strongly affects the magnetism in the RCo_5 compounds and their derivatives. The theory of this type of transition was investigated thoroughly.[2] .

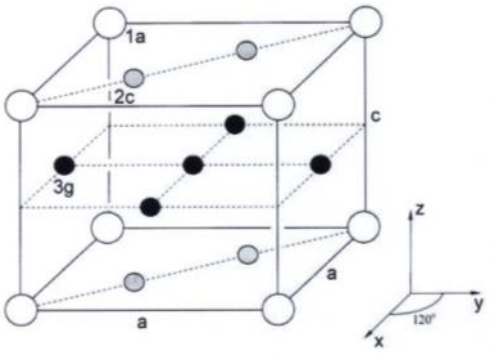

Figure 1 The $CaCu_5$ type crystallographic structure of RCo_5, in which the R sub-lattice consists of the '1a' site and the Co sub-lattices consist of the '2c' and the '3g' sites .

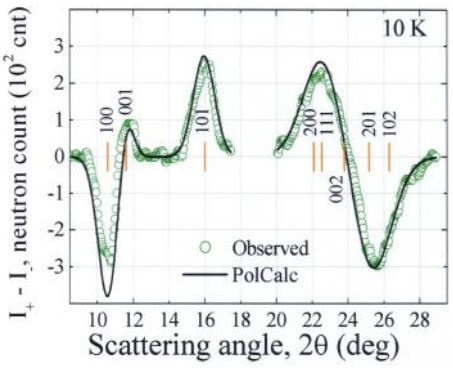

Figure 2 : I+ - I- profile of $TbCo_2Ni_3$ at 10 K. The circles represent the observed PNPD profile and the solid line is the PolCalc refinement profile. The reflections calculated 2q positions are marked and their Miller (P6/mmm) indices are given.

Partial substitution of the Co by Ni in the ternary compounds $R(Co_{1-x}Ni_x)_5$, enables a gradual change in the magnetic exchange field, originating from the Co sub-lattices, without altering the crystal structure.

PNPD experiments were performed at the 'VIP' (former 5C1) polarized diffractometer, at the Laboratoire Léon Brillouin, CEA - CNRS Saclay, France.

The flipping difference intensity of the PNPD: I+ - I-,[3] eliminates all non-magnetic background (*i.e.* nuclear scattering, scattering from the cryomagnet, multiple scattering, constant background) hence enhancing sensitivity to magnetic scattering contribution and enabling study of magnetic structures having small ordered magnetic moments. This technique was originally devel-

oped for the case of isotropic (soft) ferromagnetic (ferrimagnetic) single crystals and powders, and locally anisotropic parameters.[1] In the present work, we extend and apply the PNPD technique to the case of highly anisotropic (hard) ferromagnetic powder.[1,4] In this case the magnetization direction in an individual grain depends on its crystallographic orientation with respect to the external field. As a consequence, only a component of the magnetization, $\langle\cos\beta\rangle_{hkl}$, in each powder grain, is parallel to the polarization of the neutron beam[4]. The appropriate cross section for the flipping difference (FD), in powders, is calculated by averaging over all grains which contribute to the hkl Bragg reflection,[4] and considering the appropriate geometrical and physical intensity corrections (Eq. (1)). [3,4]

$$I_+ - I_- \propto D(2\theta)T(2\theta)\langle\cos\beta\rangle_{hkl}\frac{e^{-2B_T\sin^2\theta/\lambda^2}}{\sin\theta\,\sin 2\theta}m_{hkl}\mathrm{Re}\left\{F_N F_M^{\dagger}\right\} \quad (1)$$

where $D(2\theta)$ is the beam depolarization inside the sample, $T(2\theta)$ is the absorption corrected geometrical transmition function (in Debye-Scherrer geometry).[4] A computer routine (PolCalc4) was created to refine by iterations the magnetic parameters until best fit of the calculated to the observed I+ - I- (Eq. (1)) is achieved.

The observed PNPD magnitude of μ_{Tb} as a function of temperature agrees with that observed using neutron powder diffraction (Fig. 3).[1] At 10 K, we observed μ_{Tb} = 8.1(2) μ_B. This value is reduced compared to the free Tb^{3+} ion (9μB). Such a reduction (in rare earth ions) in the magnetic moment was previously found when there is a competition between magnetic exchange field and crystal electric field.[2] Furthermore, the observed temperature dependence of the magnitude of this moment (Fig. 3) does not follow spontaneous magnetization curvature, as described within the framework of the mean field approximation.[1] .

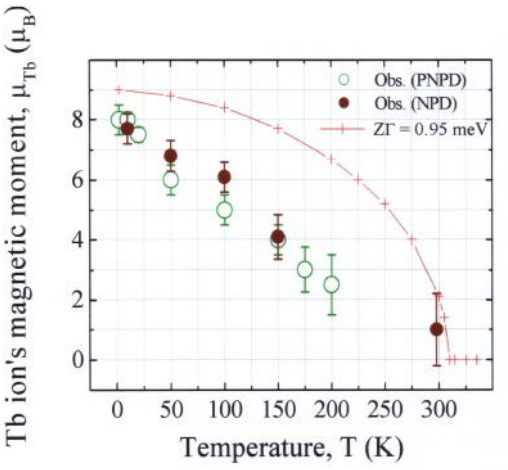

Figure 3 : Temperature dependence of the Tb magnetic moment from NPD and PNPD, and a calculated spontaneous magnetization curve, based on the mean field approximation, using the exchange coupling constant, G, and the number of nearest neighboring ions, Z.

References

1. O. Rivin, E. N. Caspi, H. Ettedgui, H. Shaked and A. Gukasov, Phys. Rev. B 88, 054430 (2013).
2. B. R. Cooper and O. Vogt, J. De Physique 32 Cl, 958 (1971).
3. A. Gukasov, M. Braden, R. J. Papoular, S. Nakatsuji and Y. Maeno, Phys. Rev. Lett. 89, 087202-1 (2002).
4. O. Rivin, E. N. Caspi, H. Ettedgui, H. Shaked and A. Gukasov, J. Neut Research, *submitted*.

A spin liquid that does not freeze at 0.07K : $Tb_2Ti_2O_7$

S. PETIT[A], J. ROBERT[A], S. GUITTENY[A], P. BONVILLE[B], A. GUKASOV[A], C. DECORSE[C], I. MIREBEAU[A]

A Laboratoire Léon Brillouin, CEA-CNRS, CEA-Saclay, 91191 Gif sur Yvette, France

B Service de Physique de l'état Condensé, CEA-CNRS, CEA-Saclay, 91191 Gif sur Yvette, France.

C ICMMO, Université Paris-Sud, 91400 Orsay France

Isabelle.mirebeau@cea.fr

Geometrical frustration has been studied extensively for the last two decades. In the context of magnetism, the geometry of the underlying lattice is such that the magnetic moments cannot find any configuration that satisfies simultaneously all pair-wise interactions, leading to novel and exotic ground states.

Pyrochlore magnets, with their lattice of corner-sharing tetrahedra, are model systems in this field. The celebrated terbium titanate $Tb_2Ti_2O_7$ belongs to this class of materials. It is an extreme case since, because of frustration, the Tb magnetic moments do not show long range ordering, but keep fluctuating, like in a "spin-liquid", down to temperatures as low as 0.05 K. This phenomenon remains so far a theoretical puzzle.

Neutron scattering is a powerful technique in this context, as it allows one to determine correlations between Tb magnetic moments, by measuring maps in the reciprocal space. Theoretical models are then tested in the light of these experiments. Researchers from LLB addressed this issue by measuring maps of inelastic and elastic diffuse scattering at very low temperature (0.07 K) on 4F and 6T2 spectrometers at Saclay (Figure 1, top). In collaboration with SPEC, they developed a model that invokes a dynamical Jahn-Teller effect (or similarly quadrupolar interactions), which would appear at

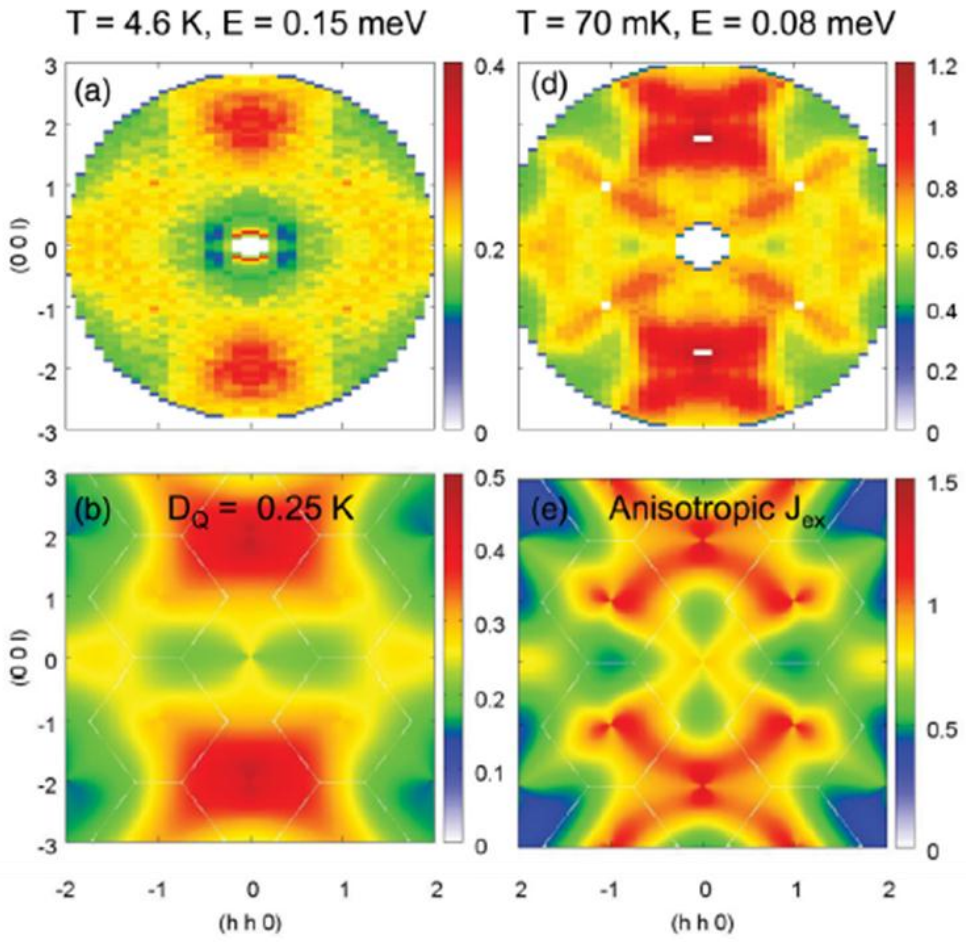

Figure 1: Inelastic neutron scattering maps at 0.07 K (right) and 4.2 K (left), performed on the spectrometer 4F of LLB: comparison between experiment (top) and theory (bottom).

very low temperatures, and that would lead to a spin-liquid ground state. This model accounts quite well for the inelastic scattering maps (Figure 1, bottom) and also reproduces the main features of the diffuse scattering maps at 0.07 K measured on D7 at the ILL by other teams (Figure 2). The proposed model is however semi-phenomenological and a more complete theory, taking into account the complex set of interactions, along with spin and lattice degrees of freedom, remains to be developed.

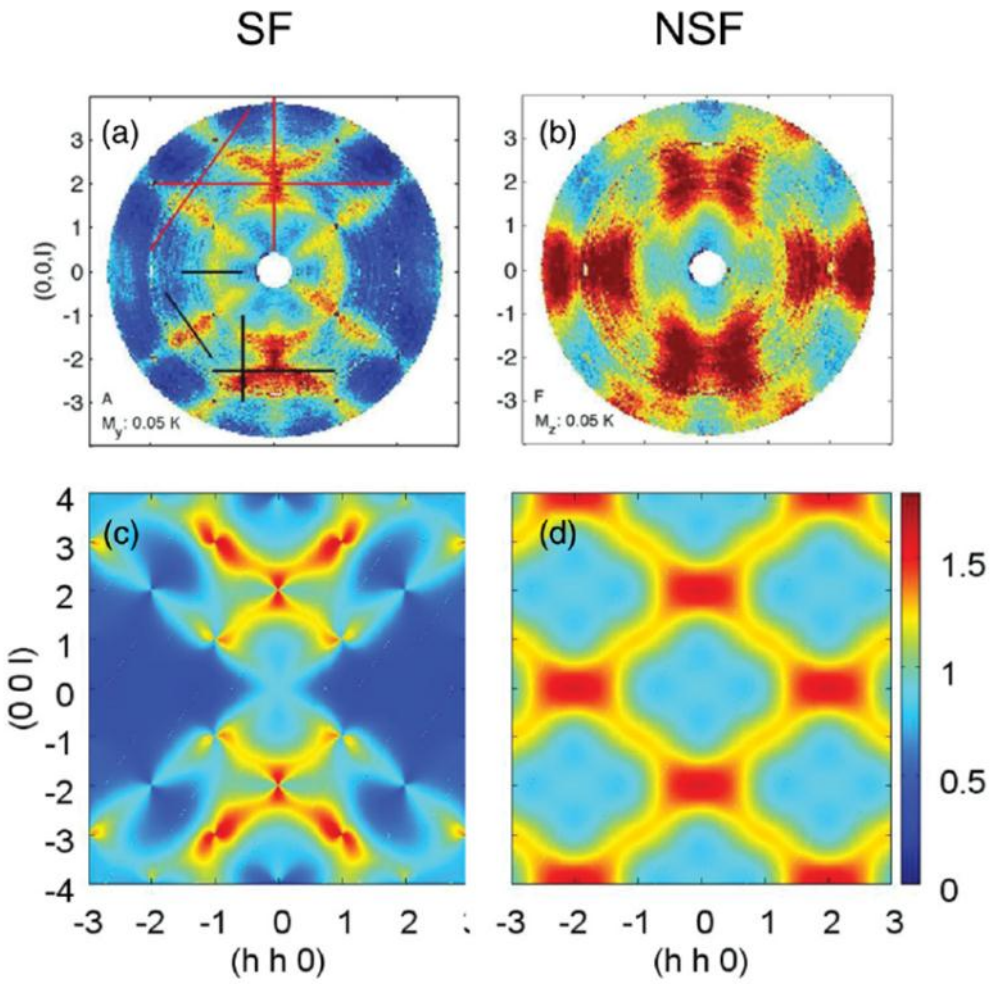

Figure 2 : Diffuse scattering maps of polarized neutrons at 0.07K: comparison between experiment (top, alleging T. Fennell et al, PRL 109, 017201 (2012)) and theory (bottom). The initial SF (Spin-Flip) and NSF (Non-Spin Flip) refer to a neutron polarization reversed or not after interaction.

References

1. Tetragonal distortion yielding a two-singlet spin liquid in pyrochlore $Tb_2Ti_2O_7$, P. Bonville, I. Mirebeau, A. Gukasov, S. Petit, J. Robert, Phys. Rev. B 84, 184409 (2011)

2. Low temperature phase diagram for the pyrochlore compound $Tb_2Ti_2O_7$, P. Bonville, I. Mirebeau, A. Gukasov, S. Petit, J. Robert, J. Phys.: Conf. Series 320, 012006 (2011)

3. Spin dynamics in the ordered spin ice $Tb_2Ti_2O_7$, S. Petit, P. Bonville, I. Mirebeau, H. Mutka, J. Robert, Phys. Rev. B 85, 054428 (2012)

4. Spin liquid correlations, anisotropic exchange and symmetry breaking in $Tb_2Ti_2O_7$, S. Petit, P. Bonville, J. Robert, C. Decorse, I. Mirebeau, Phys. Rev. B 86, 174403 (2012)

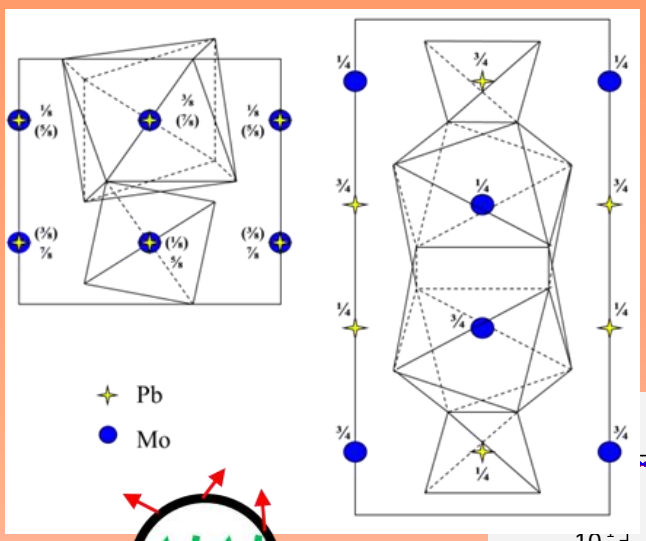
Pb
Mo

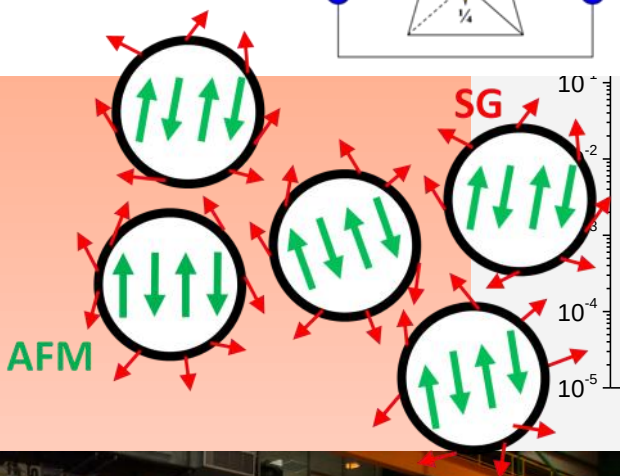
SG
AFM

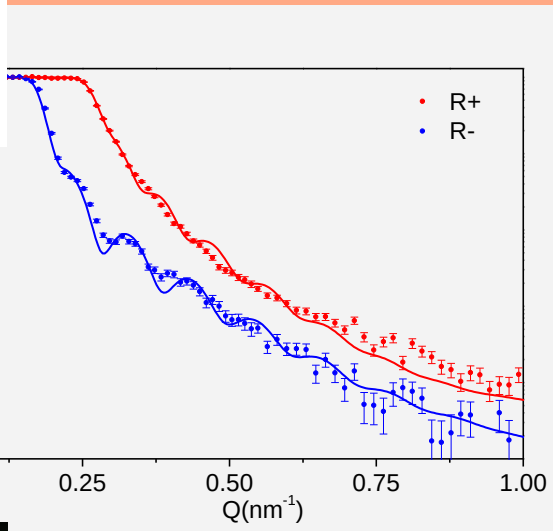
R+
R-
Q(nm-1)

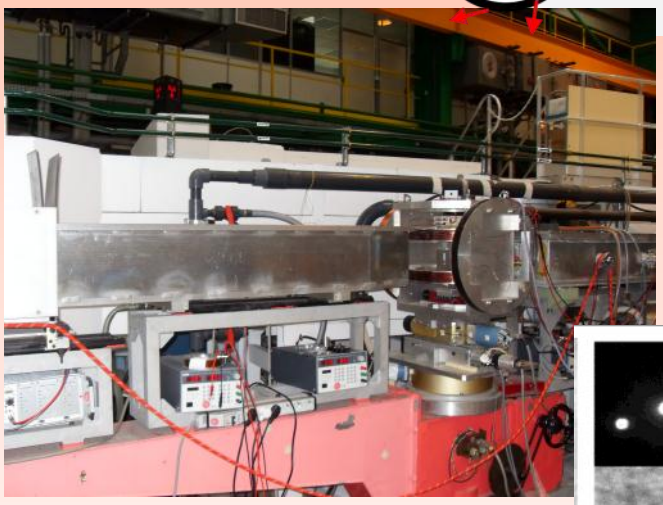

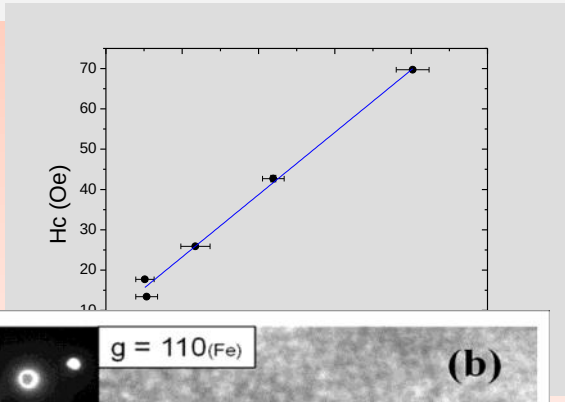
Hc (Oe)

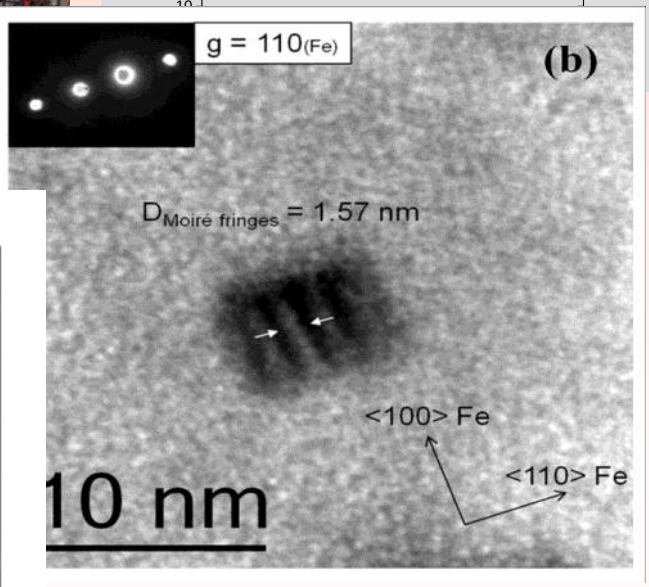
g = 110(Fe)
(b)
DMoiré fringes = 1.57 nm
<100> Fe
<110> Fe
10 nm

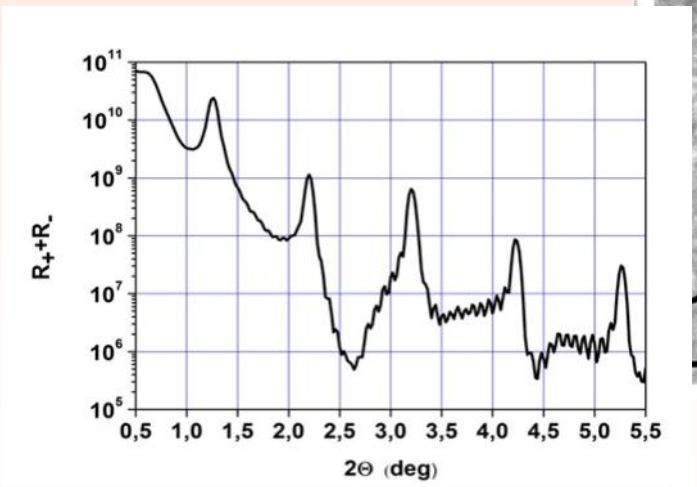
R+R-
2Θ (deg)

AXE 2:

Materials and Nanosciences : Fundamental Studies and Applications.

The second axis, "Materials and Nanosciences: Fundamental Studies and Applications", covers the activities related to the research in materials sciences and more generally in hetero-systems (interfaces, alloys, composites materials, confined systems). The studies cover detailed structures of nano-objects, interactions between nano-objects, and the role of nanostructures in composite materials. The length-scales which characterize the properties of the systems range between 1-100 nm. More specifically, the following areas are addressed at the LLB: *Magnetic nanostructures* (metallic layers, oxide epitaxial layers, nanoparticles) studied by diffraction, SANS and reflectometry; *Composite materials* (polymer reinforcement by nanoparticles, metallurgical composites) whose properties are studied by SANS; *Metallurgy* (both fundamental and industrial) where Textures and Strain heterogeneities are studied by diffraction in various alloys or nuclear materials; *Confined systems (*microporous materials and organized guest-hosts systems, mesoporous materials and organized guest-hosts systems) in which the dynamics of the confined elements can be studied by inelastic scattering techniques; *Amorphous materials* (disordered systems – glasses) where the local atomic order is also investigated by diffraction.

- **Metallic superantiferromagnetic $TbCu_2$ nanoparticles**
  C. Echevarria-Bonet, 1; D. P. Rojas; J. I. Espeso, J. Rodríguez Fernández, L. Rodríguez Fernández, P. Gorria, J. A. Blanco, M. L. Fernández-Gubieda, E. Bauer, G. André, L. Fernández Barquín

- **Polarised neutron reflectivity reveals enhanced moment on Fe^+ irradiated iron films**
  K. Mergia, K. Papamichail, F. Ott, Y. Serruys, Th. Speliotis, G. Apostolopoulos, S. Messoloras

- **Point defects in $PbMoO_4$ both undoped and doped with Nd^{3+}**
  I. Kaurova, G. Kuz'micheva, V. Rybakov, A. Cousson, Yu. Gorobets

- **Effect of chemical composition on the coalescence kinetics of oxides in the reinforced steel ODS Fe-14%Cr**
  S. Zhong, M.-H. Mathon, V. Klosek, Y. de Carlan, J. Ribis

- **Temperature driven interlayer exchange coupling in Fe/Cr/Gd multilayers**
  M. V. Ryabukhina, E. A. Kravtsov

Metallic superantiferromagnetic $TbCu_2$ nanoparticles

C. ECHEVARRIA-BONETA[a]; D. P. ROJAS[B]; J. I. ESPESO[A], J. RODRÍGUEZ FERNÁNDEZ[A], L. RODRÍGUEZ FERNÁNDEZ[C], P. GORRIA[D], J. A. BLANCO[D], M. L. FDEZ-GUBIEDA[E], E. BAUER[F], G. ANDRÉ[G], L. FERNÁNDEZ BARQUÍN[A]

a Depto. CITIMAC, Universidad de Cantabria, 39005 Santander, Spain

b Depto. Física e Instalaciones Aplicadas. ETSAM- UPM, 28040 Madrid, Spain

c SERMET, Universidad de Cantabria, 39005 Santander, Spain

c Depto. Física, Universidad de Oviedo, 33007 Oviedo, Spain

e Depto. Electricidad y Electrónica, Universidad del País Vasco (UPV/EHU), 48940 Leioa, Spain

f Institut für Festkörperphysik, Technische Universität Wien, 1040 Wien, Austria

g LLB, CEA-SACLAY, 91191 Gif-sur-Yvette Cedex, France

echevarriac@unican.es

The novel superantiferromagnetic arrangement in metallic $TbCu_2$ nanoparticles has been revealed by the full analysis of the magnetic structure. Such an arrangement coexists at low temperatures with the spin glass canting of surface spins. TEM and XRD evidence that the lattice structure at the nanoscale retains the bulk crystallographic symmetry, with particle sizes around 9 nm. Macroscopic measurements of static and dynamic magnetic susceptibility disclose that there is a collective Néel temperature of 46 K and the glassy freezing is below ≈9 K, governed by a critical slowing down process.

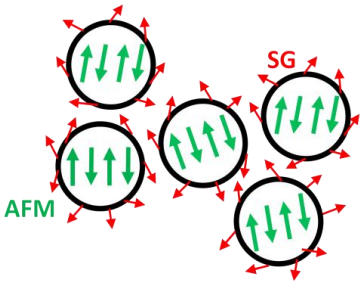

The effects of interparticle interactions of different strengths among magnetic nanoparticles gives rise to a variety of magnetic states from the weakly correlated Superparamagnetism [1], passing through the Super Spin Glass state [2] and reaching the Superferromagnetism [3], the latter two included within the so-called Supermagnetism [4]. The appearance of metallic Superantiferromagnetic (SAFM) state and its coexistence with a Spin Glass (SG) behavior has very recently been disclosed in nanoparticles of $TbCu_2$ [5]. The characterization of those systems is essential to extend the magnetic phase diagrams, which, in turn, constitute the roadmap for technological transfer.

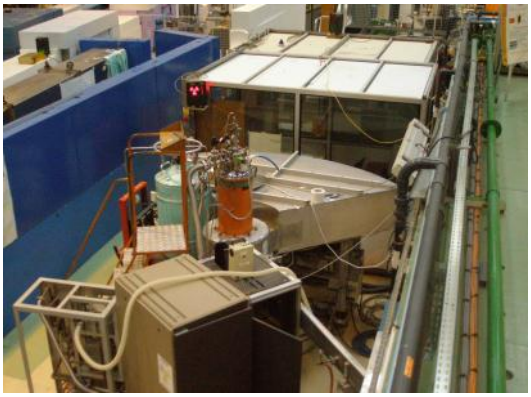

Figure 1: G4.1 instrument at the LLB with an orange cryostat mounted for the low temperature nano-$TbCu_2$ measurements.

The existence of SAFM and SG states was revealed by DC- and AC-susceptibility measurements, and additionally by microscopic magnetic structure analysis (neutron scattering) [5]. The metallic state is now confirmed by electrical resistivity. Neutron diffraction measurements have been carried out at Laboratoire Léon Brillouin (G4.1 instrument) with $\lambda = 2.423$ Å. G4.1 is a two axis powder diffractometer (Fig. 1) equipped with a vertical focusing pyrolytic graphite monochromator and a 800-cell multidetector covering a $80^o - 2\theta$ range. The instrumental resolution of the spectrometer is maximum at low 2θ scattering angles ($2\theta < 600$), so G4.1 is well adapted for magnetic structure determination and for phase transition studies.

Both DC- and AC-susceptibility showed a peak at the Néel transition (46 K) and a broader hump at the freezing point (9 K) [5]. The critical slowing down of the low temperature SG transition was studied for the $TbCu_2$ milled alloy by extracting quantitative values for the zv and ß dynamic exponents. This analysis yielded $zv = 6$ and $ß = 0.7$, in the range of supermagnetic systems (see Ref. [5] for details). In Fig. 2, we are confirming the metallic character of the $TbCu_2$ nanoparticles by displaying the electrical resistivity (ρ), which resembles the behavior found in bulk alloys. Moreover, there is a clear change of slope at the Néel temperature, which is smooth due to the nanoscopic nature of the alloy in question.

Neutron diffraction spectra were taken at different temperatures: 1.8 K and 10 K ($T < T_f$), 25 K and 36 K ($T_f < T < T_N$) and 60 K and 140 K ($T > T_N$). The spectra were taken for 8 hours/temperature to get good stats with an amount of sample of

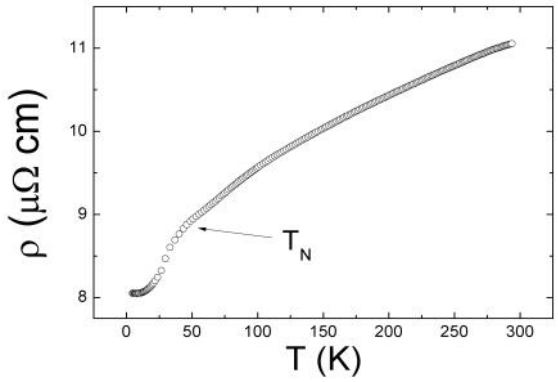

Figure 2: Electrical resistivity (ρ) of compacted nanometric $TbCu_2$ particles, showing their metallic character and the Néel transition (T_N). Such a transition is rounded up in comparison to bulk alloys.

As a result, a thin layer of random spins favors the SG behavior, enabling the coexistence with the antiferromagnetic order, which is scarcely reported [6]. Overall, the neutron diffraction spectra provide crucial evidences to understand the magnetic structure at the nanoscale. [1, 5].

Consequently, this system should be considered as a superantiferromagnet with reentrant behavior ensured by the nanoparticle spin-disordered surface.

around 2 g. The magnetic structure (Fig. 3) corresponds to a commensurate antiferromagnetic with two propagation vectors, $q_1 = (0, 0, 0)$ and $q_2 = (1/3, 0, 0)$. The magnetic structure is collinear AF with large Tb atoms (blue) holding the magnetic moment (arrows) (see the inset of Fig. 3). Thus, the magnetic structure is not modified respect to that of the bulk alloy. The particle size is also confirmed to be around 9 nm, in agreement with the TEM & X-ray data. The resulting ordered Tb^{3+} magnetic moment, at 1.8 K, is $\mu = 7.76(2)\mu B$, with $R_{mag} = 4.2\%$ and $R_B = 1.1\%$. A rough estimate assuming the ratio of surface atoms (N_s) with respect to those in the total volume (N_V) results in $N_s/N_V \approx 40\%$, remarking the role of surface spins and supporting the surface moment reduction. In our $TbCu_2$ nanomagnets, the uncompensated spins provide a source for randomness at the particle surface.

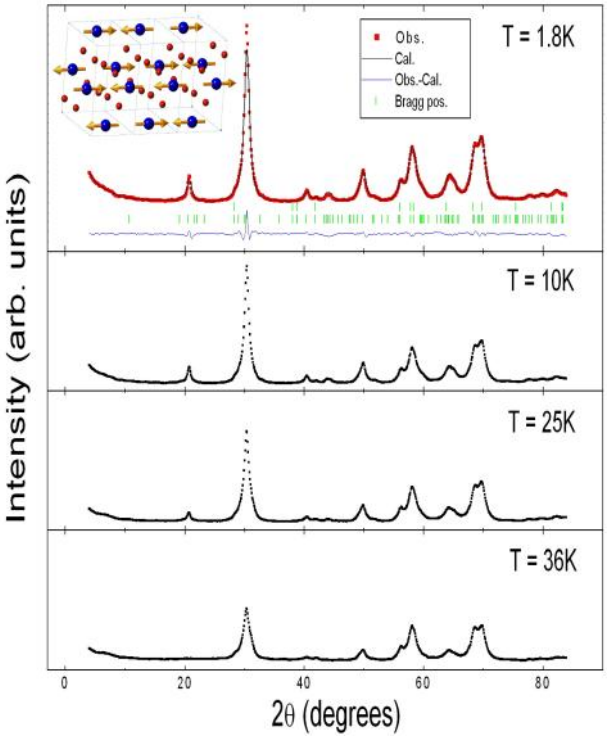

Figure 3: Neutron diffraction spectra at different temperatures for the milled $TbCu_2$ alloy. (Upper plot) vertical marks correspond to the position of the allowed Bragg reflections. Blue line corresponds to the difference between the observed (red dots) and the calculated (black line) intensity, by a Rietveld refinement. Inset: magnetic structure of nano-$TbCu_2$.

References

1. L. Fernández Barquín *et al.*, Phys Rev B 76, 172404 (2007).
2. C. Binns *et al.*, Phys Rev B 66, 184413 (2002).
3. X. Chen *et al.*, Phys. Rev. Lett. 89, 137203 (2002).
4. S. Bedanta *et.al.*, J. Phys. D 42, 13001 (2009).
5. C. Echevarria-Bonet *et al.*, Phys. Rev B 87, 180407(R) (2013).
6. W. Kleemann *et al.*, Phys. Rev. Lett. 105, 257202 (2010). .

Polarised neutron reflectivity reveals enhanced moment on Fe^+ irradiated iron films

K. MERGIA[A], K. PAPAMICHAIL[A], F. OTT[B], Y. SERRUYS[C], TH. SPELIOTIS[A], G. APOSTOLOPOULOS[A], S. MESSOLORAS[A]

a NCSR Demokritos, Athens, Greece

b Laboratoire Léon Brillouin, CEA, Saclay, France

c DEN/DMN/SRMP - Laboratoire JANNUS, CEA, Saclay, France rance

kmergia@ipta.demokritos.gr

kpapmih@ipta.demokritos.gr

frederic.ott@cea.fr

yves.serruys@cea.fr

tspeliotis@ims.demokritos.gr

gapost@ipta.demokritos.gr

Thin Fe films had been irradiated at CEA-JANNuS multi-ion beam facility with 490 keV iron ions at four different doses causing displacements per atom (dpa) from 1.2 to 57. PNR measurements revealed a dose dependent increase in the magnetic moment of iron above its bulk value. In addition, structural changes have been investigated using X-ray reflectivity (XRR) and grazing incidence diffraction measurements (GIXRD) before and after irradiation. These measurements, have shown lattice constant increase and grain growth versus dose.

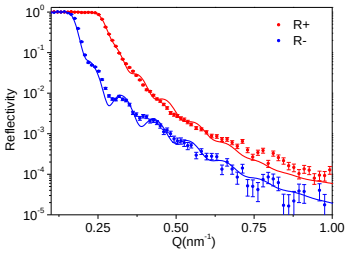

The interplay between magnetism and radiation damage of Fe and Fe based alloys by energetic ions or neutrons is an area of extensive current international research effort [1]. This activity not only addresses an important physics problem but it is also interrelated to the international effort for the development of new radiation resistant FeCr based alloys for the future fusion reactor. Neutron based techniques are unique in revealing structural and magnetic changes induced in the Fe and its alloys after irradiation.

Within the above described science and technology framework we initiated a research programme to study irradiation induced changes in the magnetic properties of Fe. As radiation damage inducing agent mono-energetic Fe ions were chosen. The reasons for this choice were: a) the interaction of Fe ion with Fe can be easily simulated, b) the expected defect structures are relatively simple and c) more importantly the Fe^+ bombardment can simulate also the interaction of the fusion produced neutrons with Fe. The 14 MeV fusion neutrons create primary Fe knock-ons which in their turn produce the radiation damage of the material. As the mean energy of the produced primary Fe knock-ons is about 490 keV, this energy was chosen for the Fe ion bombardment. Since the aim was to study initially only radiation damage effects simulations on the interactions of 490 keV Fe^+ with Fe films were carried out. The simulations showed that in Fe film thickness of around 50 nm the Fe implantation is negligible whereas the radiation damage considerable.

With the above reasoning Fe thin films of 50 nm thickness were fabricated by magnetron sputtering. Prior to irradiation the Fe films were characterized by GIXRD, XRR and magnetomentry measurements. The irradiation with 490 keV Fe^+ ions was carried out at the CEA-JANNUS multi-ion beam facility under the auspices of the European Fusion Programme. Four doses were chosen causing displacements per atom from 1.2 to 57.

Structural changes induced by the Fe ion irradiation were assessed by GIXRD and XRR measurements. As the dose increases the lattice constant increases from a value lower than that of the bulk to that of the bulk. In addition the grain size increases reaching a plateau for doses above $1x10^{16}$ ions/cm^2 (Fig.1). The final increase of the grain size is 53%. X-ray reflectivity measurements have shown that for the high dose irradiations swelling has occurred leading to an average film thickness increase of about 3 nm. Swelling is caused by the movement of the interstitial defects to the grain surfaces.

However, the most crucial irradiation induced changes refer to the magnetic properties of the Fe films [2]. Polarised neutron reflectivity (PNR) is the most sensitive, accurate and indisputable method to reveal those. The structural changes induced by the irradiation and described above are limited and thus any magnetic changes would be expected also small [3]. PNR measurements were carried out at PRISM reflectometer, Laboratoire Léon Brillouin. To our surprise the effects were not small as would have been expected but a remarkable magnetic moment enhancement was observed. The magnetic moment increases from

2.1 (for the unirradiated film) up to 2.5 μ_B/atom for the highest dose which corresponds to 57 displacements per atom (Fig.2).

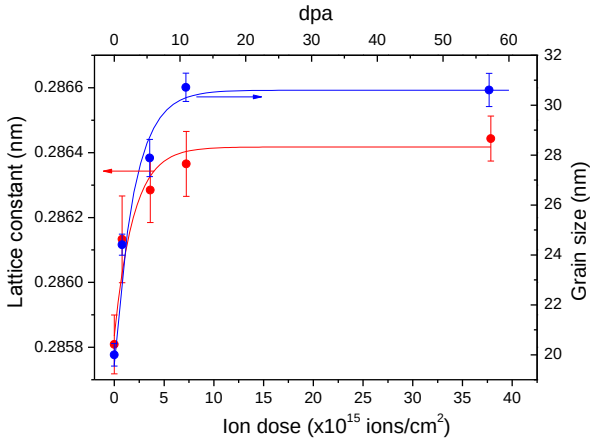

Figure 1: Lattice constant and grain size as a function of irradiation dose.

Furthermore, the irradiation makes the iron films magnetically softer and this is reflected in the reduction of the coercive field, H_c, with the increase of the irradiation dose. The highest dose of about $4x10^{16}$ ions/cm^2 results in 80% reduction of the coercive field to about 13 Oe. This decrease of the coercive field is related with the grain size increase and Fig.3 shows that H_c varies linearly with the inverse of the grain size.

In conclusion the different structural changes observed in Fe^+ irradiated films *e.g.* lattice constant increase, swelling are expected and have been observed in many instances after irradiation. However, the drastic increase of the Fe magnetic moment revealed by PNR has never been observed before and it is quite unexpected. Fe magnetic moment increase arising from lattice constant increase would be very small [4] and thus could not explain the results. This magnitude increase of magnetic moment has to do with the formation of vacancy clusters as it is known

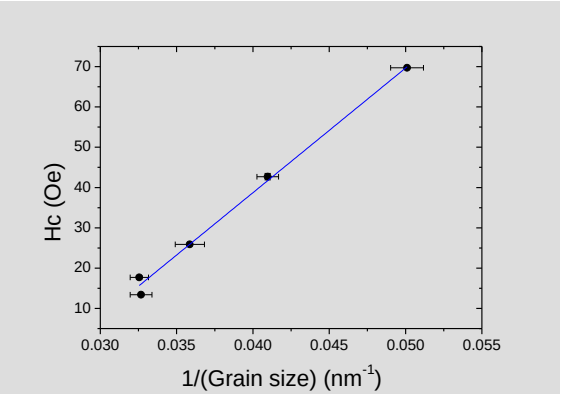

Figure 3: Coercive field as a function of the inverse grain size.

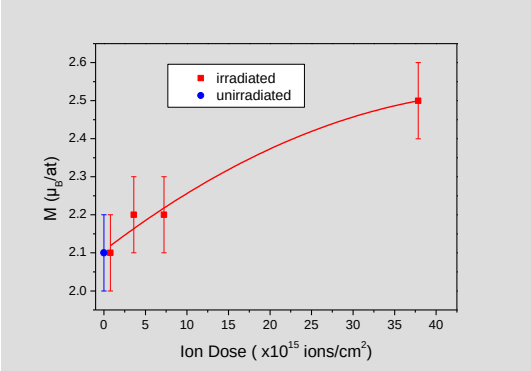

Figure 2: Lattice Magnetic moment of 490 keV Fe^+ irradiated iron 50 nm films .

that the neighbouring and next neighbours Fe atoms of the cluster have increased magnetic moments. Dislocation formation due to irradiation could not explain the magnetic moment increase as a large number of dislocations is formed after cold working and such effects have not been observed

References

1. S. L. Dudarev and P. M. Derlet, J Computer-Aided Mater Des (2007) 14, 129–140
2. K. P. Lieb K. Zhang, G. A. Müller, R. Gupta and P. Schaaf, Hyperfine Interactions (2005) 160, 39–56
3. Yasuhiro Kamada, *et al.*, Materials Transactions (2009) 50, 2134 – 2138
4. H. C. Herper, E. Hoffmann, and P. Entel, Phys. Rev. B (1999) 60, 3839-3848 .

Point defects in $PbMoO_4$ both undoped and doped with Nd^{3+}

I. KAUROVA[A], G. KUZ'MICHEVA[B], V. RYBAKOV[C], A. COUSSON[D], YU. GOROBETS[A]

a Mineral Ltd., Alexandrov, Russia

b Lomonosov State University of Fine Chemical Technologies, Moscow, Russia

c Lomonosov State University, Moscow, Russia

d Laboratoire Leon Brillouin, CEA Saclay, France

e Institute for Single Crystals of NAS of Ukraine, Kharkiv, Ukraine

kaurchik@yandex.ru

Nominally pure and Nd^{3+}-doped $PbMoO_4$ single crystals grown by the Czochralski technique with using Nd_2O_3, $Nd_2(MoO_4)_3$, $NaNd(MoO_4)_2$, and $NdNbO_4$ compounds have been investigated by single crystal neutron diffraction. It was revealed the presence of additional reflections (~3÷~6%) for all the crystals caused by kinetic growth effects that give grounds to assign them to the space group $I4$ rather than to $I4_1/a$. The type and concentration of point defects have been determined. Explanation of crystals color has been proposed.

Lead molybdate - $PbMoO_4$ (PMO) - is an acousto-optic material which belongs to the family of crystals with $CaWO_4$ scheelite structure (sp. gr. $I4_1/a$, Z = 4) [1]. In the PMO crystal structure, the Pb^{2+} atoms occupy dodecahedral positions with two sets of interatomic distances (CN = 4+4; CN - coordination number). The Mo^{6+} atoms are in the center of a slightly distorted tetrahedra MoO^4 (CN = 4). Each oxygen atom is coordinated by two Pb atoms and one Mo atom (CN = 3) (Fig. 1).

The presence of color caused by associates of point defects and antisite defects, or by photochromic effect restricts the use of lead molybdate as an optical material [2].

Presence in the structure of point defects, their types and their associates will be determined by the charge synthesis conditions, the concentration of impurities, and by single crystal growth conditions.

$PbMoO_4$ crystals are usually grown by the Czochralski method using the charge prepared by solid phase synthesis of PbO and MoO_3 oxides combined in a stoichiometric ratio. The main problem is stoichiometry violation due to the higher vapor pressure of MoO_3 compared with PbO. As a result, the formation of defective phases and distorted crystal structure is possible. It will affect crystal color and properties.

Introduction of laser-active ions, in particular neodymium ions, allows to obtain the lasing of $PbMoO_4$ crystal [3]. However heterovalent activation by Nd^{3+} ions can lead to the formation of additional types of defects.

It was suggested that Nd^{3+} ions may occupy different crystallographic positions in $PbMoO_4$ crystal lattice depending on the method of activation [4].

The motivation of this work was the lack of consensus about the possible types of point defects in undoped and doped PMO crystals, and their influence on the physical properties taking into account the further use of the material in different areas of optoelectronics. Therefore, the precise definition of each crystallographic position composition is critical.

The purpose of this work is to determine the type and concentration of point defects in nominally pure and Nd^{3+}-doped $PbMoO_4$ single crystals grown by the Czochralski technique in Pt crucible along <001> direction using the neutron diffraction analysis (NDA) of single crystals (~3x3x3 mm; λ=0.83Å; 5C2, Orphée-reactor, LLB, France; SHELXL-97).

The Nd^{3+} ions were introduced to PMO in the form of Nd_2O_3, $NdNbO_4$, $Nd_2(MoO_4)_3$ and $NaNd(MoO_4)_2$. The crystals had different color: nominally pure $PbMoO_4$ sample was transparent and had a yellowish tint; $PbMoO_4$:Nd_2O_3 and $PbMoO_4$:$Nd_2(MoO_4)_3$ samples had a deep yellow color; $PbMoO_4$:$NdNbO_4$ and $PbMoO_4$:$NaNd(MoO_4)_2$ had a deep lilac color.

As a result of the NDA, the following results were obtained:

1. The neutron diffraction investigation of PMO and PMO:Nd^{3+} crystals within the framework of sp. gr. $I4_1/a$ allowed to reveal the presence of additional reflections $PbMoO_4$ (4.8%), $PbMoO_4$:Nd_2O_3 (4.6%), $PbMoO_4$:$NdNbO_4$ (5.7%), $PbMoO_4$:$Nd_2(MoO_4)_3$ (3%), $PbMoO_4$:$NaNd(MoO_4)_2$ (5.4%) which were indexed within the framework of noncentrosymmetric sp. gr. . In this case we may deal with a kinetic phase transition of order-disorder type, *i.e.* a partially ordered noncentrosymmetric phase is formed in the sta-

bility area of the disordered centrosymmetric phase under the influence of kinetic factors.

2. The crystal compositions refined from the neutron diffraction analysis of PMO and PMO:Nd^{3+} single crystals within the framework of sp. gr. $I4_1/a$ are the following (□ - vacancy):

- $Pb^{2+}\ Mo_{1.000(16)}O_{3.960(44)}$

  (R1 =0.065; $PbMoO_4$);

- $(Pb^{2+}_{0.865(45)}Nd^{3+}_{0.085}\square_{0.050})Mo^{6+}O_4$

  (R1 =0.080; $PbMoO_4$:Nd_2O_3);

- $(Pb^{2+}_{0.968(16)}Nd^{3+}_{0.032})(Mo^{6+}_{0.970(20)}Nb^{5+}_{0.030})O_4$

  (R1 =0.068; $PbMoO_4$:$NdNbO_4$);

- $(Pb^{2+}_{0.964(15)}Nd^{3+}_{0.025}\square_{0.011})Mo^{6+}O_4$

  (R1 = 0.070; $PbMoO_4$:$Nd_2(MoO_4)_3$);

- $(Pb^{2+}_{0.935(12)}Nd^{3+}_{0.033}Na^{+}_{0.033})Mo^{6+}O_4$

  (R1 = 0.060 ; $PbMoO_4$:$NaNd(MoO_4)_2$).

According to NDA, the composition of undoped $PbMoO_4$ is almost stoichiometric taking into account the standard deviation in the determination of oxygen position. It was found that the type and concentration of point defects are changed depending on the type of activator which is a heterogeneous impurity. But it should be noted that Nd^{3+} ions occupy dodecahedral position in the structure of all the samples. As a result of refinement of crystallographic position compositions of $PbMoO_4$:Nd_2O_3, $PbMoO_4$:$Nd_2(MoO_4)_3$, $PbMoO_4$:$NaNd(MoO_4)_2$ samples, the presence of defects in molybdenum and oxygen positions was not revealed. At the same time, the use of neutron radiation allowed to determine the composition of dodecahedral and tetrahedral position of the $PbMoO_4$:$NdNbO_4$ sample.

3. It's not excluded that yellow color or yellowish tint of crystals under investigation is due to the formation of $(V_{Pb}^{n'}, nh\cdot)^x$ or (and) $(V_{Mo}^{n'}, nh\cdot)^x$ color centers.

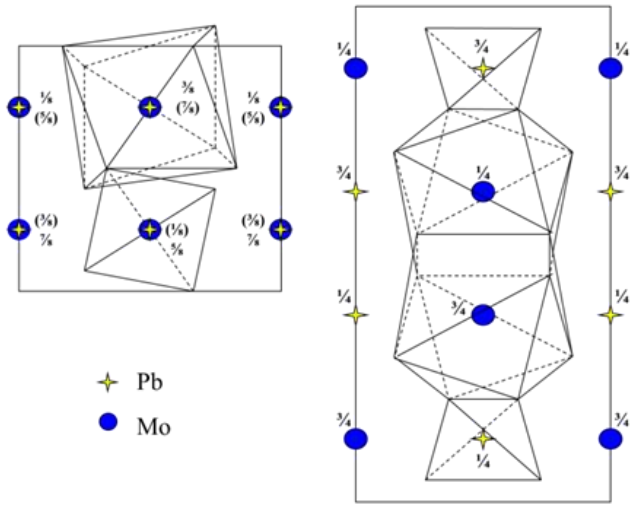

Figure 1: Coordination polyhedra in the $PbMoO_4$ structure:

(a) XY projection ; (b) XZ projection

References

1. D. Errandonea *et al.*, Phys Rev. B 72, 174106 (2005)
2. G. Kuz'micheva *et al.*, Russian J of Inorg Chem 57, 1128 (2012)
3. T. T. Basiev *et al.*, Optics Letters 31, 65 (2006)
4. Yu. N. Gorobets *et al.*, J Cryst Growth 318, 687 (2011)

Effect of chemical composition on the coalescence kinetics of oxides in the reinforced steel ODS Fe-14%Cr

S. ZHONG[A], M.-H. MATHON[A], V. KLOSEK[A], Y. DE CARLAN[B], J. RIBIS[B]

a Laboratoire Léon Brillouin, CEA-CNRS, CEA-Saclay, 91191 Gif sur Yvette, France.

b DEN/DANS/SRMA, CEA-Saclay, 91191 Gif sur Yvette, France

marie-helene.mathon@cea.fr

In designing the heart of a nuclear reactor structural materials should be selected with a good working knowledge of their mechanical properties and their behavior under irradiation. The nanostructured oxide dispersion (ODS steels: Oxide Dispersion Strengthening) is a method for hardening steel. These materials are considered as structural materials for future nuclear reactors (Generation IV, especially for fuel cladding in fast reactors RNR) or the first walls of fusion reactors.

To validate these guidelines, a perfect mastery of the development of these ODS steels is required. The present study shows that the initial contents of Ti, Y and O are crucial for the kinetics of coalescence of the oxide particles and the temperature behavior of the material, which determine its mechanical properties.

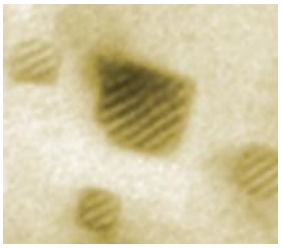

The strengthening of steels with a fine dispersion of oxides such as Y_2O_3 or $Y_2Ti_2O_7$ imparts excellent creep resistance properties. These materials are prepared by mechanical alloying. It is assumed that this process provides these nanostructured materials by dissolving the yttrium and oxygen atoms introduced in the form of nano compounds during co-grinding, which, during annealing, better control precipitation phase of hardening particles. The resulting mechanical properties are closely related to the fine oxide particles, and the mastery of precipitation is thus an important issue in the development of these steels.

Early work showed that the initial levels of Y, Ti and O affect the precipitation kinetics. One of the objectives of the thesis of S. Y. Zhong was to determine the effect on the microstructure of a change in levels around the reference values usually used. The approach was twofold: specify the precipitation kinetics, and recrystallization conditions between 850° and 1450°C. The chosen material as reference is a ferritic Fe-14Cr-1W-0, 0-3Ti, $3Y_2O_3$, which was available in four other shades having contents of Ti, O and Y different. The microstructural analysis was performed by coupling the techniques of neutron scattering at small angles (SANS) and transmission electron microscopy (TEM).

Dispersions of nano-oxides formed after consolidation in different alloys are quite similar (bimodal centered on 2 and 5 nm). After annealing, the detailed study by TEM reveals a consistent crystallographic structure with the pyrochlore phase of $Y_2Ti_2O_7$ expected for all alloys. On the other hand changes during annealing at high temperature (between 1300 and 1450°C) show a wide disparity (Figure 1): the shape, size and orientation relationship between the particles and the matrix are clearly dependent on the material. For alloys with a concentration ratio [Ti]/[Y] close to or greater than 1, nano -oxides are cubic (Fig. 2), with an orientation coherent with the matrix (cubic on cubic ([100] oxide // [100] matrix) and remain small, irrespective of the temperature and time of annealing. by contrast, the highly doped yttrium alloys ([Ti]/[Y] < 1), oxides are spherical of large size after prolonged annealing and relationships orientations are not coherent with

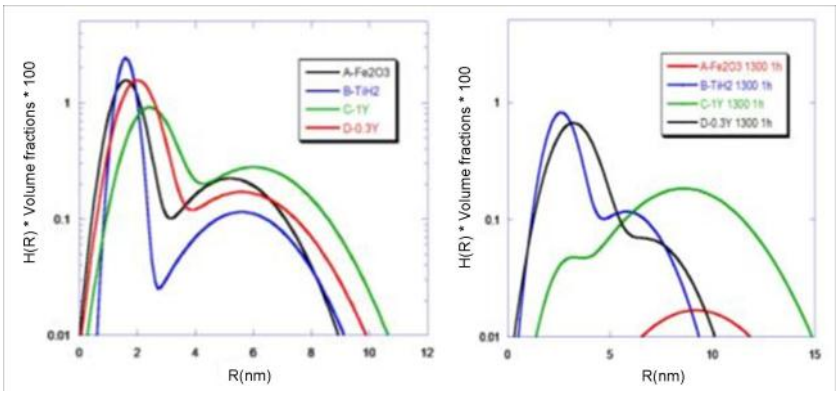

Figure 1: Study of the kinetics of particle coalescence.

Distribution of nano-oxides determined by SANS in different alloys in the consolidated state then after 1h annealing at 1300°C.

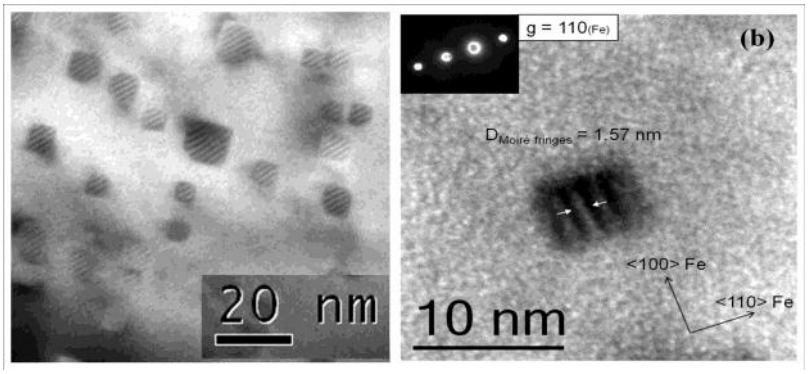

Figure 2: TEM observations performed on the alloy doped titanium (B) highlighting the cubic oxides and orientation relationships perfectly coherent with the iron matrix.

the matrix.

The difference in the relative orientation between the precipitates and the matrix can explain the differences in behavior during annealing. Energy of oxides/matrix interface is strongly dependent on orientation relationship and increases with disorientation. This parameter is involved in the kinetics of coalescence (the period during which the particles grow at the expense of dissolution of smaller). It is normal to observe a pseudo stable oxides for alloys [Ti] / [Y] ≥ 1 even at high temperature (1450°C), the phenomenon of recrystallization is blocked. On the other hand it is observed in shades rich in oxygen and yttrium (Ti] / [Y] <1) where the coalescence is rapid due to the strong interface energy associated with oxides/matrix disorientation.

This work thus highlights the differences in kinetics of coalescence of oxide precipitates, depending on the initial content of Ti, Y and O. The differences result from the form of oxides $Y_2Ti_2O_7$ and of orientation relations of particle/matrix, which directly affect the behavior of the material under annealing. The implications are abundant especially on the mechanical properties, crystallization behavior, etc. This research continues the study of the germination process, seeking the origin of coherence relations between the precipitates and the matrix depending on the alloy composition.

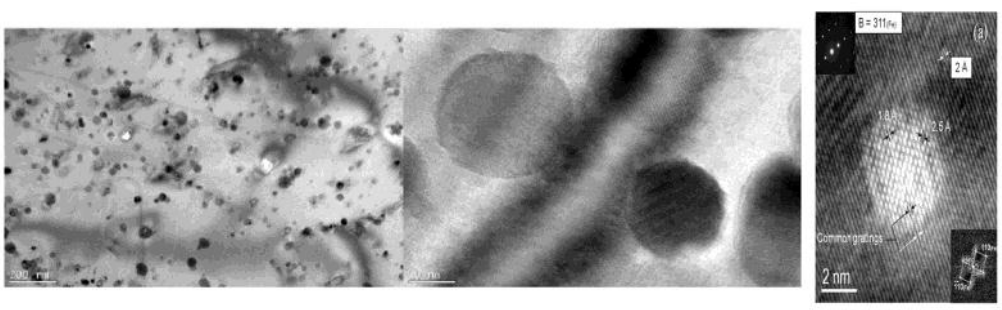

Figure 3: TEM observations performed on the alloy doped yttrium (C) showing the spherical shape of oxides and relationships orientation incoherent with the iron matrix

References

1. Étude des évolutions microstructurales à haute température en fonction des teneurs initiales en Y, Ti et O et, de leur incidence sur les hétérogénéités de déformation dans les aciers ODS Fe-14Cr1W, Thesis of S. Y. Zhong (July 2012).

Temperature driven interlayer exchange coupling in Fe/Cr/Gd multilayers

M.V.. RYABUKHINA[A]., E.A. KRAVTSOV[A]

a Institute of Metal Physics, Russia

ryabukhina@imp.uran.ru

Ferromagnetic 4f rare-earth/ 3d transition metal (RE/TM) multilayers are popular model systems showing a rich variety of magnetic phases in applied field.

In particular, complex magnetic order in Fe/Gd multilayers is governed by several competing mechanisms: enhancement and temperature-independence of Gd magnetic moment in the interfacial region near Fe, strong RE-TM antiferromagnetic coupling at interfaces, and Zeeman interaction with external fields.

It was recently shown that RE/Cr/TM multilayers, where RE-TM exchange is mediated by antiferromagnetic Cr, display a number of novel magnetic phases, including switching an otherwise AFM Gd-Fe coupling to ferromagnetic coupling, together with a dominant biquadratic RE-TM exchange coupling over bilinear coupling at certain Cr thicknesses near where the oscillatory interlayer coupling (with Cr thickness) changes sign. The latter should lead to non-collinear ordering. Cr layer thickness in the samples was chosen in order to cover 3 different types of magnetic ordering in the system: ferromagnetic, antiferromagnetic and non-collinear.

The [Fe(35 Å)/Cr(t Å)/Gd(50 Å)] (t = 0-60 Å) multilayer was grown via magnetron UHV sputtering onto a Si substrate with Cr buffer (50 Å) and cap (30 Å) layers. The structural properties of the multilayer were characterized with resonant x-ray magnetic reflectometry (RXMR). Magnetometry measurements were performed with a superconducting quantum interference device (SQUID).

Two samples of the series ([Fe(35 Å)/Cr(t)/Gd(50 Å))/Cr(t)]$_{12}$ (t = 4.4, 7.2 Å)) were successfully measured with PNR (PRISM). The PNR experiment has been performed at T= 15, 50, 100 and 300 K in magnetic field 500 Oe within saturation. In the experiment, the mag-

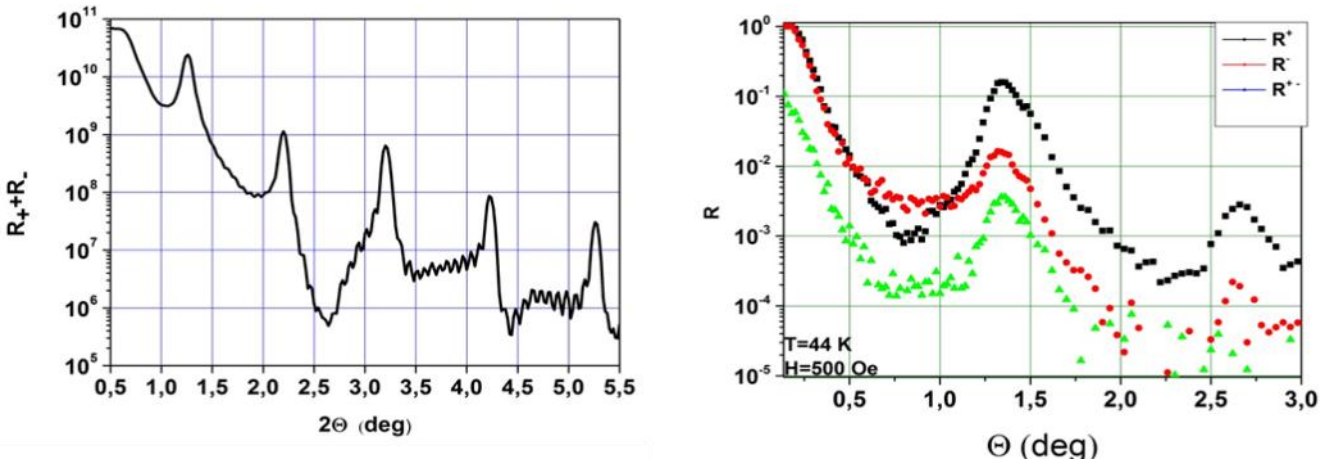

Figure 1 : Experimental RXMR, PNR spectra of sample [Fe(35 Å)/Cr(4.4 Å)/Gd(50 Å)/Cr(4.4 Å)]$_{12}$ for T=44 K, H=500 Oe

netic field was applied in the plane of the sample. The measurement has shown excellent structural quality of the sample and interesting magnetic behavior at different temperatures.

In Fig. 1 we show RXMR, PNR spectra measured for samples [Fe(35 Å)/Cr(4.4 Å)/Gd(50 Å)/ Cr(4.4 Å)]$_{12}$.

We expect to discover novel effects associated with strong temperature – dependent non-collinear ordering due to dominated biquadratic coupling that has not been observed so far in TM-RE multilayers so we need investigate samples with different Cr layer thicknesses at low temperatures from 20 K to 320 K in magnetic fields.

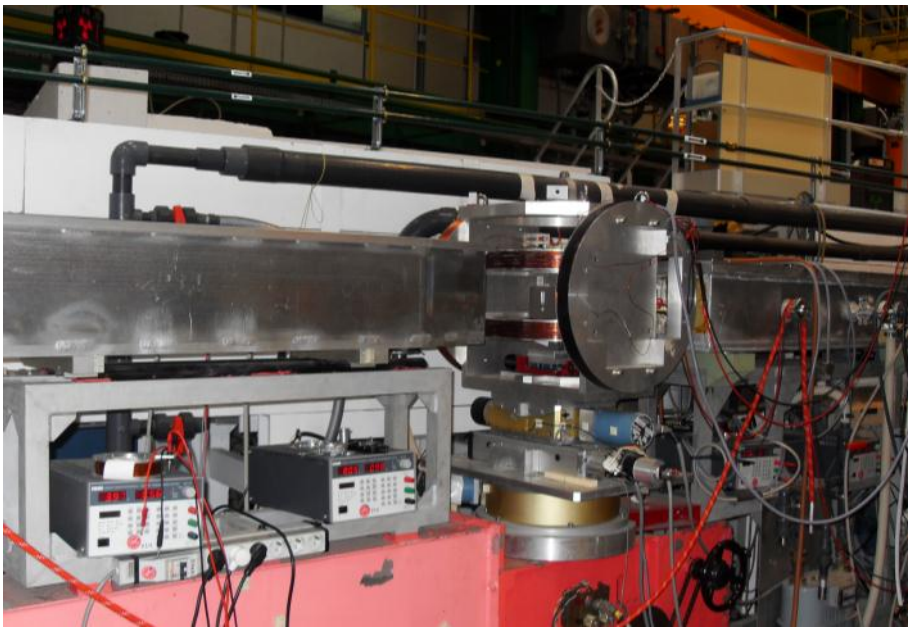

The PRISM (G2.4) polarized reflectometer at LLB

References

1. *R.E. Camley in Nanomagnetism: Ultrathin Films, Multilayers and Nanostructures, eds D. L. Mills,J. Anthony C. Bland, Elsevier, 2006.*
2. *R. Sanyal, C. Antoniak, T. Burkert, B. Krumme, A. Warland, F. Stromberg, Ch. Praetorius, K. Fauth, H. Wende, O. Eriksson Forcing ferromagnetic coupling between rare-earth-metal and 3d ferromagnetic films, Phys. Rev. Letters 104, 156402 (2010).*
3. *E. Kravtsov, D. Haskel, S. G. E. te Velthuis, J. S. Jiang, and B. J. Kirby Complementary polarized neutron and resonant x-ray magnetic reflectometry measurements in Fe/Gd heterostructures: Case of inhomogeneous intralayer magnetic structure, Phys. Rev. B 79, 134438 (2009).*

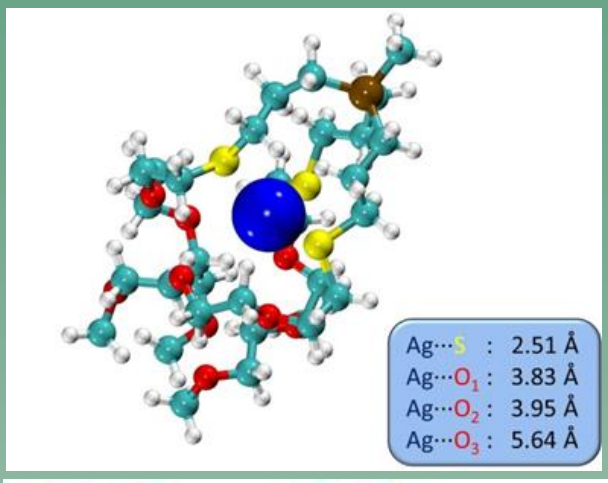
Ag···S : 2.51 Å
Ag···O1 : 3.83 Å
Ag···O2 : 3.95 Å
Ag···O3 : 5.64 Å

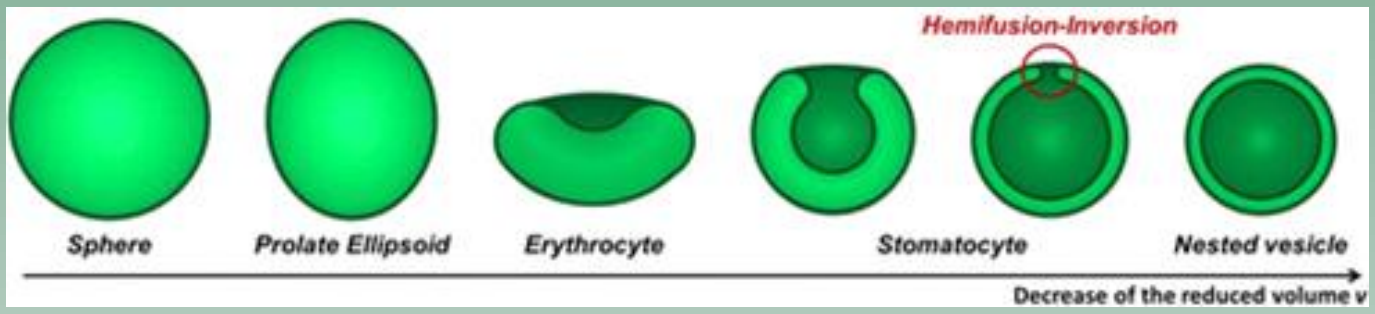
Hemifusion-Inversion
Sphere
Prolate Ellipsoid
Erythrocyte
Stomatocyte
Nested vesicle
Decrease of the reduced volume v

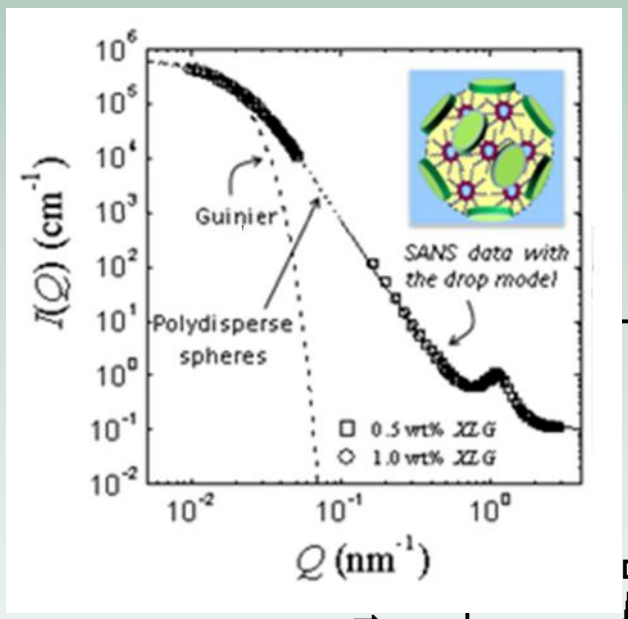
I(Q) (cm-1)
Guinier
Polydisperse spheres
SANS data with the drop model
0.5 wt% XLG
1.0 wt% XLG
Q (nm-1)

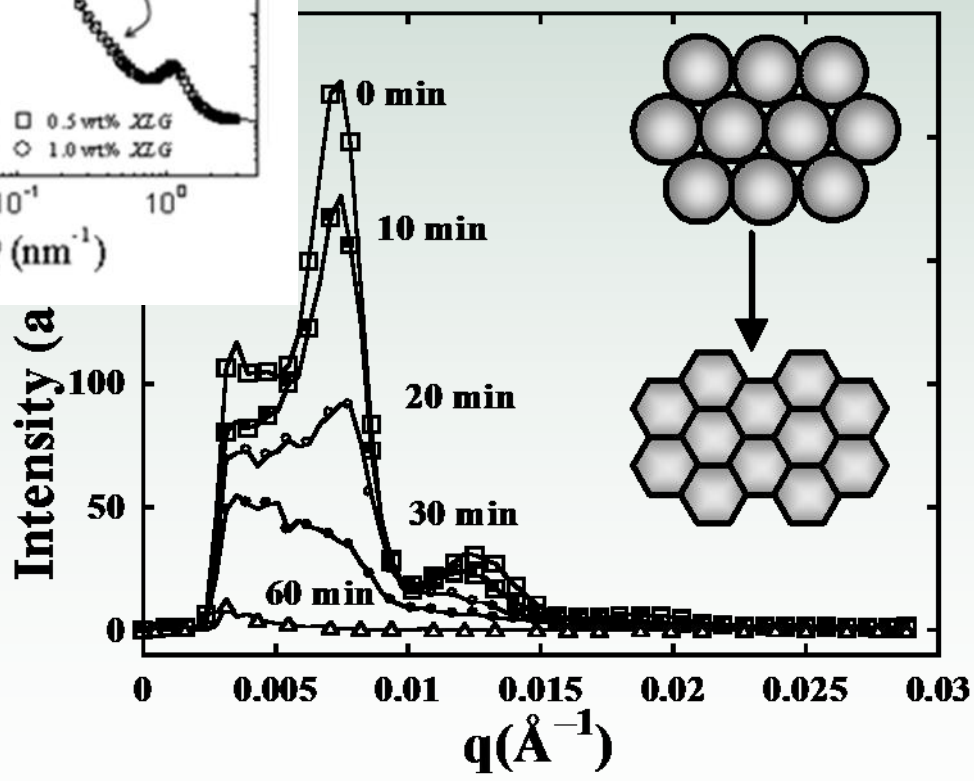
0 min
10 min
20 min
30 min
60 min
Intensity (a
q(Å−1)

AXE 3:

Soft Matter and Biophysics.

The third scientific axis concerns soft matter and biophysics. Flourishing of many new systems, combining different components, many involving nanoscales (1-100 nm) has become a major current trend in soft mater. At LLB, researchers have developed in similar directions keeping some of the historical specificities of the lab.: involving polymers is one of the components illustrating the advantages of neutron scattering, *i.e.* labelling and contrast matching, while we often marry the reciprocal space (SANS but also SAXS) with other techniques, in real space or at macroscopic scales. The following topics are investigated: nanoparticles and hybrid systems; organic systems and self-organization; polymer dynamics; electrostatics complexes. The research at the interface of physics and biology is based on three main topics: 1) Proteins in complex media viewed as model systems for living environments. Experiments are concerned with macro- or supra-molecular scales and their analysis is strongly influenced by our background in polymer physics, statistical physics and phase transition physics; 2) Local dynamics of proteins and hydration water in relation with the dynamical transition of proteins and their enzymatic activity. Neutron scattering techniques, that are very sensitive to protons, are particularly suitable for these studies; 3) Water and its specific properties are fundamentally related to life and to the very peculiar properties of some biological molecules like proteins. Here, water properties are studied in relation with the dynamics of hydrogen bonds network, the notions of hydrophobicity and confinement.

- **Dendronized Polymers with Silver and Mercury Cations Recognition: Complexation Studies and Polyelectrolyte behavior**
  J. Roeser, B. Heinrich, C. Bourgogne, M. Rawiso, S. Michel,V. Hubscher-Bruder, F. Arnaud-Neu, S. Méry

- **The glassy dynamic of confined polymer nanoparticles**
  Y. Rharbi, F. Boué, Q. Nawaz

- **Manipulation of the shape of polymeric vesicles**
  R. Salva, J.-F. Le Meins, O. Sandre, A. Brûlet, M. Schmutz, P. Guenoun, S. Lecommandoux

- **Structure of colloidal thermosensitive systems**
  J.-D. Marty, N. Lauth-de Viguerie, A. Brûlet

- **Impact of sucrose replacement by maltitol on cacao butter crystallisation, texture and fat blooming**
  E. Angelard, C. Brochet, A. David, L. Gehin, E. Gorlin, A. Leboullenger, A. Mourched, C. Alba-Simionesco, D. Bonnet, P. Cayot, D. Champion, F. Cousin, C. Loupiac, F. Porcher, P. Smith

Dendronized Polymers with Silver and Mercury Cations Recognition: Complexation Studies and Polyelectrolyte behavior

J. ROESER[A,B], B. HEINRICH[A], C. BOURGOGNE[A], M. RAWISO[C], S. MICHEL[B], V. HUBSCHER-BRUDER[B], F. ARNAUD-NEU[B], S. MÉRY[A]

a IPCMS, UMR7504, Strasbourg, France

b IPHC, UMR7178, Strasbourg, France

c ICS, UPR022, Strasbourg, France

mery@ipcms.unistra.fr

Aqueous solutions of wormlike dendronized polymers were investigated. Solutions exhibit a lower critical solution temperature (LCST) transition, vanishing in presence of either Ag^+ or Hg^{2+} cations. The change of solubility is due to the specific Ag^+ sequestration and to the formation of complexes with ligand sites in the depth of the polymer shell. SANS proved the concomitant appearance of a polyelectrolyte behavior while preserving the polymer morphology.

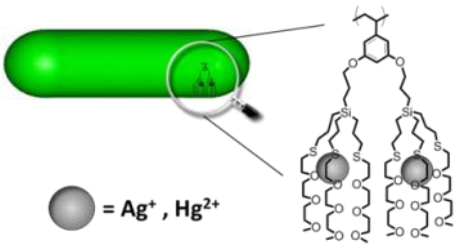

The dendronization of a linear polymer chain by dendrons wedges on each monomer repeat unit leads to a new class of macromolecules, called dendronized polymers (denpol). The interest of such materials arises from their ability to adopt a wormlike morphology and from their large number of peripheral chains accessible to functionalization.

We recently reported the synthesis by post-polymerization functionalization of a series of denpols carrying oligo-(ethyleneoxy) peripheral branches, whose wormlike core-shell structure was established by a combined SAXS-SANS investigation.[1] The hydrophobic-hydrophilic balance between the core and the shell of the denpols makes them thermoresponsive and their water solutions show sharp lower critical solution temperature (LCST) transitions.

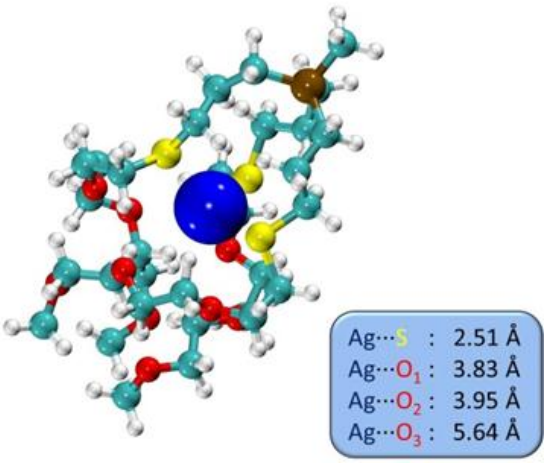

Figure 1: Lower energy conformation for Ag+ interacting with a dendron. In the frame the calculated distances from Ag+ to the sulfur and oxygen atoms of the dendritic chains

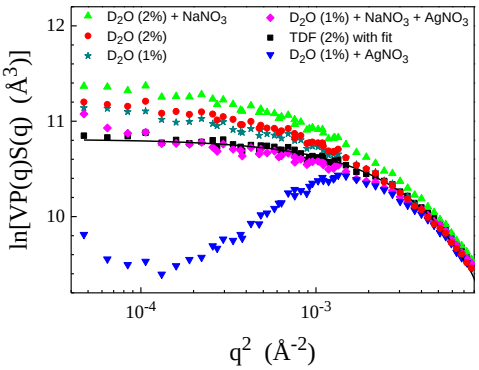

Figure 2 : Scattered intensities normalized to the contrast and particle volume fraction at small scattering vectors determined by SANS for a polymer (DP = 24) solutions in D2O or TDF (1 or 2 wt%), in the presence or not of AgNO3 (1 equiv per monomer repeat unit) and of background salt NaNO3 (50 g.L-1).

The observation of the vanishing of the LCST in the presence of certain cations revealed a recognition process, whose comprehensive investigation is the subject of this new work. Despite the broad screening of cations, recognition was only encountered for Ag^+ and Hg^{2+} and titration experiments confirmed that these cations are extracted from water. Thermodynamic properties, shifts in NMR spectra and molecular modeling confirmed the formation of denpol-cation complexes involving ligand sites within the solvated shell (Fig. 1). The work was then focused on silver-denpol complexes. Any silver charge fraction could be sequestrated by the denpols up to charge fractions of two cations per repeat unit. The neutral denpols should then become polycations, with a possible change of the morphology and the appearance of a

polyelectrolyte behavior. These points were investigated by SANS.

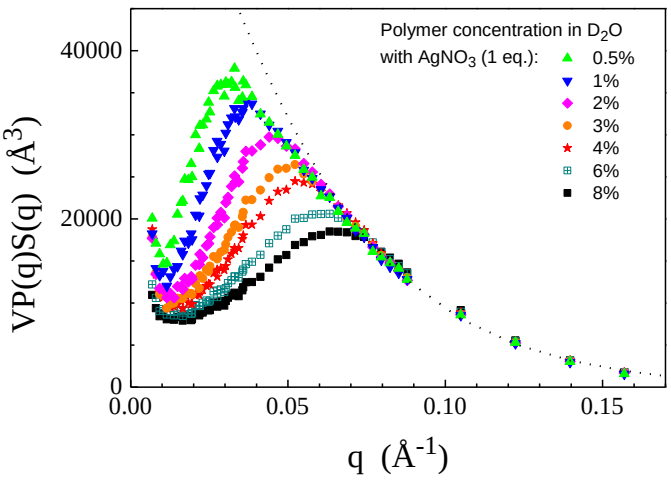

Figure 3 : Scattered intensities normalized to the contrast and the particle volume fraction at small scattering vectors determined by SANS for solutions in D_2O, with 1 equiv of $AgNO_3$ of polymer (DP = 24) at variable concentration of polymer.

In a previous work, [1] the scattering curves of the diluted neutral denpol solutions established average shapes fitting with spherocylinders of roughly 40 Å diameter, whatever the polymer chain length and the solvent. The present work demonstrates that the polymer shape is preserved by the incorporation of the cations, since the SANS curves of neutral and charged denpols solutions overlap in the Porod and intermediate regions. [2] This result confirms the expectations from the neutral denpol architecture, as it is constrained by the dense packing at the core shell interface and therefore excludes substantial swelling or elongation effects. At small scattering vectors, the curves however start deviating from each other, due to the contribution of the different regimes of interactions between polymers (fig. 2).

In the neutral polymer solutions, the scattering curve in D_2O (deuterated water) lies above that in TDF (deuterated tetrahydrofurane), because of the existence of aggregates in aqueous solution even below the LCST. In presence of background salt, a further increase is observed, in consistency with the enhancement of the aggregation process lowering the LCST. To the contrary, the addition of a stoichiometric amount of Ag^+ reduces the scattered intensities at small q values and leads to the appearance of a correlation peak due to the electrostatic repulsions between polymers and to the decrease of the osmotic compressibility. Further addition of background salt restores a scattering curve coinciding with the one in TDF. Indeed, the aggregation process is then prevented by the sequestrated ions, but the ions in solution screen up the repulsive interactions between charged polymers and restore the diluted regime. In the absence of background salt, the correlation peak is logically found all the more pronounced given the sequestrated charge fraction is high. The location of the peak maximum is independent of the charge fraction, but regularly changes with the concentration (fig. 3), as it follows the variation of the average distance between neighboring charged polymers.
To conclude, SANS studies proved without doubt that the high sequestration of Ag^+ by a dendronized polymer with oxathiaether branches transforms this polymer in a novel type of polyelectrolyte with all typical features of polyelectrolytes but with a specific dendronized polymer worm shape. This shape is not significantly modified by the formation of the polyelectrolyte, but the process involves the dissociation of the aggregates and the rapid vanishing of the LCST. Finally, the remarkable chelating properties of the dendritic polymer shell in regard to Ag^+ could be used in the design of materials with potential applications for waste treatment, chemosensors, or antimicrobial and antibacterial surfaces.

References

1. J. Roeser, F. Moingeon, B. Heinrich, P. Masson, F. Arnaud-Neu, M. Rawiso, S. Méry, Macromolecules. 44, 8925-8935, (2011)
2. J. Roeser, B. Heinrich, C. Bourgogne, M. Rawizo, S. Michel, V. Hubscher-Bruder, F. Arnaud-Neu, S. Méry, Macromolecules, 46, 7075-7085 (2013)

The glassy dynamic of confined polymer nanoparticles

Y. RHARBI[A], F. BOUÉ,[B] Q. NAWAZ[A]

a Laboratoire de Rhéologie et procédés, UJF/INPG/CNRS, BP 53, Domaine universitaire 38041, Grenoble, France.

b Laboratoire Léon Brillouin, CEA Saclay, 91191 Gif-sur-Yvette, France.

rharbi@ujf-grenoble.fr

The dynamic of confined polystyrene in nanoparticles was investigated in particles as small as 42 nm. The relaxation time was extracted from the dynamic of closure of voids between close packed particles. The particles deform under the effect of the surface tension energy (polystyrene/air), and the deformation is probed via small angle neutron scattering. Both the shift factor and relaxation time of the confined PS was found to follow a bulk dynamic between bulk T_g and T_g -50°C, for particles as small as 42 nm. This data was interpreted to indicate that cooperativity resulting from the contacts between particles inhibits the eventual activation of the surface dynamic.

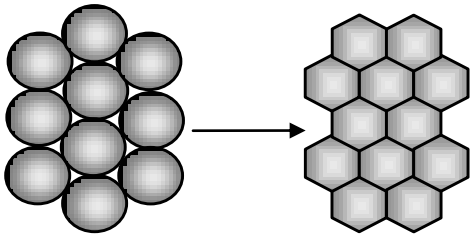

This work aims to investigate the role of the confinement on the polymer dynamic. While most of the confinement studies were dedicated to thin films geometry, only a few were being conducted on the nanoparticles geometry. The nanoparticle geometry has several advantages as it leads to a larger surface area than thin films and an isotropic confinement. We have shown that it is possible to probe directly the relaxation time of polystyrene in nanoparticles using the kinetic of void closure between close-packed particles. In these experiments, we found that when water is evaporated from the particle suspension in the glassy regime, the particles remain spherical and form close-packed structures separated by interstices (voids).

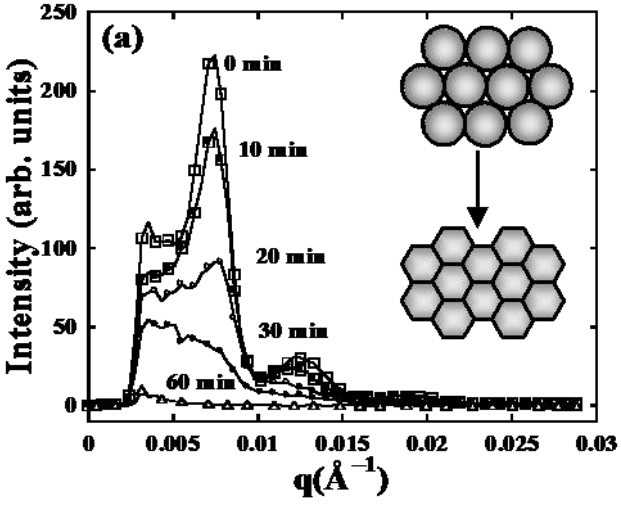

Figure 1 : SANS spectra of 93 nm during annealing at 100 °C (a). Inset: schema of particle deformation and void closure during annealing.

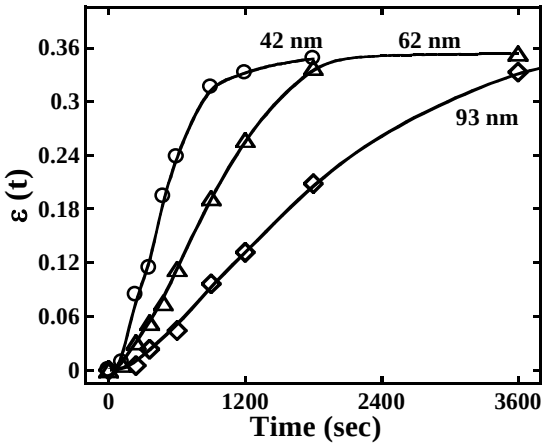

Figure 2 : Deformation strain ε(t) calculated from the intensity peak at 100°C for various particle size polystyrene.

The presence of free surface area within these interstices (Fig. 1) is what gives the confined particularity to the polymer.

The air/polystyrene surface tension

$$\gamma_{P/a}\ (\gamma_{P/a} = 0.03\ N/m^2)$$

in the voids generates negative Laplace pressure

$$P_{lap} = \gamma_{P/a}\, S_{void}/V_{void}$$

(where S_{void} and V_{void} are the surface and volume of the voids) which close the voids and deform the particles. The scattering peaks vanish within a few minutes when the samples are annealed at bulk T_g (Fig. 1) but remain unchanged over 3 years at room temperature.

The scattering intensity reflects the evolution of the void volume ($V_{void}(t)$) as

$$I(t) \propto (V_{void}(t))2 \propto (V_{void}(0))^2 (1-\varepsilon(t)/0.36)^2,$$

where $\varepsilon(t)$ is the deformation rate of the particles

$$\varepsilon(t) = 0.36\times(1-(I(t)/I(0))^{1/2}) \text{ (Fig. 2).}$$

The deformation is creep-like particularly for small $\varepsilon(t)$ values where the stress can be considered constant leading to a linear dependence of $\varepsilon(t)$ on time

$$\varepsilon(t) \propto t/\tau_{void}$$

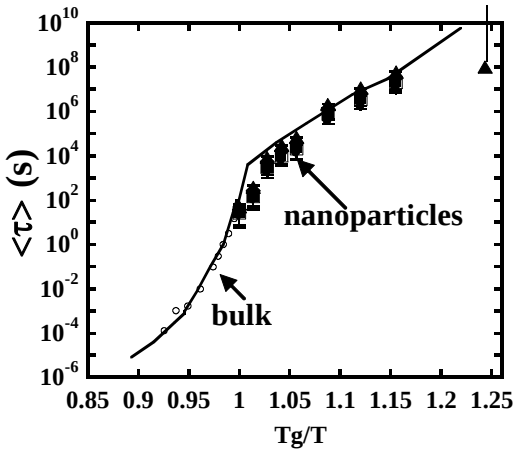

Figure 3: The average relaxation time $<\tau>$ vs. the inverse of temperature during void closure for particle sizes 42 (¨), 62 (■) and 93 nm (▲). The $<\tau>$ for nanoparticles is compared to the $<\tau>$ of bulk PS made from the same particles using the creep compliance (○) and to the bulk $<\tau>$ form the SHG on other PS sample. The temperature is normalized to the bulk T_g. The error bar is estimated is estimated from the various models for calculating $<\tau>$.

(τ_{void} is the characteristic time for void closure). The shift factor and relaxation time of the polymer within the particles can be estimated form model independent method (shift factor) or using Frenckel modified JKR or Russel models for void closure

$$\frac{6.69(1-\nu)\,\gamma_{P/a}}{R} = \int_0^t G(t-t')\,\frac{d\varepsilon^{3/2}}{dt'}dt' \quad .$$

The $<\tau>$ from nanoparticles is found to be similar to the bulk $<\tau>_\alpha$ from the SHG for temperatures between bulk T_g and T_g-50 °C for all the particle sizes between 93 nm and 42 nm.

The $<\tau>$ at room temperature represent an estimate of the lower limit of the relaxation time and is added in Fig. 3 as indication. These results prove beyond a doubt that the dynamic of polystyrene in particles adopts all aspects of the bulk a relaxation in the glassy regime when the particles are in a close packed morphology. These results suggest that the free surface between the particles does not activate the polystyrene dynamic contrary to what is expected. We suggest that the eventual depression of T_g in freestanding particles and the activation of the dynamic could be inhibited *via* dynamical cooperativity between neighboring particles.

References

1. Y. Rharbi, F. Boué & Q. Nawaz, Macromolecules, 2013, 46 ,7812–7817

Manipulation of the shape of polymeric vesicles

R. SALVA[A,B], J.-F. LE MEINS[A], O. SANDRE[A], A. BRÛLET[C], M. SCHMUTZ[D], P. GUENOUN[B], S. LECOMMANDOUX[A]

a Université Bordeaux/IPB

b LIONS, SIS2M, CEA-Saclay, 91191 Gif sur Yvette, France

c Laboratoire Léon Brillouin, CEA-CNRS, CEA-Saclay, 91191 Gif sur Yvette, France

d Institut Charles Sadron, UPR 22 CNRS, Université de Strasbourg

annie.brulet@cea.fr

Vesicles, simple membrane compartments isolating two aqueous media, are proposed as chemical nano-reactors or carriers capable of transporting and delivering to a targeted location molecules of interest, in imitation of biological functions (the study of the exchange between cells via vesicles is the object of the Nobel Prize in Physiology or Medicine, 2013). Consisting of a single membrane vesicle is also a coarse model, but simpler, of a biological cell.

The present study focused on vesicles enclosed by a membrane composed of self-assembled copolymers (polymersomes), whose properties of mechanical resistance and permeability are very high. This research, a collaboration between researchers of CEA-Saclay and the University of Bordeaux-ENSBCP published in ACS Nano, shows that polymersomes made of diblock copolymers can form double-walled vesicles, under the effect of intense constraints sustained during osmotic shock. These effects have been widely explored, because the shape of the vesicles is an essential element of bio-distribution and cellular internalization (endocytosis), for which the polymersomes are excellent candidates today.

The vesicles or liposomes, closed structures separating an aqueous domain equally aqueous continuous phase thanks to a lipid bilayer, represent a basic model of a biological cell. A cell remains however more complex, since the membrane has in fact several types of lipids, many membrane proteins and is connected to an internal cytoskeleton.

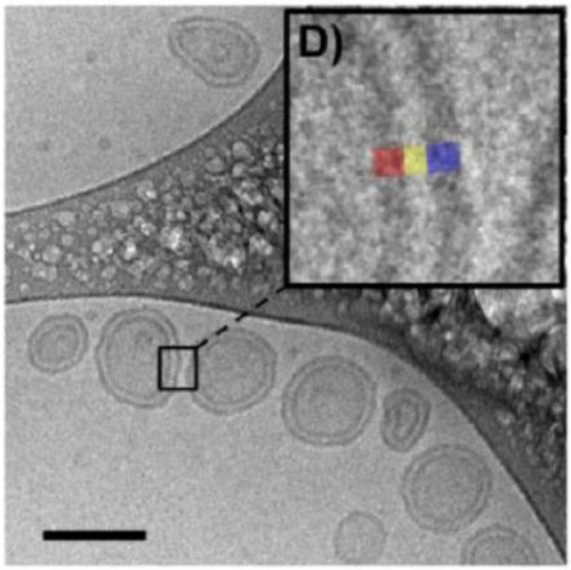

Figure 1 : Double wall vesicles.

However vesicles are also objects that one seeks to control for transporting molecules of interest as drugs and release them in a controlled manner. They can also become nano-reactors where one seeks to replicate the conditions of confinement for chemical reactions. If the lipid bilayers are fragile and difficult to use, vesicles made of a polymer membrane (polymersomes) can be handled more easily and featured of various chemical functions thanks to the richness of the polymers used.

A complication, which may also be a benefit factor is that the vesicles change shape during their transfer from one medium to the other due to the variation of osmotic pressure (due to the concentration of solute). The polymers membranes, although less permeable to water than their counterparts lipid, react to these situations of osmotic imbalance in letting through water (rejection of water in a solution of excess solute, water absorption for internal concentration higher than that of the environment). In the case of a water rejection, which form does a nanoscale polymersome (typically 100 nm in diameter) adopt when it has too much surface relative to the enclosure volume to remain spherical?

The answer depends on the size of the polymersome and the nature of the membrane.

For membranes made of a bilayer of copolymer as with PDMS-g-PEO, hypertonic osmotic disequilibrium allows the vesicle to achieve an original state of nested vesicles resulting in a membrane fusion during the wall folding when the internal volume is reduced. These double-walled vesicles

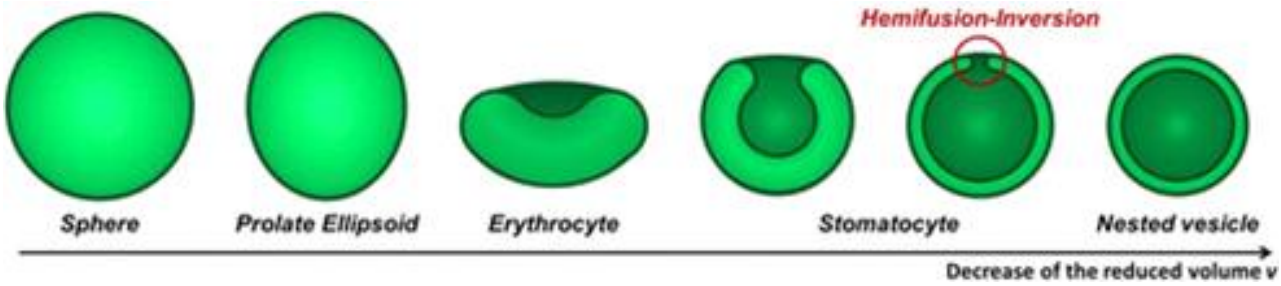

Figure 2 : Scheme of the transformation by an osmotic deflation of an initially spherical vesicle to form a "nested" bi-lamellar vesicle. The form obtained is the function of reducing the volume of the vesicle. The color (light green and dark green) are respectively, the inner and outer faces of the initial vesicle. All forms preserve a symmetry of rotation about the vertical axis.

are highlighted by electron microscopy under low temperature (cryoTEM) but also by neutron scattering. The combination of both techniques can eliminate observation artifacts and achieve a very good statistics on the membrane thickness measurements when changing shape. It is observed that for polymersomes too small (less than 23 nm radius), the complete folding requires too much bending energy and nested vesicles are not formed.

It is also possible to form the polymersomes with triblock polymers and the membrane is then formed as a monolayer like for the PEO-b-PDMS-b-PEO polymer. Then the conformation of the polymer prevents the formation of double-walled vesicles because membrane fusion would require to lose too much conformational entropy (hairpin formation), or interfacial energy.

The discovery of these deformation pathways of polymersomes were obtained through a collaboration between the LIONS IRAMIS/SIS2M, the Laboratoire Léon Brillouin, the LCPO ENSBCP Bordeaux and Charles Sadron Institute in Strasbourg. These results were published in ACS Nano.

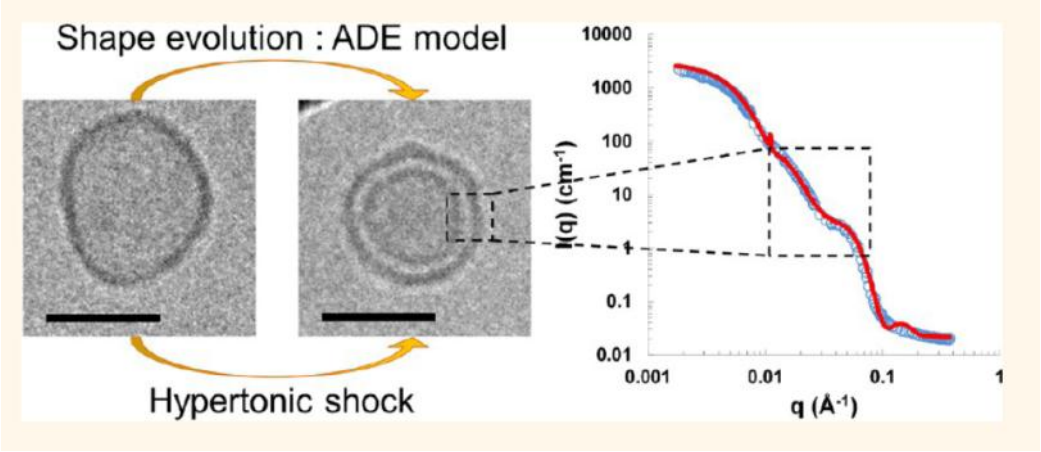

Figure 3 : Left: in a hypertonic osmotic shock polymersome shape evolves towards two nested polymersomes. Right: intensity of neutron scattering at small angles by polymersomes. The waveform bears the signature, at the dotted square, of the formation of nested

References

1. Polymersome shape transformation at the nanoscale, R. Salva, J.-F. Le Meins, O. Sandre, A. Brûlet, M. Schmutz, P. Guenoun & S. Lecommandoux, ACS Nano, 7 (10) (2013) 9298.

Structure of colloidal thermosensitive systems

J.-D. MARTY[A], N. LAUTH-DE VIGUERIE[A], A. BRÛLET[B]

a IMRCP UMR CNRS 5623, Université de Toulouse, France.

b Laboratoire Léon Brillouin, CEA Saclay, France

marty@chimie.ups-tlse.fr

Amphiphilic block polymers, exhibiting a thermosensitive block and various types of architecture (di-block, tri-block,…) or chemical composition have been synthesized. Their aggregation in solution below and over the cloud point was probed using Small Angles Neutrons Scattering. This study shows the influence of macromolecular parameters on the size of the objects formed and on their aggregation kinetics.

The use of controlled polymerization methods in recent years has led to the development of polymers with temperature-sensitive blocks whose architecture can be modulated and controlled and which can self-organize in different aggregates depending on the temperature. These stimulable compounds have many applications, *eg* in nanomedicine and catalysis. We have shown that the catalytic activities (induction time, kinetic constant, activation energy …) of gold nanoparticles stabilized by heat-sensitive polymers are modulated at will by the chemical nature and the architecture of the polymer, in addition to temperature. [1,2,3].

In this study, our aim is, firstly, to characterize by Small Angles Neutron Scattering (SANS) the objects formed in aqueous solution by thermosensitive block-polymers as a function of temperature (Figure 1). Secondly, we will analyze the behavior of these polymers when nanoparticles are present in solution. The different families of copolymers were synthesized at IRMCP by RAFT/MADIX-type controlled radical polymerization

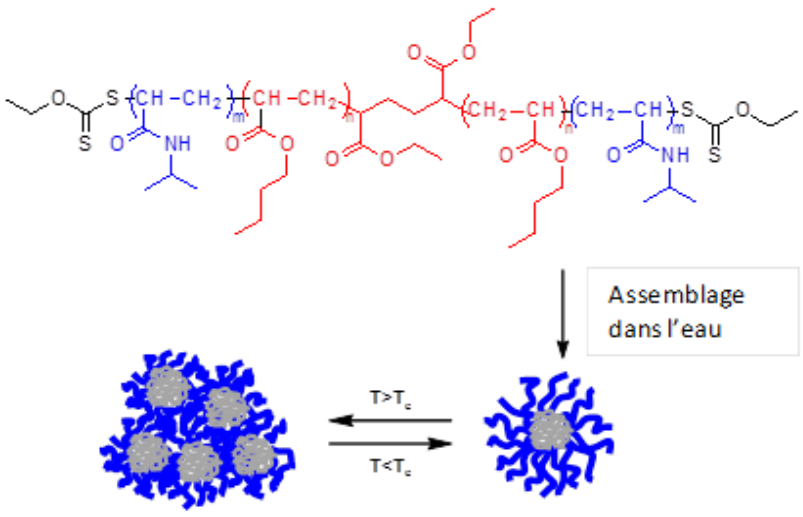

Figure 1:Agrégation of gold particles stabilized by thermosensitive polymers in aqueous solution.

The thermosensitive block is the poly(N-isopropyl acrylamide) (PNIPAM). The hydrophobe block is made from poly(n-butyl acrylate) (PABu). Various polymers with different architecture and chemical content were elaborated on that basis:

- di-block polymers: $PAbu_{2k}$-*b*-$PNIPAM_{8k}$, $PABu_{5k}$-*b*-$PNIPAM_{5k}$ and PBA_{8k}-*b*-$PNIPAM_{2k}$

- tri-block polymers: $PNIPAM_{4k}$-*b*-PBA_{2k}-*b*-$PNIPAM_{4k}$, $PNIPAM_{2.5k}$-*b*-PBA_{5k}-*b*-$PNIPAM_{2.5k}$ and $PNIPAM_{1k}$ -*b*-PBA_{8k}-*b*-$PNIPAM_{1k}$

These polymers were charaterised by size exclusion chromatography which evidenced the di– or tri – block character of these polymers, their molar mass and their dispersivity; NMR spectroscopy confirmed the PABu/PNIPAM composition of these polymers.

These polymers are solved in aqueous solution. Due to their amphiphilic character, they lead to the formation of colloids at 25°C, which are characterized by dynamic light scattering and SANS. In addition, the thermosensitive group of PNIPAM possesses a transition at about 32°C which induces the formation of new aggregates which are also characterized. Consequently, in a previous study (experiment #9820 at LLB), we have demonstrated that the di-block polymers (PABu-*b*-PNIPAM) evolve from a structure made from nm-size spheres at 25°C to one made from spherical aggregates of 35-40 nm size at 40°C, according to the mass of the polymers considered.

In this new set of experiments, the tri-block pol-

ymers considered were characterized. In order to obtain the scattering curves, three Q-ranges (17Å - 5m), (7Å - 3m) et (7Å - 1m) were explored.

The scattering curves obtained from three samples in D_2O with various compositions were recorded at 2 temperatures (20°C and 36°C). The Figure 2 shows an example of such a curve for a thermosensitive solution made from tri-blocks $PNIPAM_{4k}$-*b*-$PABu_{2k}$-*b*-$PNIPAM_{4k}$ at 0.5% concentration and the corresponding fits by a core-polydisperse shell model.

The tri-block polymers have shown aggregation modes at high or low temperature which are more or less similar (in a matter of size or morphology) to those observed for di-blocks polymers: at low temperature, nm-size objects are observed, which aggregate when the temperature rises and form spherical objects with a radius of ~27nm (Figure 2a). However, their aggregation/disaggregation kinetics are significantly different, with slower observed speeds of reaction.

The addition of gold nanoparticles to these solutions leads to a clear modification of the SANS signal. This demonstrates the restructuration of the polymer around the gold nanoparticles. Analyses are currently performed in order to understand better this reorganization and the influence of temperature on it.

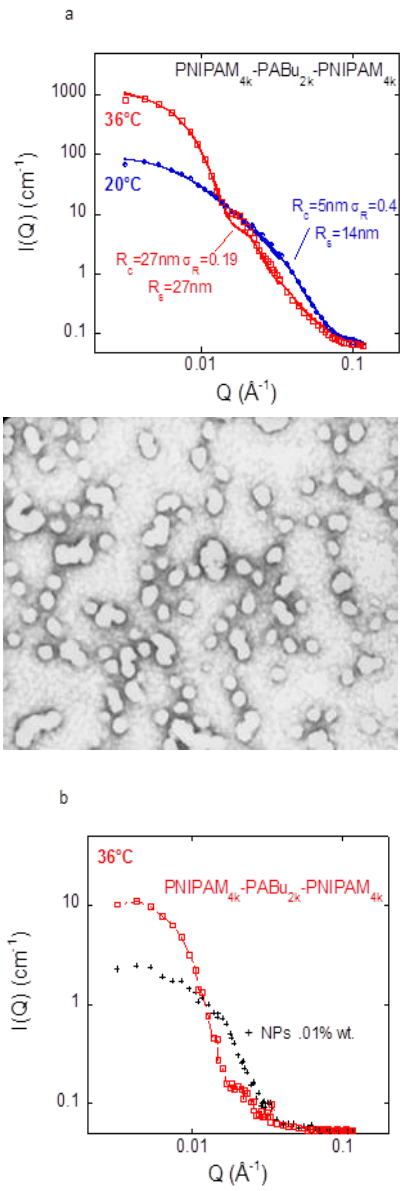

Figure 1 a) Scattering by a thermosensitive solution of tri-block PNIPAM-PABu-PNIPAM polymers and best fit by a core-polydisperse shell model. Corresponding diameter and electron microphotograph at T=36°C. Scattering curves at 36°C showing a modification of the aggregation in the presence of a low concentration of 4-5 nm particles.

References

1. S. Sistach, M. Beija, V. Rahal, A. Brûlet, J. D. Marty, M. Destarac and C. Mingotaud, Chem. Mat. 2010, 22, 3712-3724.

2. S. Sistach, Thèse de l'Université de Toulouse, 2011.

3. M. Beija, J. D. Marty and M. Destarac, Chem. Com. 2011, 47, 2826-2828 .

Impact of sucrose replacement by maltitol on cacao butter crystallisation, texture and fat blooming

E. ANGELARD[A], C. BROCHET[A], A. DAVID[A], L. GEHIN[A], E. GORLIN[A], A. LEBOUILLENGER[A], A. MOURCHED[A], C. ALBA-SIMIONESCO[B], D. BONNET[C], P. CAYOT[A], D. CHAMPION[A], F. COUSIN[B], C. LOUPIAC[A,B], F. PORCHER[B], P. SMITH[C]

a AgroSup Dijon, Dominante Formulation et Qualité des Aliments, Département Sciences des Aliments et Nutrition, 21079 Dijon cedex, France

b Laboratoire Léon Brillouin, CEA Saclay, 91191 Gif-Sur-Yvette cedex, France

c Cargill R&D Centre Europe, Global Food Research, Havenstraat 84, B1800 Vilvoorde, Belgique

camille.loupiac@cea.fr

Crystallization is the critical step in making chocolate and confectioneries. Poorly crystallized chocolate or chocolate stored under wrong conditions suffer the formation of fat bloom, a white film at the chocolate surface. Bloomed chocolate not only looks less appealing, but it also has a less attractive mouthfeel on the palate.

The preliminary work performed at LLB aimed to observe the crystallization behavior of 3 different samples of cacao butter and examine the role of sweeteners in sugar-free chocolate sample.

http://fr.wikipedia.org/wiki/Chocolat

Although cocoa-butter crystallization has been subject to research for many years, no uniform nomenclature for the various phases of cocoa-butter exists. A combination of the greek letters (γ, α, β' and β) and Roman numbering system (I–VI) is used (Wille and Lutton, 1966) to denote the different phases, resulting in a puzzling ensemble with γ, α, β' and two β phases: β (V) and β (VI). Each cocoa-butter phase has its own physical characteristics, such as melting range and relative stability. Chocolate preferably should be crystallized in β (V) or β (VI) phases, but the crystallization of these phases from the melt under static conditions is only possible using the memory effect of cocoa-butter. Under all other conditions, undesirable polymorphs with lower melting temperatures develop. During chocolate manufacturing, the most frequently applied procedure for obtaining stable form β(V) involve a well-defined cycling in temperature of the cocoa paste under shear, which induces the formation of a small proportion (1–3 vol%) of seed crystals. Through this process, the remaining fat solidi-

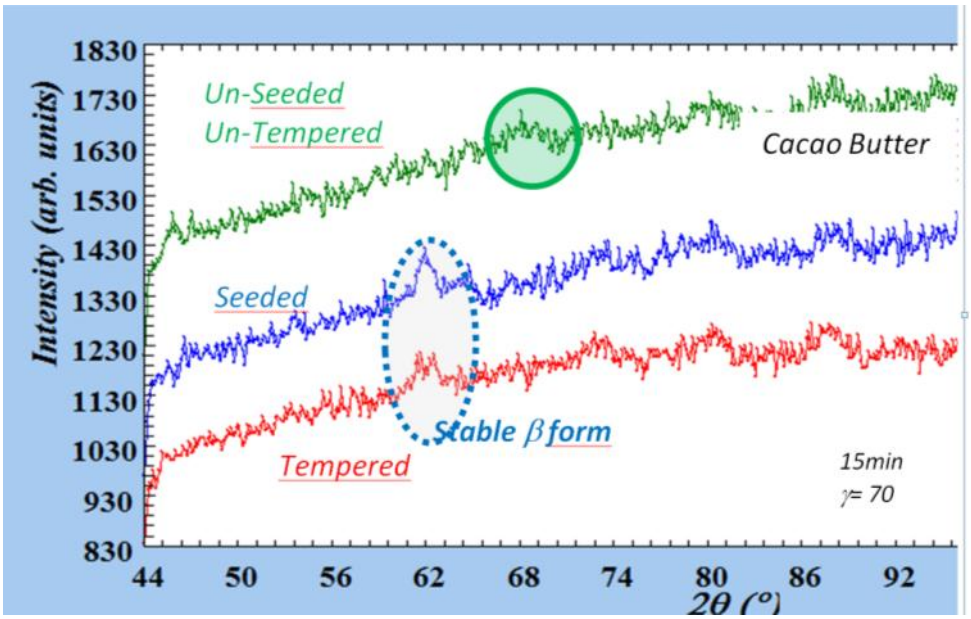

Figure 1 : Neutron diffraction patterns of seeded cacao butter (blue), tempered cacao butter (red) and un-seeded/un-tempered cacao butter (green). The results indicate that the conventional tempering process allows obtaining stable β form. (G6.1 diffractometer, λ= 4.746Å, sample-detector distance = 950cm, 15minutes scans)

fies around the seeds, which induces the correct polymorphic form (Afoakowa et al., 2008). The "conventional tempering" has four key steps: (i) complete melting at 50°C (at least); (ii) cooling to the crystallization point at 32°C; (iii) second crystallization at 27°C; and (iv) melting out unstable polymorphs at 29–31°C.

The first aim of the present work was to observe by neutron diffraction (figure 1), the crystallization behavior of 3 different samples of cacao butter: 1- first sample (called "tempered" in figure 1) corresponds to cacao butter after the "conventional tempering" ; 2- Second sample (seeded) corresponds to cacao butter after the addition of seeds (stable β form); and the third sample (un-seeded/untempered) corresponds to cacao butter obtained without any tempering steps or seeds addition ; In this case, raw cacao butter has just been melted at 60°C and then freeze at 0°C. Figure 1 presents the crystallographic patterns obtained for these 3 samples, and confirmed that the conventional tempering process allows obtaining stable β form.

The second aim of this study concerns sucrose-free chocolates, which have become popular because of their reduced calorific values, non cariogenicity and tolerance for diabetics (Olinger, 1994). As sucrose forms more than 40–50% of solids dispersed in fat, its impact on functional properties (including sweetness, stability, particle size distribution, mouthfeel), and on the rheology of the product is crucial (Jeffery, 1993). We examined the consequences of the replacement of sucrose by sweeteners, in this study, the maltitol. The results obtained by texture analysis are shown in Figure 2. The force to apply to break samples of cacao butter (7N) is smaller than the one to break mixture of sucrose-cacao butter (16N) and both are even smaller than the one to break maltitol-cacao butter mixture (24N) (see Figure 2).

We also followed the crystallization of these different samples (mixture of cacao butter with sugars) by calorimetry and neutron diffraction (G6.1, LLB). Finally, we used neutron reflectivity (EROS, LLB) to study the interface between model triglycerides and the different sugars (sucrose or maltitol).

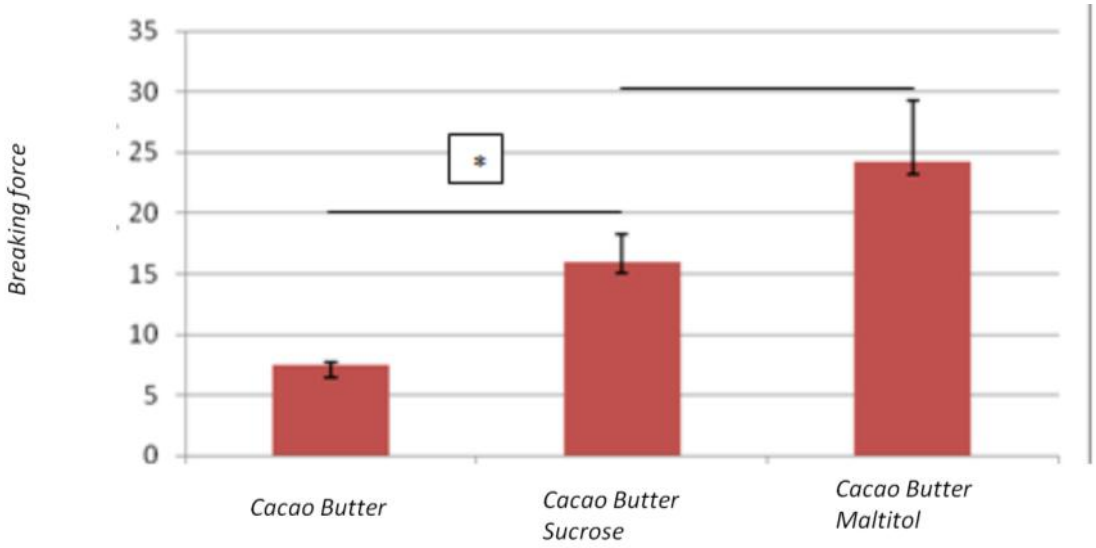

Figure 2 : Impact of sucrose replacement by maltitol on chocolate model texture. The results indicated that maltitol strongly changed the texture of model chocolate

References

1. Afoakowa et al., 2008, Journal of Food Engineering vol 89, 128–136
2. Jeffery M.S.,1993, Food Technology, vol 47(1), 141-144
3. Olinger P., 1994, The Manufacturing Confectioner, vol 74(5), 77-84
4. While RL, Lutton E.S., 1966, Journal of the American oil chemist's society, vol 43 (8), 491-

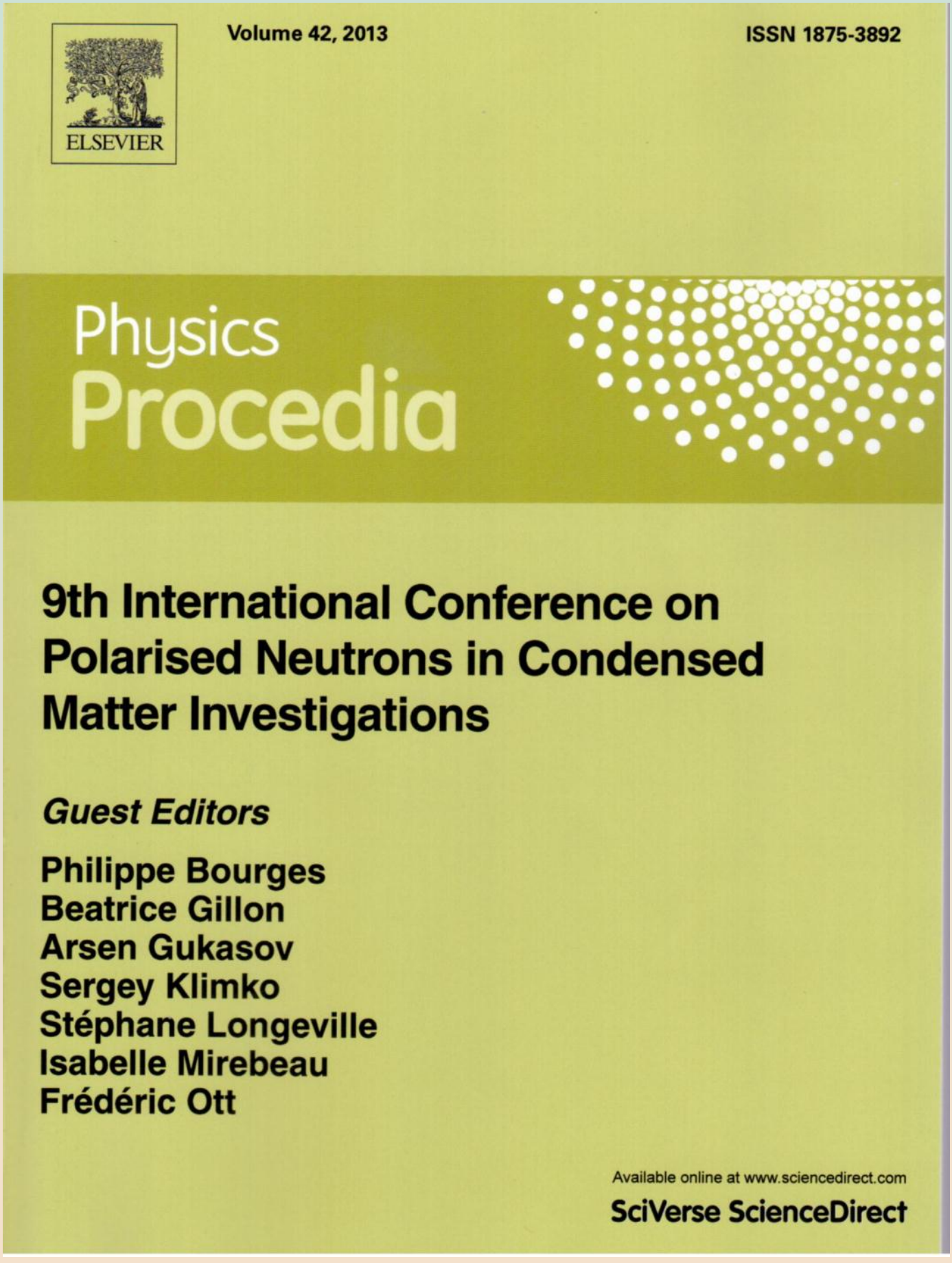
ELSEVIER
Volume 42, 2013
ISSN 1875-3892
Physics
Procedia
9th International Conference on
Polarised Neutrons in Condensed
Matter Investigations
Guest Editors
Philippe Bourges
Beatrice Gillon
Arsen Gukasov
Sergey Klimko
Stéphane Longeville
Isabelle Mirebeau
Frédéric Ott
Available online at www.sciencedirect.com
SciVerse ScienceDirect

PUBLICATIONS
2013

1. K. Ait Atmane, F. Zighem, Y. Soumare, M. Ibrahim, R. Boubekri, T. Maurer, J. Margueritat, J.-Y. Piquemal, F. Ott, G. Chaboussant, F. Schoenstein, N. Jouini and G. Viau, 'High temperature structural and magnetic properties of cobalt nanorods', Journal of Solid State Chemistry 197 (2013), 297-303.
2. M. Allix, S. Chenu, E. Veron, T. Poumeyrol, E. A. Kouadri-Boudjelthia, S. Alahrache, F. Porcher, D. Massiot and F. Fayon, 'Considerable Improvement of Long-Persistent Luminescence in Germanium and Tin Substituted $ZnGa_2O_4$', Chemistry of Materials 25 (2013), 1600-6.
3. D. L. Anastassopoulos, N. Spiliopoulos, A. A. Vradis, C. Toprakcioglu, A. Menelle and F. Cousin, 'Neutron Reflectivity Study of End-Adsorbed Bimodal Polymer Systems under Static Conditions and Shear Flow', Macromolecules 46 (2013), 6972-80.
4. M. Anoufa, J. M. Kiat, I. Kornev and C. Bogicevic, 'Energy harvesting in core-shell ferroelectric ceramics: Theoretical approach and practical conclusions', Journal of Applied Physics 113 (2013).
5. M. Anoufa, J. M. Kiat, I. Kornev and C. Bogicevic, 'Vortices of polarization in $BaTiO_3$ core-shell nanoceramics: Calculations based on ab initio derived Hamiltonian versus Landau theory', Physical Review B 88 (2013).
6. P. A. Artola, A. Raihane, C. Crauste-Thibierge, D. Merlet, M. Emo, C. Alba-Simionesco and B. Rousseau, 'Limit of Miscibility and Nanophase Separation in Associated Mixtures', Journal of Physical Chemistry B 117 (2013), 9718-27.
7. K. A. Atmane, F. Zighem, Y. Soumare, M. Ibrahim, R. Boubekri, T. Maurer, J. Margueritat, J. Y. Piquemal, F. Ott, G. Chaboussant, F. Schoenstein, N. Jouini and G. Viau, 'High temperature structural and magnetic properties of cobalt nanorods', Journal of Solid State Chemistry 197 (2013), 297-303.
8. N. Baccile, J. S. Pedersen, G. Pehau-Arnaudet and I. N. A. Van Bogaert, 'Surface charge of acidic sophorolipid micelles: effect of base and time', Soft Matter 9 (2013), 4911-22.
9. Z. Bakaeva, P. Cernoch, P. Stepanek, F. Nallet and L. Noirez, 'Critical behavior of nanoparticle-containing binary liquid mixtures', Physical Chemistry Chemical Physics 15 (2013), 5831-5.
10. F. Balima, V. Pischedda, S. Le Floch, A. Brulet, P. Lindner, L. Duclaux and A. San-Miguel, 'An in situ small angle neutron scattering study of expanded graphite under a uniaxial stress', Carbon 57 (2013), 460-9.
11. G. Barbera, G. Barone, V. Crupi, F. Longo, G. Maisano, D. Majolino, P. Mazzoleni, J. Teixeira and V. Venuti, 'Small angle neutron scattering study of ancient pottery from Syracuse (Sicily, Southern Italy)', Journal of Archaeological Science 40 (2013), 983-91.
12. P. Baroni, P. Bouchet and L. Noirez, 'Highlighting a Cooling Regime in Liquids under Submillimeter Flows', Journal of Physical Chemistry Letters 4 (2013), 2026-9.
13. N. Barrier, O. I. Lebedev, M. M. Seikh, F. Porcher and B. Raveau, 'Impact of Mn^{3+} upon Structure and Magnetism of the Perovskite Derivative $Pb_{2-x}Ba_xFeMnO_5$ (x similar to 0.7)', Inorganic Chemistry 52 (2013), 6073-82.
14. M. Bastos, N. Alves, S. Maia, P. Gomes, A. Inaba, Y. Miyazaki and J. M. Zanotti, 'Hydration water and peptide dynamics - two sides of a coin. A neutron scattering and adiabatic calorimetry study at low hydration and cryogenic temperatures', Physical Chemistry Chemical Physics 15 (2013), 16693-703.
15. A. M. Bataille, V. Auvray, C. Gatel and A. Gukasov, 'Contrast enhancement of data measured with area detectors: a way to generalize the use of neutron diffraction for thin-film studies', Journal of Applied Crystallography 46 (2013), 726-35.
16. C. Blouzon, F. Ott, L. Tortech, D. Fichou and J. B. Moussy, 'Anti-ferromagnetic coupling in hybrid magnetic tunnel junctions mediated by monomolecular layers of alpha-sexithiophene', Applied Physics Letters 103 (2013).
17. P. Bonville, S. Petit, I. Mirebeau, J. Robert, E. Lhotel and C. Paulsen, 'Magnetization process in $Er_2Ti_2O_7$ at very low temperature', Journal of Physics-Condensed Matter 25 (2013).
18. I. Boucenna, M. A. Guedeau-Boudeville, A. Lapp, P. Colinart, A. Proag, L. Royon and A. Mourchid, 'Temperature directed-assembly of coated-laponite nanoparticles in pluronic micellar solutions', Soft Matter 9 (2013), 170-6.
19. X. Boulnat, D. Fabregue, M. Perez, M. H. Mathon and Y. Decarlan, 'High-Temperature Tensile Properties of Nano-Oxide Dispersion Strengthened Ferritic Steels Produced by Mechanical Alloying and Spark Plasma Sintering', Metallurgical and Materials Transactions a-Physical Metallurgy and Materials Science 44A (2013), 2461-5.
20. L. E. Bove, S. Klotz, T. Strassle, M. Koza, J. Teixeira and A. M. Saitta, 'Translational and Rotational Diffusion in Water in the Gigapascal Range', Physical Review Letters 111 (2013).
21. A. R. Bras, C. H. Hovelmann, W. Antonius, J. Teixeira, A. Radulescu, J. Allgaier, W. Pyckhout-Hintzen, A. Wischnewski and D. Richter, 'Molecular Approach to Supramolecular Polymer Assembly by Small Angle Neutron Scattering', Macromolecules 46 (2013), 9446-54.
22. N. Brodie-Linder, J. Deschamps, F. Audonnet and C. Alba-Simionesco, 'Method to create a hydrophilic environment within hydrophobic nanostructures', Microporous and Mesoporous Materials 179 (2013), 17-21.
23. N. Brouette, G. Fragneto, F. Cousin, M. Moulin, M. Haertlein and M. Sferrazza, 'A neutron reflection study of adsorbed deuterated myoglobin layers on hydrophobic surfaces', Journal of Colloid and Interface Science 390 (2013), 114-20.
24. C. V. Cerclier, A. Guyomard-Lack, F. Cousin, B. Jean, E. Bonnin, B. Cathala and C. Moreau, 'Xyloglucan-Cellulose Nanocrystal Multilayered Films: Effect of Film Architecture on Enzymatic Hydrolysis', Biomacromolecules 14 (2013), 3599-609.
25. A. Chenneviere, E. Drockenmuller, D. Damiron, F. Cousin, F. Boue, F. Restagno and L. Leger, 'Quantitative Analysis of Interdigitation Kinetics be-

tween a Polymer Melt and a Polymer Brush', Macromolecules 46 (2013), 6955-62.
26. J. P. Coulomb, N. Floquet, C. Martin and G. Andre, 'Structural and dynamics properties of methane confined phase in $AlPO_4$-5 model aluminophosphate: An illustrative example of quasi-(1D) phase transition', Microporous and Mesoporous Materials 171 (2013), 82-6.
27. V. Crupi, A. Fontana, M. Giarola, G. Guella, D. Majolino, I. Mancini, G. Mariotto, A. Paciaroni, B. Rossi and V. Venuti, 'Cyclodextrin-Complexation Effects on the Low-Frequency Vibrational Dynamics of Ibuprofen by Combined Inelastic Light and Neutron Scattering Experiments', Journal of Physical Chemistry B 117 (2013), 3917-26.
28. V. Crupi, G. Guella, S. Longeville, D. Majolino, I. Mancini, A. Paciaroni, B. Rossi and V. Venuti, 'Influence of Chirality on Vibrational and Relaxational Properties of (S)- and (R,S)-Ibuprofen/methyl-beta-cyclodextrin Inclusion Complexes: An INS and QENS Study', Journal of Physical Chemistry B 117 (2013), 11466-72.
29. F. Damay, S. Petit, M. Braendlein, S. Rols, J. Ollivier, C. Martin and A. Maignan, 'Spin dynamics in the unconventional multiferroic $AgCrS_2$', Physical Review B 87 (2013).
30. J. del Barrio, P. N. Horton, D. Lairez, G. O. Lloyd, C. Toprakcioglu and O. A. Scherman, 'Photocontrol over Cucurbit 8 uril Complexes: Stoichiometry and Supramolecular Polymers', Journal of the American Chemical Society 135 (2013), 11760-3.
31. V. Delhorbe, C. Cailleteau, L. Chikh, A. Guillermo, G. Gebel, A. Morin and O. Fichet, 'Influence of the membrane treatment on structure and properties of sulfonated poly(etheretherketone) semi-interpenetrating polymer network', Journal of Membrane Science 427 (2013), 283-92.
32. G. Deng, N. Tsyrulin, P. Bourges, D. Lamago, H. Ronnow, M. Kenzelmann, S. Danilkin, E. Pomjakushina and K. Conder, 'Spin-gap evolution upon Ca doping in the spin-ladder series $Sr_{14-x}Ca_xCu_{24}O_{41}$ studied by inelastic neutron scattering', Physical Review B 88 (2013).
33. D. Deribew, E. Pavlopoulou, G. Fleury, C. Nicolet, C. Renaud, S. J. Mougnier, L. Vignau, E. Cloutet, C. Brochon, F. Cousin, G. Portale, M. Geoghegan and G. Hadziioannou, 'Crystallization-Driven Enhancement in Photovoltaic Performance through Block Copolymer Incorporation into P3HT:PCBM Blends', Macromolecules 46 (2013), 3015-24.
34. S. Desert, T. Panzner and P. Permingeat, 'Focusing neutrons with a combination of parabolic and elliptical supermirrors', Journal of Applied Crystallography 46 (2013), 35-42.
35. S. Devineau, J. M. Zanotti, C. Loupiac, L. Zargarian, F. Neiers, S. Pin and J. P. Renault, 'Myoglobin on Silica: A Case Study of the Impact of Adsorption on Protein Structure and Dynamics', Langmuir 29 (2013), 13465-72.
36. M. Djemel, M. Abdelhedi, M. Dammak and A. W. Kolsi, 'Phase transitions and vibrational study of $(Cs_{3.5}Rb_{0.5})[(Se_{0.85}S_{0.15})O_3]_2[Te(OH)_6]_3$ material', Journal of Molecular Structure 1033 (2013), 84-90.
37. C. Drappier, H. Oliveira, O. Sandre, E. Ibarboure, S. Combet, E. Garanger and S. Lecommandoux, 'Self-assembled core-shell micelles from peptide-b-polymer molecular chimeras towards structure-activity relationships', Faraday Discussions 166 (2013), 83-100.
38. Y. Drees, D. Lamago, A. Piovano and A. C. Komarek, 'Hour-glass magnetic spectrum in a stripeless insulating transition metal oxide', Nature Communications 4 (2013).
39. C. Echevarria-Bonet, D. P. Rojas, J. I. Espeso, J. R. Fernandez, L. R. Fernandez, P. Gorria, J. A. Blanco, M. L. Fdez-Gubieda, E. Bauer, G. Andre and L. F. Barquin, 'Size-induced superantiferromagnetism with reentrant spin-glass behavior in metallic nanoparticles of $TbCu_2$', Physical Review B 87 (2013).
40. G. Eickerling, C. Hauf, E. W. Scheidt, L. Reichardt, C. Schneider, A. Munoz, S. Lopez-Moreno, A. H. Romero, F. Porcher, G. Andre, R. Pottgen and W. Scherer, 'On the Control Parameters of the Quasi-One Dimensional Superconductivity in Sc_3CoC_4', Zeitschrift Fur Anorganische Und Allgemeine Chemie 639 (2013), 1985-95.
41. P. Escale, W. Van Camp, F. Du Prez, L. Rubatat, L. Billon and M. Save, 'Highly structured pH-responsive honeycomb films by a combination of a breath figure process and in situ thermolysis of a polystyrene-block-poly(ethoxy ethyl acrylate) precursor', Polymer Chemistry 4 (2013), 4710-7.
42. W. Essafi, A. Abdelli, G. Bouajila and F. Boue, 'Behavior of Hydrophobic Polyelectrolyte Solution in Mixed Aqueous/Organic Solvents Revealed by Neutron Scattering and Viscosimetry (vol 116, pg 13525, 2012)', Journal of Physical Chemistry B 117 (2013), 731-.
43. G. C. Fadda, D. Lairez, Z. Guennouni and A. Koutsioubas, 'Peptide Pores in Lipid Bilayers: Voltage Facilitation Pleads for a Revised Model', Physical Review Letters 111 (2013).
44. A. L. Fameau, S. Lam and O. D. Velev, 'Multi-stimuli responsive foams combining particles and self-assembling fatty acids', Chemical Science 4 (2013), 3874-81.
45. A. L. Fameau, C. Gaillard, D. Marion and B. Bakan, 'Interfacial properties of functionalized assemblies of hydroxy-fatty acid salts isolated from fruit tomato peels', Green Chemistry 15 (2013), 341-6.
46. P. Foury-Leylekian, S. Petit, I. Mirebeau, G. Andre, M. de Souza, M. Lang, E. Ressouche, A. Moradpour and J. P. Pouget, 'Low-temperature structural effects in the $(TMTSF)_2PF_6$ and AsF_6 Bechgaard salts', Physical Review B 88 (2013).
47. B. Frka-Petesic, E. Dubois, L. Almasy, V. Dupuis, F. Cousin and R. Perzynski, 'Structural probing of clusters and gels of self-aggregated magnetic nanoparticles', Magnetohydrodynamics 49 (2013), 328-38.
48. A. Gauzzi, G. Rousse, F. Mezzadri, G. L. Calestani, G. Andre, F. Bouree, M. Calicchio, E. Gilioli, R. Cabassi, F. Bolzoni, A. Prodi, P. Bordet and M. Marezio, 'Magnetoelectric coupling driven by inverse magnetostriction in multiferroic $BiMn_3Mn_4O_{12}$', Jour-

nal of Applied Physics 113 (2013).
49. G. Gebel, 'Structure of Membranes for Fuel Cells: SANS and SAXS Analyses of Sulfonated PEEK Membranes and Solutions', Macromolecules 46 (2013), 6057-66.
50. I. V. Golosovsky, N. V. Golubko, A. V. Mosunov, E. D. Politova, V. V. Murasheva, E. A. Fortalnova, V. S. Rusakov, G. Andre and F. Porcher, 'Crystal structure and phase transition in the doped super-ionic conductor bismuth vanadate $Bi_4(V,Fe)_2O_{11}$ revealed by neutron diffraction', Physica Status Solidi B-Basic Solid State Physics 250 (2013), 1345-51.
51. S. Guitteny, J. Robert, P. Bonville, J. Ollivier, C. Decorse, P. Steffens, M. Boehm, H. Mutka, I. Mirebeau and S. Petit, 'Anisotropic Propagating Excitations and Quadrupolar Effects in $Tb_2Ti_2O_7$', Physical Review Letters 111 (2013).
52. S. Guitteny, S. Petit, E. Lhotel, J. Robert, P. Bonville, A. Forget and I. Mirebeau, 'Palmer-Chalker correlations in the XY pyrochlore antiferromagnet $Er_2Sn_2O_7$', Physical Review B 88 (2013).
53. A. R. A. Hamid, R. Lefort, Y. Lechaux, A. Moreac, A. Ghoufi, C. Alba-Simionesco and D. Morineau, 'Solvation Effects on Self-Association and Segregation Processes in tert-Butanol-Aprotic Solvent Binary Mixtures', Journal of Physical Chemistry B 117 (2013), 10221-30.
54. B. Hammouda, D. F. R. Mildner, A. Brulet and S. Desert, 'Insight into neutron focusing: the out-of-focus condition', Journal of Applied Crystallography 46 (2013), 1361-71.
55. V. Hardy, C. Martin, F. Damay and G. Andre, 'Magnetic couplings in the quasi-2D triangular Heisenberg antiferromagnets α-ACr_2O_4 (A=Ca, Sr, Ba)', Journal of Magnetism and Magnetic Materials 330 (2013), 111-8.
56. I. Harsanyi, L. Pusztai, P. Jovari and B. Beuneu, 'Acidic properties of aqueous phosphoric acid solutions: a microscopic view', Journal of Physics-Condensed Matter 25 (2013).
57. M. C. Hatnean, L. Pinsard-Gaudart, M. T. Fernandez-Diaz, S. Petit, A. Dixit, G. Lawes and R. Suryanarayanan, 'Structural and magnetic properties of the $M_2Ga_2Fe_2O_9$ (M=In, Sc) oxides', Journal of Solid State Chemistry 200 (2013), 110-6.
58. B. Hehlen, A. Al-Zein, C. Bogicevic, P. Gemeiner and J. M. Kiat, 'Soft-mode dynamics in micrograin and nanograin ceramics of strontium titanate observed by hyper-Raman scattering', Physical Review B 87 (2013).
59. M. Hervieu, F. Damay, M. Poienar, E. Elkaim, J. Rouquette, A. M. Abakumov, G. Van Tendeloo, A. Maignan and C. Martin, 'Nanostructures in $LuFe_2O_{4+\delta}$', Solid State Sciences 23 (2013), 26-34.
60. S. Hocine, D. Cui, M. N. Rager, A. Di Cicco, J. M. Liu, J. Wdzieczak-Bakala, A. Brulet and M. H. Li, 'Polymersomes with PEG Corona: Structural Changes and Controlled Release Induced by Temperature Variation', Langmuir 29 (2013), 1356-69.
61. D. S. Inosov, G. Friemel, J. T. Park, A. C. Walters, Y. Texier, Y. Laplace, J. Bobroff, V. Hinkov, D. L. Sun, Y. Liu, R. Khasanov, K. Sedlak, P. Bourges, Y. Sidis, A. Ivanov, C. T. Lin, T. Keller and B. Keimer, 'Possible realization of an antiferromagnetic Griffiths phase in $Ba(Fe_{1-x}Mn_x)_2As_2$', Physical Review B 87 (2013).
62. M. Jaouen, P. Chartier, T. Cabioc'h, V. Mauchamp, G. Andre and M. Viret, 'Invar Like Behavior of the Cr_2AlC MAX Phase at Low Temperature', Journal of the American Ceramic Society 96 (2013), 3872-6.
63. P. Judeinstein, S. Huet and P. Lesot, 'Multiscale NMR investigation of mesogenic ionic-liquid electrolytes with strong anisotropic orientational and diffusional behaviour', Rsc Advances 3 (2013), 16604-11.
64. I. Kaban, P. Jovari, V. Kokotin, O. Shuleshova, B. Beuneu, K. Saksl, N. Mattern, J. Eckert and A. L. Greer, 'Local atomic arrangements and their topology in Ni-Zr and Cu-Zr glassy and crystalline alloys', Acta Materialia 61 (2013), 2509-20.
65. P. Kahl, P. Baroni and L. Noirez, 'Hidden solidlike properties in the isotropic phase of the 8CB liquid crystal', Physical Review E 88 (2013).
66. I. A. Kaurova, G. M. Kuzmicheva, V. B. Rybakov, A. Cousson, O. Zaharko and E. N. Domoroshchina, 'Growth and Neutron Diffraction Investigation of $Ca_3NbGa_3Si_2O_{14}$ and $La_3Ga_{5.5}Nb_{0.5}O_{14}$ Crystals', Journal of Materials 2013 (2013), 6.
67. M. Kempa, P. Ondrejkovic, P. Bourges, J. Ollivier, S. Rols, J. Kulda, S. Margueron and J. Hlinka, 'The temperature dependence of the phononic band gap of NaI', Journal of Physics-Condensed Matter 25 (2013).
68. A. Y. Khereddine, F. H. Larbi, H. Azzeddine, T. Baudin, F. Brisset, A. L. Helbert, M. H. Mathon, M. Kawasaki, D. Bradai and T. G. Langdon, 'Microstructures and textures of a Cu-Ni-Si alloy processed by high-pressure torsion', Journal of Alloys and Compounds 574 (2013), 361-7.
69. J. M. Kiat, C. Bogicevic, P. Gemeiner, A. Al-Zein, F. Karolak, N. Guiblin, F. Porcher, B. Hehlen, L. Yedra, S. Estrade, F. Peiro and R. Haumont, 'Structural investigation of strontium titanate nanoparticles and the core-shell model', Physical Review B 87 (2013).
70. W. Kittler, V. Fritsch, F. Weber, G. Fischer, D. Lamago, G. Andre and H. von Lohneysen, 'Suppression of ferromagnetism of $CeTiGe_3$ by V substitution', Physical Review B 88 (2013).
71. R. Knoll, A. Shames, S. D. Goren, H. Shaked, S. Cordier, C. Perrin, O. Hernandez, T. Roisnel, G. Andre, R. K. Kremer and A. Simon, 'Antiferromagnetic Ordering of Magnetic Clusters Units in Nb_6F_{15}', Applied Magnetic Resonance 44 (2013), 143-51.
72. S. V. Kozhevnikov, V. K. Ignatovich, F. Ott, A. Ruhm and J. Major, 'Experimental Determination of the Neutron Channeling Length in a Planar Waveguide', Journal of Experimental and Theoretical Physics 117 (2013), 636-40.
73. X. J. Kuang, F. J. Pan, J. Cao, C. L. Liang, M. R. Suchomel, F. Porcher and M. Allix, 'Defect Structure, Phase Separation, and Electrical Properties of Non-stoichiometric Tetragonal Tungsten Bronze $Ba_{0.5-x}TaO_{3-x}$', Inorganic Chemistry 52 (2013), 13244-52.
74. D. Langevin, Q. T. Nguyen, S. Marais, S. Karademir, J.-Y. Sanchez, C. Iojoiu, M. Martinez, R. Mercier, P. Judeinstein and C. Chappey, 'High-Temperature Ionic-

Conducting Material: Advanced Structure and Improved Performance', The Journal of Physical Chemistry C 117 (2013), 15552-61.
75. D. Le Strat, F. Dalmas, S. Randriamahefa, J. Jestin and V. Wintgens, 'Mechanical reinforcement in model elastomer nanocomposites with tuned microstructure and interactions', Polymer 54 (2013), 1466-79.
76. C. Lefevre, F. Roulland, A. Thomasson, C. Meny, F. Porcher, G. Andre and N. Viart, 'Magnetic and Polar Properties' Optimization in the Magnetoelectric $Ga_{2-x}Fe_xO_3$ Compounds', Journal of Physical Chemistry C 117 (2013), 14832-9.
77. V. Legrand, W. Kockelmann, C. D. Frost, R. Hauser and D. Kaczorowski, 'Neutron diffraction study of the non-Fermi liquid compound $CeNiGa_2$: magnetic behaviour as a function of pressure and temperature', Journal of Physics-Condensed Matter 25 (2013), 7.
78. A. Lerbret, A. Hedoux, B. Annighofer and M. C. Bellissent-Funel, 'Influence of pressure on the low-frequency vibrational modes of lysozyme and water: A complementary inelastic neutron scattering and molecular dynamics simulation study', Proteins-Structure Function and Bioinformatics 81 (2013), 326-40.
79. M. A. Leroy, A. M. Bataille, F. Bertran, P. Le Fevre, A. Taleb-Ibrahimi and S. Andrieu, 'Electronic structure of the Cr(001) surface and Cr/MgO interface', Physical Review B 88 (2013).
80. O. L. Makarova, J. Bourgeois, M. Poienar, I. Mirebeau, S. E. Kichanov, G. Andre, E. Elkaim, M. Hanfland, M. Hervieu, A. Maignan, J. Haines, J. Rouquette, C. Martin and F. Damay, 'Pressure effect on the magnetic order of $LuFe_2O_4$', Applied Physics Letters 103 (2013).
81. H. Maluszynska, Z. Tylczynski and A. Cousson, 'Ferroelastoelectric ordering in $(NH_4)_2CuBr_4.2H_2O$ single crystal', Crystengcomm 15 (2013), 7498-504.
82. V. Maneeratana, J. D. Bass, T. Azais, A. Patissier, K. Valle, M. Marechal, G. Gebel, C. Laberty-Robert and C. Sanchez, 'Fractal Inorganic-Organic Interfaces in Hybrid Membranes for Efficient Proton Transport', Advanced Functional Materials 23 (2013), 2872-80.
83. C. Mariette, L. Guerin, P. Rabiller, C. Ecolivet, P. Garcia-Orduna, P. Bourges, A. Bosak, D. de Sanctis, M. D. Hollingsworth, T. Janssen and B. Toudic, 'Critical phenomena in higher dimensional spaces: The hexagonal-to-orthorhombic phase transition in aperiodic n-nonadecane/urea', Physical Review B 87 (2013).
84. V. Marry, E. Dubois, N. Maikova, J. Breu and W. Haussler, 'Anisotropy of Water Dynamics in Clays: Insights from Molecular Simulations for Experimental QENS Analysis', Journal of Physical Chemistry C 117 (2013), 15106-15.
85. C. Mathe, S. Devineau, J. C. Aude, G. Lagniel, S. Chedin, V. Legros, M. H. Mathon, J. P. Renault, S. Pin, Y. Boulard and J. Labarre, 'Structural Determinants for Protein adsorption/non-adsorption to Silica Surface', Plos One 8 (2013).
86. M. Mayo, E. Yahel, Y. Greenberg, E. N. Caspi, B. Beuneu and G. Makov, 'Determination of the structure of liquids: an asymptotic approach', Journal of Applied Crystallography 46 (2013), 1582-91.
87. H. Mendil-Jakani, P. Baroni, L. Noirez, L. Chancelier and G. Gebel, 'Highlighting a Solid-Like Behavior in RTILs: Trioctylmethylammonium Bis (trifluoromethanesulfonyl)imide TOMA-TFSI', Journal of Physical Chemistry Letters 4 (2013), 3775-8.
88. F. Michel, L. Cormier, P. Lombard, B. Beuneu, L. Galoisy and G. Calas, 'Mechanisms of boron coordination change between borosilicate glasses and melts', Journal of Non-Crystalline Solids 379 (2013), 169-76.
89. A. Morin, Z. Peng, J. Jestin, M. Detrez and G. Gebel, 'Water management in proton exchange membrane fuel cell at sub-zero temperatures: An in operando SANS-EIS coupled study', Solid State Ionics 252 (2013), 56-61.
90. W. Mueller, C. Dejugnat, T. Zemb, J. F. Dufreche and O. Diat, 'How Do Anions Affect Self-Assembly and Solubility of Cetylpyridinium Surfactants in Water', Journal of Physical Chemistry B 117 (2013), 1345-56.
91. F. Muller, B. Jean, P. Perrin, L. Heux, F. Boue and F. Cousin, 'Mechanism of Associations of Neutral Semiflexible Biopolymers in Water: The Xyloglucan Case Reveals Inherent Links', Macromolecular Chemistry and Physics 214 (2013), 2312-23.
92. B. Nabi, A. L. Helbert, F. Brisset, G. Andre, T. Waeckerle and T. Baudin, 'Effect of recrystallization and degree of order on the magnetic and mechanical properties of soft magnetic FeCo-2V alloy', Materials Science and Engineering a-Structural Materials Properties Microstructure and Processing 578 (2013), 215-21.
93. T. Nagata, Y. Fukada, M. Kawai, J. Kano, T. Kambe, E. Dudzik, R. Feyerherm, P. E. Janolin, J. M. Kiat and N. Ikeda, 'Nonlinear Electric Conductivity of Charge Ordered System RFe_2O_4 (R = Lu, Yb)', Ferroelectrics 442 (2013), 45-9.
94. L. Noirez, C. Stillings, J. F. Bardeau, M. Steinhart, S. Schlitt, J. H. Wendorff and G. Pepy, 'What Happens to Polymer Chains Confined in Rigid Cylindrical Inorganic (AAO) Nanopores', Macromolecules 46 (2013), 4932-6.
95. I. Panagiotopoulos, W. Q. Fang, F. Ott, F. Boue, K. Ait-Atmane, J. Y. Piquemal and G. Viau, 'Packing fraction dependence of the coercivity and the energy product in nanowire based permanent magnets', Journal of Applied Physics 114 (2013).
96. I. Panagiotopoulos, W. Fang, K. Ait-Atmane, J. Y. Piquemal, G. Viau, F. Dalmas, F. Boue and F. Ott, 'Low dipolar interactions in dense aggregates of aligned magnetic nanowires', Journal of Applied Physics 114 (2013).
97. K. S. Panesar, C. Hugon, G. Aubert, P. Judeinstein, J. M. Zanotti and D. Sakellariou, 'Measurement of self-diffusion in thin samples using a novel one-sided NMR magnet', Microporous and Mesoporous Materials 178 (2013), 79-83.
98. R. J. Papoular, S. J. Yuan, R. Roldan, M. I. Katsnelson and R. Papoular, 'Effects of structural and chemical disorders on the vis/UV spectra of carbonaceous interstellar grains', Monthly Notices of the Royal Astronomical Society 432 (2013), 2962-74.
99. E. Pavlopoulou, G. Fleury, D. Deribew, F. Cousin,

M. Geoghegan and G. Hadziioannou, 'Phase separation-driven stratification in conventional and inverted P3HT:PCBM organic solar cells', Organic Electronics 14 (2013), 1249-54.

100. E. Perricone, M. Chamas, L. Cointeaux, J. C. Lepretre, P. Judeinstein, P. Azais, F. Beguin and F. Alloin, 'Investigation of methoxypropionitrile as co-solvent for ethylene carbonate based electrolyte in supercapacitors. A safe and wide temperature range electrolyte', Electrochimica Acta 93 (2013), 1-7.
101. E. Perricone, M. Chamas, J. C. Lepretre, P. Judeinstein, P. Azais, E. Raymundo-Pinero, F. Beguin and F. Alloin, 'Safe and performant electrolytes for supercapacitor. Investigation of esters/carbonate mixtures', Journal of Power Sources 239 (2013), 217-24.
102. S. Petit, V. Baledent, C. Doubrovsky, M. B. Lepetit, M. Greenblatt, B. Wanklyn and P. Foury-Leylekian, 'Investigation of the electromagnon excitations in the multiferroic $TbMn_2O_5$', Physical Review B 87 (2013).
103. V. Peyre, S. Bouguerra and F. Testard, 'Micellization of dodecyltrimethylammonium bromide in water-dimethylsulfoxide mixtures: A multi-length scale approach in a model system', Journal of Colloid and Interface Science 389 (2013), 164-74.
104. M. Ponthieu, F. Cuevas, J. F. Fernandez, L. Laversenne, F. Porcher and M. Latroche, 'Structural Properties and Reversible Deuterium Loading of MgD_2-TiD_2 Nanocomposites', Journal of Physical Chemistry C 117 (2013), 18851-62.
105. E. Popova, A. F. F. Galeano, M. Deb, B. Warot-Fonrose, H. Kachkachi, F. Gendron, F. Ott, B. Berini and N. Keller, 'Magnetic anisotropies in ultrathin bismuth iron garnet films', Journal of Magnetism and Magnetic Materials 335 (2013), 139-43.
106. N. Qureshi, H. Ulbrich, Y. Sidis, A. Cousson and M. Braden, 'Magnetic structure and magnon dispersion in $LaSrFeO_4$', Physical Review B 87 (2013).
107. L. Ratkai, I. Kaban, T. Wagner, J. Kolar, S. Valkova, I. Voleska, B. Beuneu and P. Jovari, 'Silver environment and covalent network rearrangement in GeS_3-Ag glasses', Journal of Physics-Condensed Matter 25 (2013).
108. D. Renard, C. Garnier, A. Lapp, C. Schmitt and C. Sanchez, 'Structure of arabinogalactan-protein from Acacia gum: From porous ellipsoids to supramolecular architectures (vol 90, pg 322, 2012)', Carbohydrate Polymers 97 (2013), 864-7.
109. M. Retuerto, A. Munoz, M. J. Martinez-Lope, M. Garcia-Hernandez, G. Andre, K. Krezhov and J. A. Alonso, 'Influence of the Bi^{3+} electron lone pair in the evolution of the crystal and magnetic structure of $La_{1-x}Bi_xMn_2O_5$ oxides', Journal of Physics-Condensed Matter 25 (2013).
110. Y. Rharbi, F. Boue and Q. Nawaz, 'The Dynamic of Confined Polystyrene in Nanoparticles in the Glassy Regime: The Close Packed Morphology', Macromolecules 46 (2013), 7812-7.
111. J. Ribis, M. L. Lescoat, S. Y. Zhong, M. H. Mathon and Y. de Carlan, 'Influence of the low interfacial density energy on the coarsening resistivity of the nano-oxide particles in Ti-added ODS material', Journal of Nuclear Materials 442 (2013), S101-S5.
112. O. Rivin, E. N. Caspi, H. Ettedgui, H. Shaked and A. Gukasov, 'Magnetic structure determination of $TbCo_2Ni_3$ using polarized and nonpolarized neutron powder diffraction', Physical Review B 88 (2013).
113. K. Rode, N. Baadji, D. Betto, Y. C. Lau, H. Kurt, M. Venkatesan, P. Stamenov, S. Sanvito and J. M. D. Coey, 'Site-specific order and magnetism in tetragonal Mn_3Ga thin films', Physical Review B 87 (2013).
114. A. B. Rodriguez, M. R. Tomlinson, S. Khodabakhsh, J. F. Chang, F. Cousin, D. Lott, H. Sirringhaus, W. T. S. Huck, A. M. Higgins and M. Geoghegan, 'All-polymer field-effect transistors using a brush gate dielectric', Journal of Materials Chemistry C 1 (2013), 7736-41.
115. J. Roeser, B. Heinrich, C. Bourgogne, M. Rawiso, S. Michel, V. Hubscher-Bruder, F. Arnaud-Neu and S. Mery, 'Dendronized Polymers with Silver and Mercury Cations Recognition: Complexation Studies and Polyelectrolyte Behavior', Macromolecules 46 (2013), 7075-85.
116. G. Romanelli, M. Ceriotti, D. E. Manolopoulos, C. Pantalei, R. Senesi and C. Andreani, 'Direct Measurement of Competing Quantum Effects on the Kinetic Energy of Heavy Water upon Melting', Journal of Physical Chemistry Letters 4 (2013), 3251-6.
117. A. Ruhm, S. V. Kozhevnikov, F. Ott, F. Radu and J. Major, 'Magnetic planar waveguides as combined polarizers and spin-flippers for neutron microbeams', Nuclear Instruments & Methods in Physics Research Section a-Accelerators Spectrometers Detectors and Associated Equipment 708 (2013), 83-7.
118. D. Russo, M. A. Gonzalez, E. Pellegrini, J. Combet, J. Ollivier and J. Teixeira, 'Evidence of Dynamical Constraints Imposed by Water Organization around a Bio-Hydrophobic Interface', Journal of Physical Chemistry B 117 (2013), 2829-36.
119. D. Russo, M. G. Ortore, F. Spinozzi, P. Mariani, C. Loupiac, B. Annighofer and A. Paciaroni, 'The impact of high hydrostatic pressure on structure and dynamics of beta-lactoglobulin', Biochimica Et Biophysica Acta-General Subjects 1830 (2013), 4974-80.
120. R. Salva, J. F. Le Meins, O. Sandre, A. Brulet, M. Schmutz, P. Guenoun and S. Lecommandoux, 'Polymersome Shape Transformation at the Nanoscale', Acs Nano 7 (2013), 9298-311.
121. M. Sato, Y. Kobayashi, T. Kawamata, Y. Yasui, K. Suzuki, M. Itoh, R. Kajimoto, K. Ikeuchi, M. Arai and P. Bourges, 'On the superconducting symmetry of Fe-based systems - Impurity effect studies and neutron scattering measurements', Journal of the Korean Physical Society 62 (2013), 1726-33.
122. A. P. Sazonov, A. Gukasov, H. B. Cao, P. Bonville, E. Ressouche, C. Decorse and I. Mirebeau, 'Magnetic structure in the spin liquid $Tb_2Ti_2O_7$ induced by a 111 magnetic field: Search for a magnetization plateau', Physical Review B 88 (2013).
123. C. Schulreich, C. Angermann, S. Hohn, R. Neubauer, S. Seibt, R. Stehle, A. Lapp, A. Richardt, A. Diekmann and T. Hellweg, 'Bicontinuous microemulsions with extremely high temperature stability based on skin friendly oil and sugar surfactant', Colloids and Surfaces a-Physicochemical and Engineering Aspects 418 (2013), 39-46.

124. J. Schulz, F. Ott, C. Hulsen and T. Krist, 'Neutron energy analysis by silicon prisms', Nuclear Instruments & Methods in Physics Research Section a-Accelerators Spectrometers Detectors and Associated Equipment 729 (2013), 334-7.
125. L. Shi, F. Carn, F. Boue, G. Mosser and E. Buhler, 'Control over the electrostatic self-assembly of nanoparticle semiflexible biopolyelectrolyte complexes', Soft Matter 9 (2013), 5004-15.
126. F. X. Simon, T. T. T. Nguyen, N. Diaz, M. Schmutz, B. Deme, J. Jestin, J. Combet and P. J. Mesini, 'Self-assembling properties of a series of homologous ester-diamides - from ribbons to nanotubes', Soft Matter 9 (2013), 8483-93.
127. K. Singh, M. B. Lepetit, C. Simon, N. Bellido, S. Pailhes, J. Varignon and A. De Muer, 'Analysis of the multiferroicity in the hexagonal manganite $YMnO_3$', Journal of Physics-Condensed Matter 25 (2013).
128. L. P. Singh, C. Alba-Simionesco and R. Richert, 'Dynamics of glass-forming liquids. XVII. Dielectric relaxation and intermolecular association in a series of isomeric octyl alcohols', Journal of Chemical Physics 139 (2013).
129. A. Slodczyk, P. Colomban, N. Malikova, O. Zaafrani, S. Longeville, J. M. Zanotti, O. Lacroix and B. Sala, 'Bulk protons in anhydrous perovskites-neutron scattering studies', Solid State Ionics 252 (2013), 7-11.
130. G. Sudre, D. Hourdet, C. Creton, F. Cousin and Y. Tran, 'pH-Responsive Swelling of Poly(acrylic acid) Brushes Synthesized by the Grafting Onto Route', Macromolecular Chemistry and Physics 214 (2013), 2882-90.
131. G. Tresset, V. Decouche, J.-F. Bryche, A. Charpilienne, C. Le Coeur, C. Barbier, G. Squires, M. Zeghal, D. Poncet and S. Bressanelli, 'Unusual self-assembly properties of Norovirus Newbury2 virus-like particles', Archives of Biochemistry and Biophysics 537 (2013), 144-52.
132. D. Uhrikova, L. Hubcik, P. Pullmannova, Lacinova, S. S. Funari, F. Devinsky and J. Teixeira, 'DNA - cationic liposomes supramolecular assemblies: the structure and transfection efficiency', European Biophysics Journal with Biophysics Letters 42 (2013), S208-S.
133. F. Weber, D. N. Argyriou, O. Prokhnenko and D. Reznik, 'Large lattice distortions associated with the magnetic transition in $La_{0.7}Sr_{0.3}MnO_3$', Physical Review B 88 (2013).
134. V. Wintgens, C. Le Coeur, C. Amiel, J. M. Guigner, J. G. Harangozo, Z. Miskolczy and L. Biczok, '4-Sulfonatocalix 6 arene-Induced Aggregation of Ionic Liquids', Langmuir 29 (2013), 7682-8.
135. E. Wu, G. Sun, B. O. Chen, J. Zhang, V. Ji, V. Klosek and M.-H. Mathon, 'Neutron Diffraction Study of Strain/Stress States and Subgrain Defects in a Creep-Deformed, Single-Crystal Superalloy', Metallurgical and Materials Transactions A (2013), 1-8.
136. Y. J. Yadav, B. Heinrich, G. De Luca, A. M. Talarico, T. F. Mastropietro, M. Ghedini, B. Donnio and E. I. Szerb, 'Chromonic-Like Physical Luminescent Gels Formed by Ionic Octahedral Iridium(III) Complexes in Diluted Water Solutions', Advanced Optical Materials (2013), n/a-n/a.
137. K. Younsi, J. C. Crivello, V. Paul-Boncour, L. Bessais, F. Porcher and G. Andre, 'Study of the magnetic and electronic properties of nanocrystalline $PrCo_3$ by neutron powder diffraction and density functional theory', Journal of Physics-Condensed Matter 25 (2013), 10.
138. O. Zaharko, M. Pregelj, A. Zorko, R. Podgajny, A. Gukasov, J. van Tol, S. I. Klokishner, S. Ostrovsky and B. Delley, 'Source of magnetic anisotropy in quasi-two-dimensional XY $\{Cu_4(tetrenH_5)[W(CN)_8]_4.7.2H_2O)\}n$ bilayer molecular magnet', Physical Review B 87 (2013).
139. M. Zidani, S. Messaoudi, F. Dendouga, T. Baudin, C. Derfouf, A. Boulagroun and M. H. Mathon, 'Study of the Relation between Microstructure and Properties (Mechanical/Electrical) of Copper Wire Drawing and Annealed', Acta Physica Polonica A 123 (2013), 470-2.

Other publications

1. C. Alba-Simionesco, C. Dalle-Ferrier and G. Tarjus, 'Effect of pressure on the number of dynamically correlated molecules when approaching the glass transition', AIP Conference Proceedings 1518 (2013), 527-35.
2. M. Deutsch, N. Claiser, M. Souhassou and B. Gillon, 'Joint Refinement of Charge and Spin Densities', Physics Procedia 42 (2013), 10-7.
3. A. Gukasov, S. Rodrigues, J.-L. Meuriot, T. Robillard, A. Sazonov, B. Gillon, A. Laverdunt, F. Prunes and F. Coneggo, 'Very Intense Polarized (VIP) Neutron Diffractometer at the ORPHEE Reactor in Saclay', Physics Procedia 42 (2013), 150-3.
4. S. Kozhevnikov, T. Keller, Y. Khaydukov, F. Ott, A. Ruhm and J. Major, 'Polarizing Fe-Co-Fe Planar Waveguides for the Production of Neutron Microbeams', Physics Procedia 42 (2013), 80-8.
5. T. Maurer, F. Zighem, S. Gautrot, F. Ott, G. Chaboussant, L. Cagnon and O. Fruchart, 'Magnetic Nanowires Investigated by Polarized SANS', Physics Procedia 42 (2013), 74-9.
6. K. S. Nemkovski, P. A. Alekseev, J. M. Mignot and A. S. Ivanov, 'Resonant Mode in Rare-earth based Strongly Correlated Semiconductors', Physics Procedia 42 (2013), 18-24.
7. K. S. Panesar, P. Judeinstein and J.-M. Zanotti, 'Selective Deuteration Reveals Interference Caused by Side-Chain Dynamics on Measurements of Self-Diffusion in Ionic Liquid Cations', Journal of the Physical Society of Japan 82SA, SA013.
8. M. Zidani, S. Messaoudi, F. Dendouga, T. Baudin, C. Derfouf, A. Boulagroun and M. H. Mathon, 'Multi-scale analysis by SEM, EBSD and X-ray diffraction of deformation textures of a copper wire drawn industrially', MATEC Web of Conferences 5 (2013).
9. Zighem, F. Ott, T. Maurer, G. Chaboussant, J. Y. Piquemal and G. Viau, 'Numerical Calculation of Magnetic form Factors of Complex Shape Nano-Particles Coupled with Micromagnetic Simulations', Physics Procedia 42 (2013), 66-73.

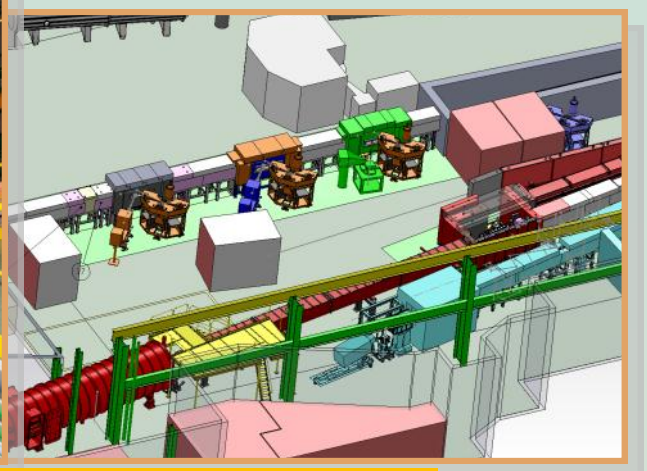

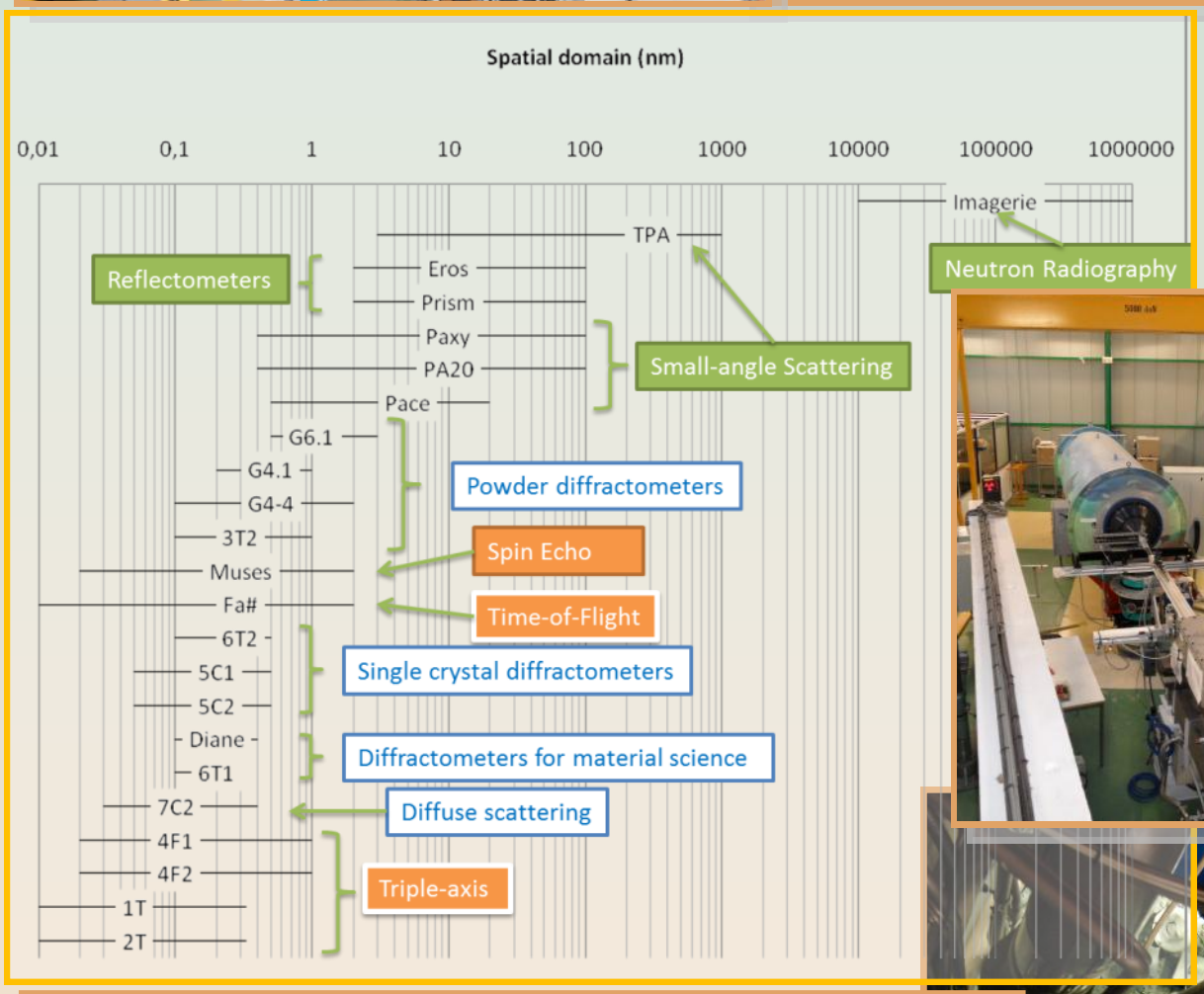
Spatial domain (nm)
0,01
0,1
1
10
100
1000
10000
100000
1000000
Imagerie
TPA
Reflectometers
Eros
Prism
Paxy
PA20
Pace
Small-angle Scattering
Neutron Radiography
G6.1
G4.1
G4-4
3T2
Muses
Fa#
6T2
5C1
5C2
Diane
6T1
7C2
4F1
4F2
1T
2T
Powder diffractometers
Spin Echo
Time-of-Flight
Single crystal diffractometers
Diffractometers for material science
Diffuse scattering
Triple-axis

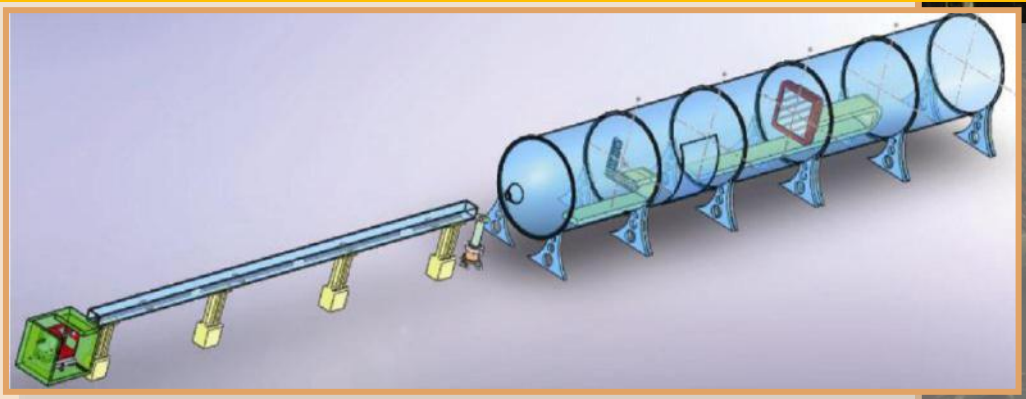

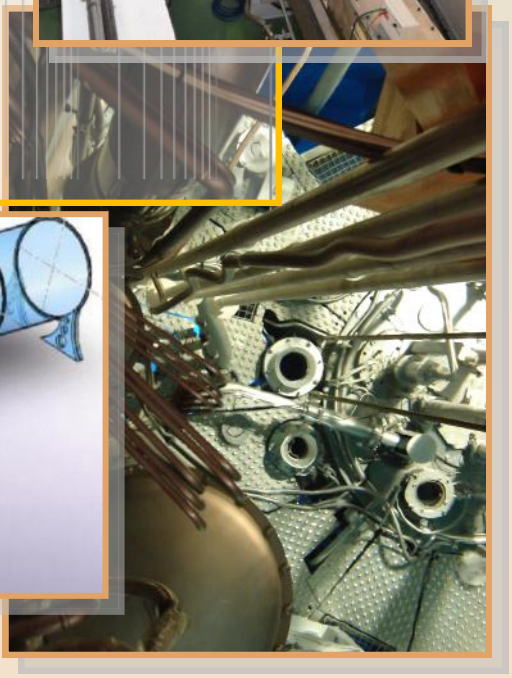

NEWS FROM THE SPECTROMETERS

THE NEUTRON SPIN-ECHO SPECTROMETER

S. Klimko[A], F. Legendre[A], S. Longeville[A], N. Malikova[B]

The neutron spin-echo spectrometer at the in Laboratoire Léon Brillouin in Saclay uses mixed resonance and conventional spin-echo principle to cover 4 decades in time for a given wavelength. Solenoid type coils are used for the measurements of the short times whereas the long time range is covered by the neutron-resonance principle. We recently installed new resonance coils in order to achieve longer times and better stability. The coils were designed to perform up to a radiofrequency of 1 MHz, which corresponds to static fields around 350 Gauss. With a wavelength of 5Å (maximum of the wavelength distribution) the accessible time ranges from 0.5 ps to 6.2 ns, and from 4 ps to 50 ns at λ=10Å.

A Laboratoire Léon Brillouin CEA/CNRS UMR 12, CEA Saclay, Gif sur Yvette, France

B Sorbonne Universités, UPMC Univ. Paris 06, CNRS, UMR 8234, PHENIX, F-75005, Paris, France

slongeville@cea.fr

The "MUSE" spectrometer

The spin-echo spectrometer produced his first echoes back in 1996, it was constructed jointly by the Technische Universität München, who was preparing the construction of the FRMII reactor and the Laboratoire Léon Brillouin. It uses the resonance principle, as an alternative to the spin echo introduced by Ferenc Mezei in 1972 [1], developed by Roland Gähler and Bob Golub in the late 80s [2]. In Neutron Resonance spectroscopy, the echo is produced by four radiofrequency flippers that combine a static (B_0) and a radiofrequency field (RF pulsation w), linked by resonance condition for the neutron spin ($w=\gamma_N B_0$), where γ_N is the neutron gyromagnetic ratio. In fact, the range of frequency of such coils is rather limited and the resonance spin echo is bounded in the low frequency range by the Bloch-Sieger shift; the oscillating field can be described by an association of two counter rotating fields. One follow the spin rotation and the opposite field (in the clockwise direction since γ_N is negative) can be considered as a perturbation. The lower the static field (*i.e.* small spin echo times) the more the perturbation induces a loss of the beam polarization. In practice, for frequency below 50kHz there is a strong decrease of the amplitude of the echo and static coils are used to produce a Mezei-type spin-echo. Above 1MHz which corresponds to static field of 350 G, the coil cooling becomes an issue. Due to the necessary transparency to neutrons, the coils must be built of aluminum. Despite the limited time range covered by resonance option it is nevertheless an interesting choice for at least two reasons: 1) the fields remain localized and 2) the continuity of the field line around sample position is not an issue. Therefore this type of spectrometer is very compact and it is well adapted for high angle measurements. Whereas other parts of the spectrometer were progressively replaced since 1996, the resonance coils remained the same. In 2012, we replaced the 4 bootstrap resonance coils by in house constructed ones [3] with higher frequency ranges (Figure 1). The changes in the characteristics of the coils necessitate a rather long period of tuning to obtain the optimum possibilities of the RF circuits. At present they are routinely used up to 400 kHz in the bootstrap mode, the 1MHz frequency should be reached after changes in the impedance adaptor which is under construction. A few years ago we also decided to start the development and construction of a multi-angle option to gain a significant counting rate by covering simultaneously scattering angles spanning over 25°. The critical aspect of the project is the construction of curved resonance coils with a sufficient homogeneity, which is not obvious if one considers the loss of a symmetry plane. Figure 2 presents

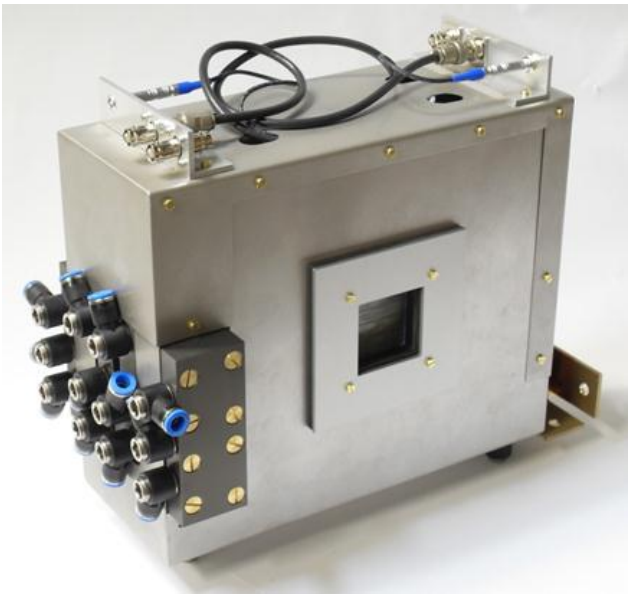

Figure 1: New flat resonance coils of the spin echo spectrometer

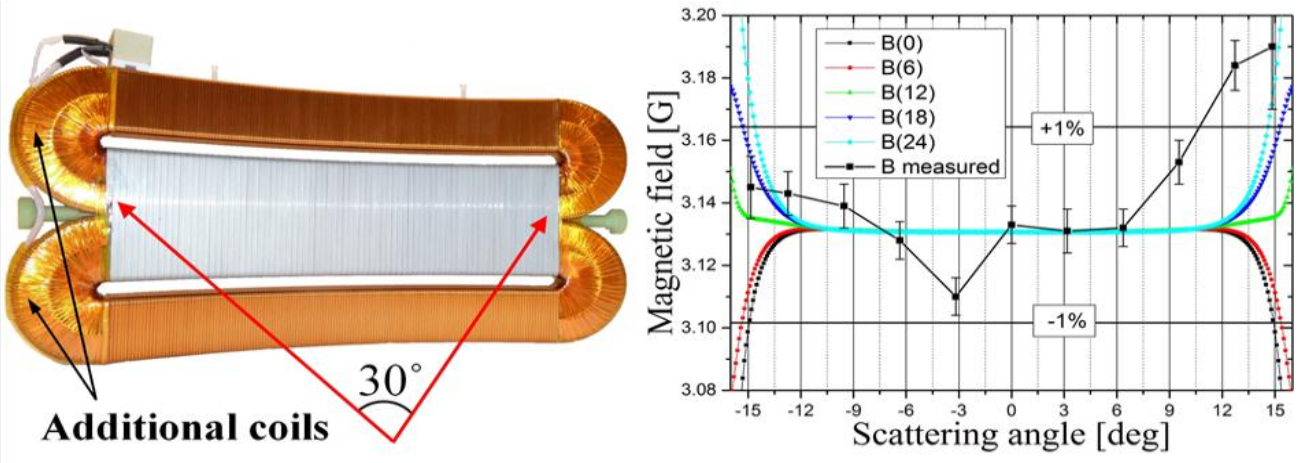

Figure 2: Left: curved radiofrequency coils for the future multi-angle option, with a radius of curvature is 40 cm (coil 3) it covers a scattering angle of 30°. Right: measurement of the homogeneity of the field as a function of the angle in degrees. The homogeneity is better than 1% over more than 25°.

the first prototype of RF coils with a radius of curvature of 40 cm, as well as test measurements of the homogeneity of the RF field. The deviation of the amplitude of the RF field remains below 1% of the central value over 30°. Figure 3 shows the drawing of the same RF coil imbedded in its static coil together with the cooling device. As for the new flat coils, simultaneous air and water cooling circuits are used. The full device is under construction. When the multi angle option of the spectrometer will be operational we expect to increase the counting rate by 2 orders of magnitude, while keeping the same time domain in a single wavelength measurement (4 orders of magnitude). For a measurement at 5Å, which corresponds to the maximum of the neutron flux distribution, we expect to cover simultaneously a time domain ranging from 0.5 ps to 6.2 ns, over a scattering angle of 25 degrees. At longer wavelengths we expect to reach a maximum time of 50ns.

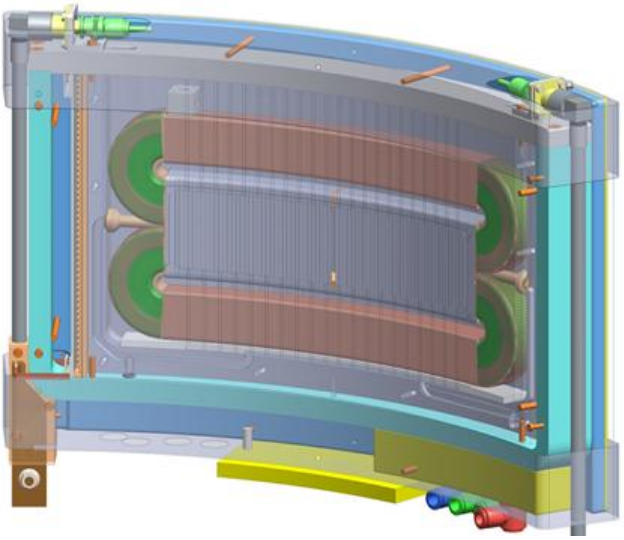

Figure 3 : Drawing of the RF coil embedded in the static coil B_0.

References

1. Mezei, F.; Neutron spin echo - New concept in polarized thermal neutron techniques, Zeit. Phys. 1972, 255, 1461
2. Ghäler R. & Golub R., A high resolution neutron spectrometer for quasielastic scattering on the basis of spin-echo and magnetic resonance, Z. Physik B – Condensed Matter, 1987, 65, 269-293.
3. Klimko S. &. Legendre F. , Private Communication

IMAGINE: A NEW COLD NEUTRON IMAGING STATION AT LLB

C. Loupiac[A,B]. S. Desert[B], A. Helary[B], F. Ott[B]

a Equipe PAPC, UMR PAM, AgroSup Dijon-Université de Bourgogne, Dijon, France

b Laboratoire Léon Brillouin CEA/CNRS UMR 12, CEA Saclay, Gif sur Yvette, France

c Institut Universitaire de la Vigne et du Vin, Université de Bourgogne, Dijon, France

d Laboratoire Interdisciplinaire Carnot de Bourgogne, UMR 6303, Université de Bourgogne, Dijon France

e UMR1347 Agroécologie, AgroSup dijon –INRA-Université de Bourgogne, Pôle IPM ERL CNRS 6300, 17 rue Sully, Dijon, France

camille.loupiac@cea.fr

frederic.ott@cea.fr

Technical specifications

IMAGINE (Fig.1) is located in the neutron guide hall on a cold neutron guide. The guide cross section is 25 mm x 50 mm and delivers cold neutrons with 3Å <λ<20 Å. The spectrometer sits on a marble floor and the detector position can be easily moved up to 10 m from the source allowing L/D = 400. In a typical configuration (FOV = 80 mm, source 20 mm diameter, L = 4m), the flux is 2x107 neutrons/s/cm². In the present state, a sCMOS camera (from Photonics Science) coupled with various scintillators (50 - 100 µm thickness) is used for the data acquisition. The sample is set on a table which allows up and down movements together with a 360° sample rotation for tomographic measurements. The table can accept loads above 100kg. A concrete casemate is after the pin-hole gives access to a velocity selector or a chopper. Various sample environments are (or will) be available shortly: humidity chamber, gas chamber, furnace, liquid cell, pressure cell. Future evolutions include the setup of the velocity selector and access to polarized neutrons. At longer term, time-of-flight measurements shall be performed, when a proper detection system is available.

Scientific case

Neutrons imaging is a non-destructive and non-invasive technique which allows to obtain materials structural characterization and defects at the microscopic length scale. Neutrons penetrate most materials to depths of several centimeters. Classically, neutron imaging has been used for quality control in industries that require precision machining such as aircraft or motor engineering. Neutron tomography has also been used in the cultural heritage studies to authenticate paintings and examine artifacts made of metal or stone. Due to its high sensitivity to hydrogen, neutron radiography and tomography can be used to measured humidity transport in soil. It is also a valuable non-invasive tool to study in situ root development in soil. Today, one important application of neutron radiography is in testing the performance of fuel cells (in operando) by imaging water or hydrogen flow in situ. The scientific case of IMAGINE station already allows to cover all these classical topics.

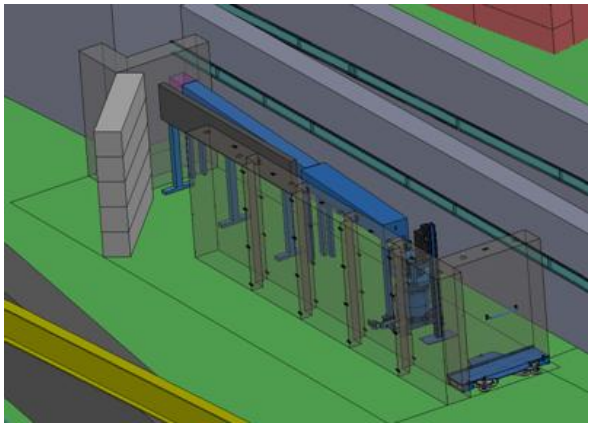

Figure 1: The IMAGINE station

First Experiments on IMAGINE

The first measurements performed on IMAGINE station deal mostly with agro-food science.

1- Quality grading of cork stoppers: amount of defects inside the material

A. Tachon[A,B,C], T. Karbowiak[A], C. Loupiac[A,B], R. Gougeon[A,C], J-P.Bellat[D]

Cork is used in a variety of products going from construction materials to gaskets, but its most important use is as a stopper for premium wines. The technology of stopping wine bottles with cork originated in 1680 with the first use of cork to seal Champagne by Dom Pierre Pérignon. The principle requirements for using cork as stoppers are the homogeneity of the cork and the loss of cavities and / or cracks. The quality grading of cork is based on visual analysis taking into account the three main types of defects: pores (lenticular channels), physiological anomalies (nails, clay), pathogenic anomalies (insect galleries). All these inspections allow to analyzing only the external surface of the stoppers. Thus cracks or holes inside the stopper are not detected. When viewed from a radial perspective, the cork cellular structure is a homogeneous tissue of thin walled cells orientated in an alveolar, honeycomb type pattern of hexagonal sections with no intercellular spaces. When viewed from an axial or a tangential perspective, the cells appear as rectangular prisms stacked base to base, parallel to the radial axis (Silva et al, 2005). Average cork cells are 45 µm tall with a hexagonal face of 20 µm and with a thickness of 1 µm. The first objective of the experiments performed by neutron imaging on cork stoppers with IMAGINE was to compare the amount of defects between natural cork Grade 0 (high quality) and Grade 4 (low quality), evaluating the empty space volume into different samples of each quality. Figure 2 presents the image obtained for two samples of different grades.

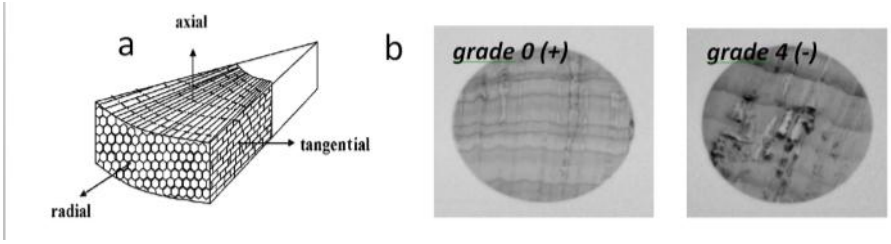

Figure 2: a- three dimensional structure of the cork from Silva et al. 2005 / b: Neutron radiographies of two slides of different qualities cork stoppers (IMAGINE instrument, 120 s exposure, 100 µm scintillator)

2- Milk powders dissolution in water: impact of agglomeration and formulation

C. Loupiac[A,B] and A. Assifaoui[A]

Milk protein powders are used as ingredients by the food industry in many applications which generally require the powder to be dissolved back into aqueous medium. The process of reconstitution of the powder in water can be divided into different steps: wetting, dispersing and dissolving (Marabi, 2007). Among these steps, the wetting of the particles is very often the rate -controlling step (Gaiani, 2009). The study of flow of liquid through porous materials finds a big importance in numerous domains and various imaging techniques (X-Ray, NMR and Neutron) were developed to visualize it through a material. The aim of these experiments was to better understand the impact of powders agglomeration (tableting), and composition on the dispersion steps and more particularly on wetting, and dissolution. Skimmed milk and sodium caseinates powders (functional milk powders) have been studied. These powders were formulated in the presence of various excipients which have to either allow the faster dissolution of the tablet, or on the contrary delay it, for example: methylcellulose (thickener used for tablet coating) maltodextrin and lactose (dispersing agents). Milk powders have been agglomerated to form tablets of 3 mm. Kinetics of dissolution of these different samples have been studied by neutron imaging after addition of water. Images acquisition have been as fast as possible (40 s) to be able to follow the fast kinetics. Figure 3 presents a tablet of milk powder after few minutes of hydration.

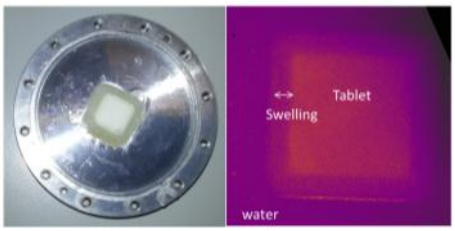

Figure 3 : (left) Tablet of milk powder after few minutes of hydration in its aluminum cell (right) Neutron radiography performed in 40s on IMAGINE

3- Grapevine root growth: beneficial effects of arbuscular mycorrhizal fungi

M. Adrian[E], S. Trouvelot[E], E. Bernaud[E], D. Wipf[Z], L. Bonneau[E], C. Salon[E], C. Loupiac[A,B], R. Gougeon[A,C]

Most grapevine varieties are susceptible to cryptogamic diseases and numerous treatments are required to ensure the quantity and quality of the harvest. In an objective of sustainable viticulture, there are increasing societal request, political incitation and winegrower's awareness to reduce the use of pesticides. For these reasons, alternative / complementary strategies of protection are investigated. One of them is the use of elicitors to induce plant resistance to pathogens by stimulation of their innate immune system (for review, see Adrian et al., 2012). Some plants know how to recognize and exploit other bodies, in particular germs present in the soil, which help them by facilitating the access to the water and to the mineral elements which, with the CO2 of air, constitute their nutrients. For example, Arbuscular Mycorrhizal (AM) fungi are able to establish a symbiotic interaction with the roots of 80% of plant families. AM fungi lead to a root morphology modification and development of a complex ramifying network in soil which allows for the plant to better explore the soil.

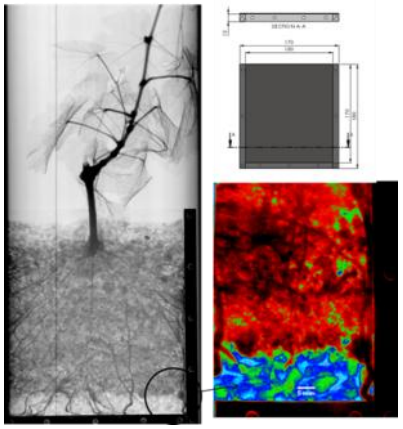

Figure 4: Neutron images of a grapevine herbaceous cutting cultivated by the AgroEcology team (Dijon) in an aluminium flat container (LLB design, Helary A.). The left « black and white » image has been performed with an image plate detector (neutronography station G4.5) and the right color one comes from the IMAGINE station (40 s of exposure)

References

1. Trouvelot , A.M., Gamm S., Poinssot M., Héloir MC. Daire X,.2012.Progress in Biological Control, Plant Defence: Biological Control. JM. Mérillon and KG. Ramawat eds, Part 4, Vol12, 313-331
2. Silva, S. P.; Sabino, M. A.; Fernandes, E. M.; Correlo, V. M.; Boesel, L. F.; Reis, R. L., Int. Mater. Rev. 2005, 50, 345-365
3. Marabi A., Mayor G., Raemy A., Bauwens I., Claude J., Burbidge A., Wallach R., Sam Saguy I., 2007, Food Research International, 40, 2007, 1286-1298
4. Gaiani C., Scher J., Schuck P., Desobry S., Banon S., 2009, Powder Technology, vol190, 2-5

A NEW DETECTOR FOR PAXY

A. Lapp[A], V. Thevenot[A],

A Laboratoire Léon Brillouin CEA/CNRS UMR 12, CEA Saclay, Gif sur Yvette, France

alain.lapp@cea.fr

Context

PAXY BF_3 multidetector (1.2 bar) dated from 1971, its replacement by a ^{3}He detector was decided in 2009. Selection of LLB went towards a unitary 12 bar ^{3}He multi-tube multidetector, named MAM 128, designed and produced by ILL. The contract for this production also included an identical detector with associated electronics for the small angle spectrometer PA20. After preliminary tests on the D33 spectrometer at the ILL, the first detector, named MAM128 # 2 (the first being that of D33), was installed in the detector tank of PAXY from July 2013 to January 2014. Installing this new hardware called the joint

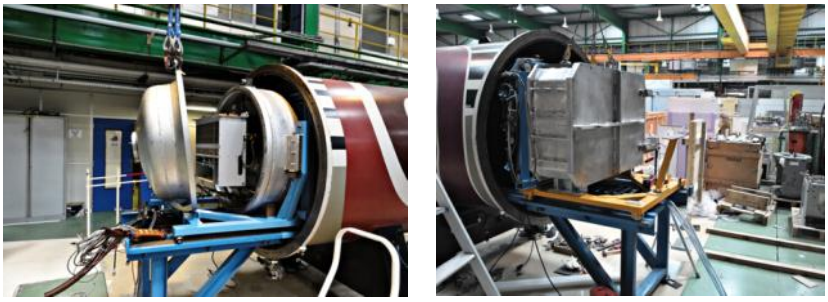

Figure 1: Unmouting the old BF_3 detector and mounting the new one

expertise of the "Instrumentation", "Electronics" and "Computing" groups from the LLB.

MAM128 #2 Detector Specifications:

The technical features of the new sensor are as follows

- 128 tubes of rectangular section (5 mm * 7mm), made by electro-erosion, 64 cm long and spaced by 5 mm.
- A pressure of 12 bar ^{3}He-Ar + CO_2.
- A detection area of 4096 cm^2 (to be compared to 3217 cm^2 for the old circular detector) which multiplies the q range by $\sqrt{2}$.
- A much better efficiency than that of the former detector for wavelengths greater than $\lambda = 4$Å. At 6 Å, the efficiency rises from 18% to 91% (gain x 5). This gain is visible on the measurements of the flux received by the detector (Figure 3).

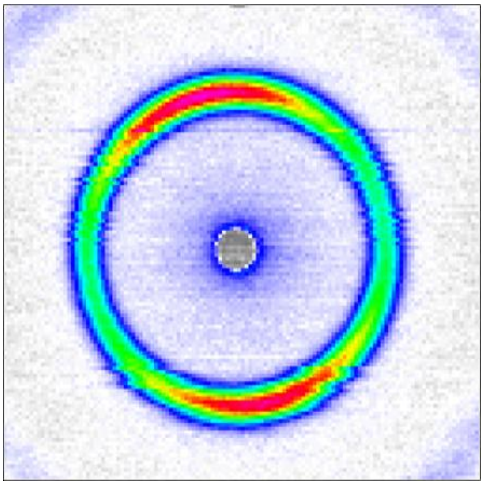

Figure 2: One of the first image : silver behenate

- A dead time τ (minimum time between the discrimination of two events) significantly reduced.

The measurement of the dynamic sensivity

$$Tr = T^2 * \frac{(1-\Sigma_{Pl} * \tau)}{T - \Sigma_{Pl} * \tau} = \frac{\sum_{plexi}}{\sum_{FV}}$$

was estimated by comparing the signal measured with variable-thickness attenuators inserted in the beam, with or without a 1 mm sample of plexiglas. This procedure showed that the dead time of the detector is (3.1 ± 0.4) x10^{-7} s. This means that a factor of 10 was won over the old detector.

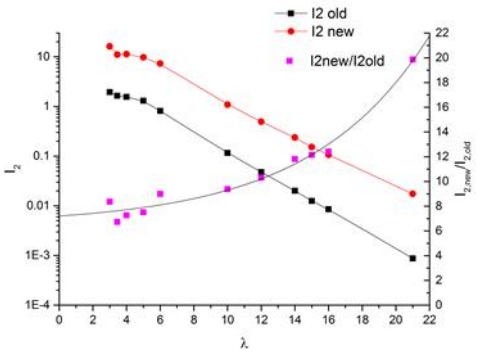

Figure 3: Comparison of the flux measured on the old and the new detector according to the wavelength.

THREE SPECTROMETERS COMING SOON: G44, PA20, HERMES!

The Powder High Resolution Diffractometer G4.4

G4.4 will be a high resolution « banana-type » diffractometer optimised for the structural studies of medium/large cell crystalline compounds. It will replace the former G4.2 diffractometer, operated in cooperation with PNPI Gatchina, which was shut down in 2004. It will complete the pool of powder diffractometers proposed by LLB (3T2/G4.1/G6.1). With its Ge(*hhl*) monochromator, it will propose 3 wavelengths (2.3/2.8/1.8Å) with a maximal diffraction angle $2\theta \sim 160°$. Typical acquisition time will be 12-24h/scan.

Testing the detection electronics of G4.4

Applications

G4.4 will be optimised for studying nuclear and magnetic structures of materials with a period of ~20Å. Typical applications will be zeolite-type systems, fuel-cell materials, pharmaceutical, (multi-)ferroic compounds…

The SANS spectrometer PA20

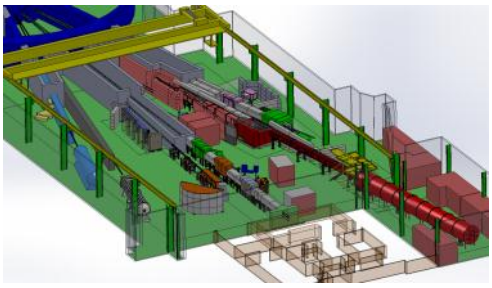

Up: 3D view of PA20 in the Hall of Guides—Down: The G5 guide and the red casemate of PA20 in 2013.

The new Small Angle Neutron Scattering (SANS) instrument PA20 will replace PAXE and PAPYRUS instruments at LLB-Orphée. It will extend LLB's capabilities in SANS, providing a polarized neutron option and a Grazing Incidence SANS (GISANS) mode, together with an improved dynamical *Q*-range. The total length of PA20 will be 40 m, including a 19 m-length collimation, a 20 m detector tank containing high-resolution/high-emciency *XY* detectors, and a casemate containing a velocity selector ($\lambda = 0.3 - 2$ nm), a chopper system for Time-of-Flight (TOF) mode, a polarizer and a RF spin flipper.

Applications

SANS is especially well adapted to research in soft matter, materials and nanosciences and SANS is particularly powerful in the studies of complex systems, with isotopic labeling and contrast variation method, but also for large-scale structures (magnetic or not). PA20 will allow faster measurements, with "single-shot" access to a wider range of scattering vectors, on possibly small samples (few mm in size). In addition, polarized neutrons will enable magnetic studies in both SANS and GISANS configurations. Studies of nanostructured surfaces and interfaces (deposited or embedded nano-objects), magnetic domain formation, multilayered materials or magnetic thin films through specular and off-specular signals will be possible through GISANS setups.

The HERMES reflectometer

The HERMES reflectometer (**H**orizontal **E**nhanced **R**eflectometer for the **ME**asurement of **S**urfaces) is the upgrade of the former EROS machine, which moved to G6.2 position at the arrival of the new IMAGINE neutronography station. Compared to EROS, HERMES will beneficiate of a new detector stage with a multidetector and a new end-guide position. Like EROS, HERMES will be specially dedicated to the study of interfaces in liquid systems, thanks to its horizontal sample stage.

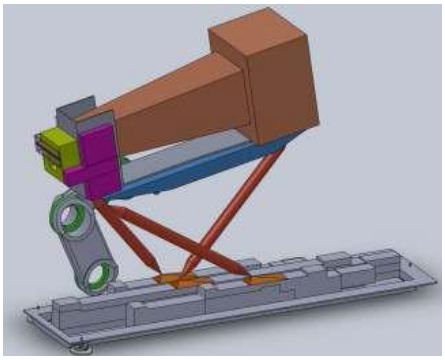

The new XY detector stage of HERMES


Young LLB
researchers
Presentations
July 1 2013

TEACHING AND EDUCATION

SECOND WINTER SCHOOL
ON NEUTRON SCATTERING ON SOFT MATTER

In the framework of the french-swedish contract on large facilities, the *2nd Swedish Winter School on Neutron Scattering on Soft Matter* was jointly organized by Maths Karlsson from Chalmers University of Technology of Göteborg, Max Wolff from Uppsala Universitet and Laboratoire Léon Brillouin. The School was targeted to attract pHD students in order to prepare the Swedish academic scientific community to the arrival of the European Spallation Source in Lund as students of 2013 may be mature researchers 10 years from now when the next european facility ESS will be in full operation. It was divided in two separated parts : *(i)* a theoretical part organized from at Chalmers University in Göteborg at Chalmers University from 25th -27th February 2013 and *(ii)* a practical part organized at LLB from 11th -14th March 2013. Although organized in Göteborg, LLB was actively involved in the theoretical part since two basic lectures (half day each) were given by LLB researchers : *Introduction to inelastic scattering* by Sylvain Petit and *Introduction to Neutron reflectometry* by Fabrice Cousin.

Blizzard on the School !

Time	Group 1	Group 2	Group 3
Day 1/ 9 - 12	General information LLB Visit of guide hall and reactor Safety training Dosimetry	General information LLB Visit of guide hall and reactor Safety training Dosimetry	General information LLB Visit of guide hall and reactor Safety training Dosimetry
Day 1/ 14 - 17	SANS	Reflectometry	NSE
Day 2/ 9- 13	SANS	Reflectometry	NSE
Day 2/ 14 - 18	NSE	SANS	Reflectometry
Day 3/ 9 - 13	NSE	SANS	Reflectometry
Day 3/ 14 - 18	Reflectometry	NSE	SANS
Day 3/ 20 - 24	Dinner	Dinner	Dinner
Day 4/ 9 - 13	Reflectometry	NSE	SANS

The involvement of the LLB staff was important to insure a good welcome to the participants, from the local organizers to the supervisors of practicals and administration staff (Fabrice Cousin, Françoise Damay, Giulia Fadda, Jacques Jestin, Lucile Mangin-Thro, Alain Menelle and Anne Touze). The visit started by a first half day devoted to the welcoming of students, a general presentation of the facility and a visit tour of the Orphée reactor. It was followed by 3 days of practical divided in three sessions of 1 day each on Inelastic Scattering (on a 3-Axis spectrometer), Small Angle Neutron Scattering and Neutron Reflectometry to offer a comprehensive overview of the useful neutron techniques in the field of soft matter. The students were split in groups and all made the 3 sessions. The organization of the school was sometimes chaotic as it was hampered by a snow storm, an exceptional weather event at this period in Paris area, but both students and supervisors did their best to reach the lab and make the practicals in the best possible conditions. These unexpected conditions finally favored very friendly relationship between all participants and made the School a very good *souvenir* for everyone.

Final day of practice under the sunny arctic atmosphere of Saclay

PRACTICALS WITH AGROSUP DIJON :

"Impact of sucrose replacement by maltitol on cacao butter crystallisation, texture and fat blooming"

E. Angelard[1], C. Brochet[1], A. David[1], L. Gehin[1], E. Gorlin[1], A. Leboullenger[1], A. Mourched[1], C. Alba-Simionesco[2], D. Bonnet[3], P. Cayot[1], D. Champion[1], F. Cousin[2], C. Loupiac[1,2], F. Porcher[2], P. Smith[3]

1-AgroSup Dijon, Dominante Formulation et Qualité des Aliments, Département Sciences des Aliments et Nutrition, 26 boulevard du Dr Petitjean, 21079 Dijon cedex, France

2-Laboratoire Léon Brillouin, CEA Saclay, 91191 Gif-Sur-Yvette cedex, France

Students from AgroSup Dijon (food engineering school) involved in the third year major on "Food Development and Quality" worked on chocolate crystallization with two partners: Cargill, producer and international supplier of services and food products, and the Laboratoire Léon Brillouin. The main objectives were to study the replacement of sucrose by maltitol and the role of lecithin (emulsifier) towards other components. One part of the experiments was realized in Agrosup Dijon by analyzing the texture, the rheology and the evolution of crystalline forms during tempering using classical tools of food science. The other part was realized at the Laboratoire Léon Brillouin by using the neutron reflectivity and diffraction. For these experiments, the aim was to observe interfaces created between the model components with reflectivity and show the crystalline structure change of components with diffraction. The aim was to show the interest of these methods for the food-processing industry.

FAN DU LLB (DECEMBER 2-5 2013)

FAN du LLB is an annual school delivered in French and offering young French-speaking researchers a first contact with real experimental neutron scattering. The school is aimed at students and post-docs working in all scientific areas where neutrons can provide valuable insights, although *priority is given to those having never had any contact with neutrons scattering*. After an introduction to neutron sources and neutron scattering, ten different thematic subjects based on different scientific problems that can be addressed by neutron scattering, are proposed to the students. In groups of four to five, the students are then introduced to two different neutrons scattering technique, during three days devoted to experiments and data analysis. One of the distinguishing features of our school is that the students often come with their own samples, which are tested during the training together with our demonstration samples. This ensures a good and efficient participation of the students. In 2012, the number of participants was 31.

Website: **http://www-llb.cea.fr/fan**

JDN 21 (JUNE 21-27 2013)

Every year a school is organized on a particular aspect of neutron scattering, with the support of French neutron centers LLB and ILL. The 21st edition, JDN 21, and was held at Club Lazaret in Sète from 21 to 27 June 2013 The school theme was « NEUTRONS AND MATERIALS FOR ENERGY ». This latter focused on the use of neutron scattering for the study of high tech materials, especially in the energy sector The development of new materials for energy is one of the major challenges of this century and is based largely on a thorough understanding of the origins of multi scale properties.

NEW PHD STUDENTS IN 2013

SONGVILAY Manila — CEA-2013-2016

"Structures et propriétés d'oxydes magnétiques à topologie frustrée"

Supervisor : F. Damay
(*Strongly Correlated Quantum Materials and Magnetism*)

PANTIATICI Claire – Grant IDEX Paris-Saclay/CEA

(**Call LLB/SOLEIL 2013**)

«DNA replication in eukaryotic cells : Relation between chromatin conformation and kinetic of DNA replication »

Supervisors : A. Goldar (CEA Saclay) / D. Lairez - (LLB)
(*Soft Complex Matter*)

GUENET Hélène – Région Bretagne/CEA-2013-2016

(**Call LLB/SOLEIL 2013**)

«Les zones humides sont-elles une source d'As pour les aquifères sous-jacents : caractérisation des interactions As-matière organique (imagerie/rayonnement synchrotron/diffraction de neutrons)»

Supervisors : M. Davranche (Géosciences Rennes) / J. Jestin - (LLB)
(*Soft Complex Matter*)

THESES DEFENDED IN 2013

SHI Li – April 5 2013

«Structure de complexes électrostatiques entre un polyélectrolyte de rigidité variable et des nanoparticules de taille contrôlée»

Supervisors : E. Buhler (Paris) / F. Boue
(*Soft Complex Matter*)

LEROY Marie-Alix– September 20 2013

«Films minces épitaxiés de chrome pour l'électronique de spin : propriétés de volume et d'interface»

Supervisors : S. Andrieu (Nancy) / A. Bataille
(*Materials and Nanosciences: Fundamental Studies and Applications*)

DUBOIS Matthieu – July 2 2013

«Apport de la diffraction neutronique dans l'étude des phases métastables de l'alliage à mémoire de forme CuAlBe sous sollicitations mécaniques et thermiques»

Supervisors : A. Lodini (Reims) / M.-H. Mathon
(*Materials and Nanosciences: Fundamental Studies and Applications*)

FANG Weiqing – November 29 2013

«Elaboration de matériaux composites nanofils magnétiques/polymères pour la fabrication d'aimants permanents»

Supervisors : F. Boue / F. Ott
(*Materials and Nanosciences: Fundamental Studies and Applications*)

BOUTY Adrien – December 3 2013

«Influence de la dispersion des charges et de la conformation des chaines sur les propriétés mécaniques de systèmes nanocomposites SBR/Silice »

HABILITATIONS TO SUPERVIZE PHD STUDENTS (HDR)

"Nanostructured particle-polymer composites: filler dispersion and chain conformation from well-defined model to "real" systems, correlation with mechanical properties "

Jacques JESTIN (November 14 2013)

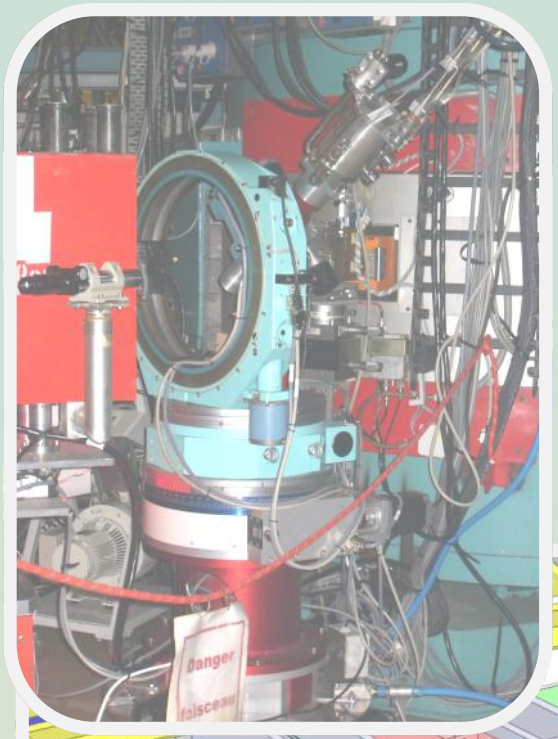
Danger

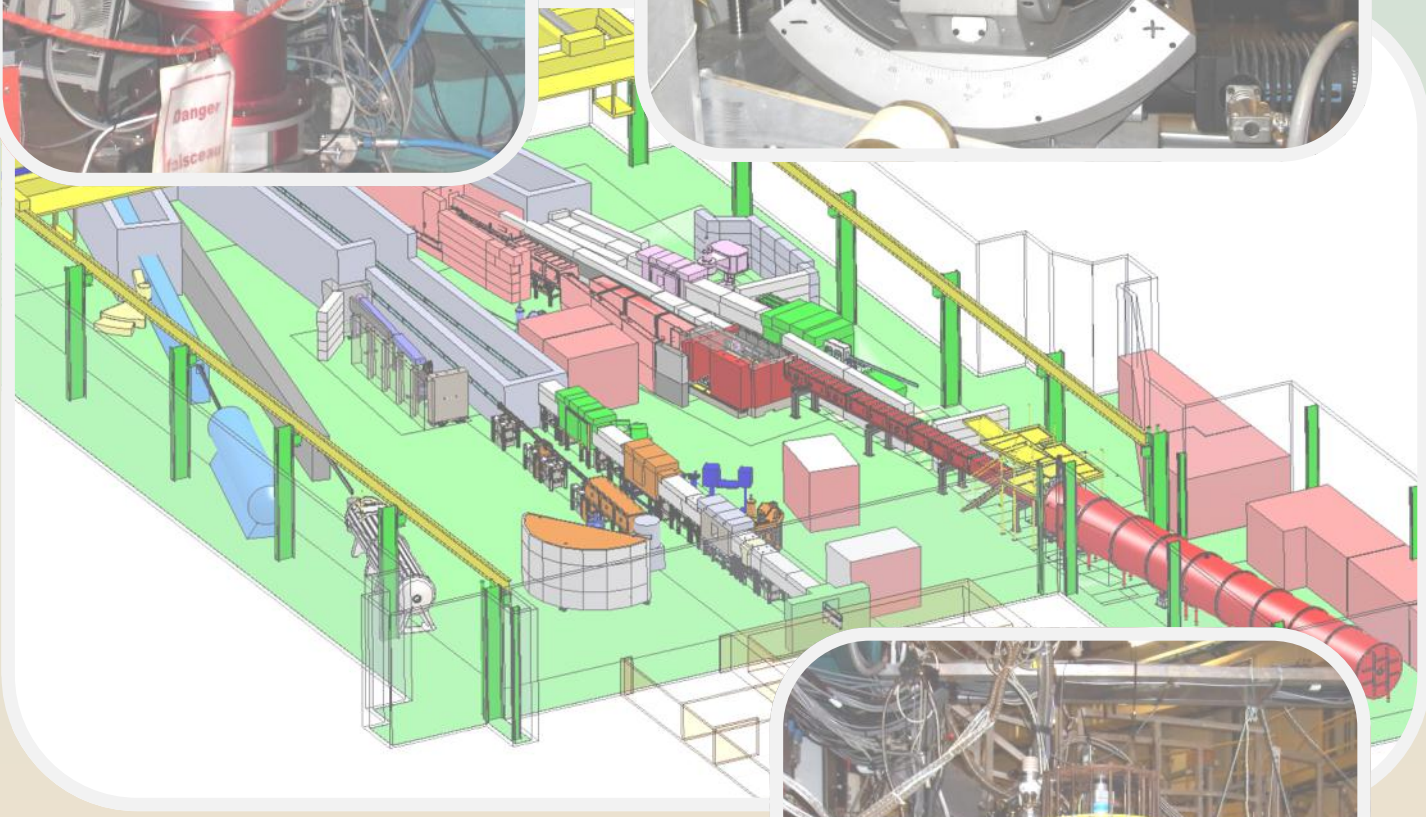

BEAMTIME ACCESS

GENERAL LAYOUT OF THE SPECTROMETERS

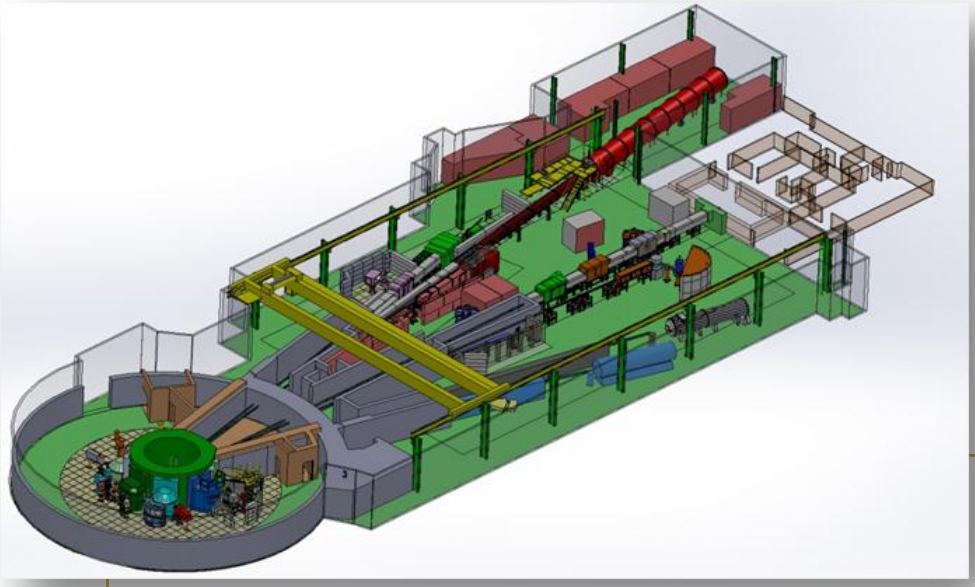

	SPECTROMETERS OPEN TO USERS	CONTACTS
	Powder diffractometers	
3T2	Florence Porcher	florence.porcher@cea.fr
G4.1	Françoise Damay	francoise.damay@cea.fr
G4.4 PHR	Florence Porcher	florence.porcher@cea.fr
G6.1	Isabelle Mirebeau	isabelle.mirebeau@cea.fr
	Single crystal diffractometers	
5C1 - VIP	Béatrice Gillon	beatrice.gillon@cea.fr
5C2	Alexandre Bataille	alexandre.bataille@cea.fr
Super 6T2	Arsen Goukassov	arsen.goukassov@cea.fr
	Diffuse scattering instrument	
7C2	Louis Hennet	louis.hennet@cea.fr
	Small-angle scattering instruments	
G1.2 - PACE	Didier Lairez	didier.lairez@cea.fr
G2.3 - PAXY	Alain Lapp	alain.lapp@cea.fr
G5bis - TPA	Annie Brûlet	annie.brulet@cea.fr
	Diffractometers for material science studies	
6T1	Marie-Hélène Mathon	marie-helene.mathon@cea.fr
G4.2 - DIANE	Vincent Klosek	vincent.klosek@cea.fr
	Reflectometers	
G3bis - EROS	Fabrice Cousin	fabrice.cousin@cea.fr
G2.4 - PRISM	Frédéric Ott	frederic.ott@cea.fr
	Triple-axis instruments	
1T	John Paul Castellan / Yvan Sidis (CRG Instrument Karlsruhe/LLB)	john-paul.castellan@cea.fr / yvan.sidis@cea.fr
2T	Philippe Bourges	philippe.bourges@cea.fr
4F1	Sylvain Petit	sylvain.petit@cea.fr
4F2	Julien Robert	julien.robert@cea.cr
	Quasi-elastic instruments	
G1bis - MUSES	Stéphane Longeville	stephane.longeville@cea.fr
	Neutron radiography	
G3bis—IMAGINE	Frédéric Ott	frederic.ott@cea.fr
G4.5	Guy Bayon	guy.bayon@cea.fr

The LLB-Orphée neutron scattering and imaging instruments

Powder diffractometers

3T2 "Thermal neutrons" 2-axis (50 detectors) high resolution, mainly for nuclear structure determination.

G4.1 "Cold neutrons" 2-axis (multidetector 800 cells) high flux, mainly for magnetic structure determination.

G4.4 "Cold neutrons" 2-axis (70 detectors) high resolution, for nuclear/magnetic structure determination of systems with large cells.

G6.1 "Cold neutrons" 2-axis (multidetector 400 cells) with long wavelength (~5Å) and high flux, for the study of very small powder samples (<1mm^3). Medium/high pressure cell available.

Single crystal diffractometers

5C1 "Hot neutrons" 2-axis with lifting arm, polarized neutrons, magnetic field (8 Tesla) for spin-density maps determination

5C2 "Hot neutrons" 4-circle for nuclear structure determination.

6T2 "Thermal neutrons" 2-axis, lifting arm and 4-circles, mainly for magnetic structure determination. 12 Tesla magnetic field available, 2D detector.

Diffuse scattering instruments

7C2 "Hot neutrons" 2-axis (multidetector 640 cells) for local order studies in liquid or amorphous systems. Cryostat and furnace available (1.2K to 1300°C).

Small-angle scattering instruments

G1.2 "Cold neutrons" (annular detector, 30 rings) for study of large scale structures in isotropic systems (mainly polymers and colloids).

G2.3 "Cold neutrons" (X-Y detector, 128x128 cells) for study of large scale structures (10 to 500 Å) in anisotropic systems (polymers under stress, metallurgical samples, vortex in superconductors).

G5bis Very Small Angle Neutrons Scattering spectrometer

Diffractometers for material science studies

6T1 "Thermal neutrons" 4-circle for texture determination.

G4.2 "Cold neutrons" 2-axis for internal strain determination in bulk samples with spatial resolution ~ 1mm^3.

Reflectometers

G3bis "Cold neutrons" reflectometer operating in time-of-flight mode for multipurpose surface studies.

G2.4 "Cold neutrons" reflectometer with polarized neutrons and polarization analysis for the study of magnetic layers.

Triple-axis instruments

1T "Thermal neutrons" high-flux 3-axis instrument with focussing monochromator and analyser, mainly devoted to phonon dispersion curves measurements. High pressure cells (100 Kbar) available. CRG Instrument operated in collaboration with the INFP Karlsruhe

2T "Thermal neutrons" high-flux spectrometer with focussing monochromator and analyser, mainly devoted to spin-waves and magnetic excitations studies (1.5 to 80 meV).

4F1
4F2 "Cold neutrons" high flux 3-axis instruments with double monochromator and analyzer, mainly devoted to the study of low-energy (15µeV to 4meV) magnetic excitations. Polarized neutrons and polarization analysis option available.

Quasi-elastic instruments

G1bis "Cold neutrons", high resolution and high flux spin-echo instrument. It can study, in a large Q range, slow dynamics of large molecules in biology or long relaxation times like in glassy transition (Fourier times ~ 20ns)

Neutron Radiography

G3bis IMAGINE: Imaging station mainly dedicated to soft matter.

G4.5 Imaging technique : white beam facility for non-destructive control or dynamics imaging (NMI3 access only).

AUXILLIARY SERVICES AVAILABLE

Laboratories for sample preparation:

- Chemistry laboratory
- Biological laboratory

Technical help for:

- Cryostat, Furnace (0.1 – 2000 K)
- Medium/High pressures
- High magnetic fields (up to 10 T)
- Mechanics, Cryogenics, *Vacuum*

http://www-llb.cea.fr/fr-en/spectros_p.php

Access to beamtime

LLB has been selected in the frame of the European Community – Access activities of the Neutron scattering and Muon spectroscopy Integrated Infrastructure Initiative (NMI3-II) which supports access to neutron beams for the selected user teams, travel and subsistence fees of visiting scientists. The program is opened to E.C. users and to scientists of the associated states.

http://nmi3.eu

Beamtime access is free of charge for any experimentalist from the French Scientific community. LLB takes in charge the expenses (travel and stay) of 2 people during the experiment.

Beamtime on the 20 open-access spectrometers can be requested by submission of:

- *An experimental application to a Selection Committee (Normal Procedure)*
  This procedure is open to any public/industrial researcher that is interested in using neutron scattering for his research. Results should be free to be totally or partially published in a Scientific Review.
  DEADLINE FOR APPLICATION: April 1st and October 1st
  http://www-llb.cea.fr/en/fr-en/proposal.php

- *An experimental application to the Directors (Exceptional)*
  This special procedure should only be used exceptionally for hot topics, confidentiality reasons or if an anomaly in the review procedure is suspected. The delay between the acceptation decision and the realization of the experiment is shortened to the minimum.
  No deadline applies for such propositions (Application all along the year).
  http://www-llb.cea.fr/en/fr-en/proposal.php

- *A fast access application*
  This procedure allows a rapid access (1 to 2 months delay) to the spectrometers in order to perform a short experiment (1 day max.). It can be used for feasibility tests, sample characterization, obtaining complementary results…
  No deadline applies for such propositions (Application all along the year).
  http://www-llb.cea.fr/en/fr-en/prop-rap.php

CONTACT AT LABORATOIRE LEON BRILLOUIN

Laboratoire Léon Brillouin

Scientific Office

CEA SACLAY

Bâtiment 563 *F - 91191 Gif-sur-Yvette Cedex*

Tel. : 33(0) 1 69 08 60 38 *Fax : 33 (0) 1 69 08 82 61*

Selection committees

Proposals are examined by 5 Selection Committees. Each is composed of 8 to 10 senior scientists that are nominated by the management of LLB for 3 years. At least half of them do not belong to the LLB and 2 or 3 are coming from foreign institutes.

For each spectrometer, LLB gives a beam-time available which is shared out by the committee; each proposal gets a grade A or B or C.

A : The experiment must be done and the committee allocates a beam-time

B : The experiment might be done if there is some extra beam-time,

C : The experiment is refused on scientific arguments.

Selection Committees are asked to take care of the educational duty of the LLB when proposal comes from new young searcher.

SELECTION COMMITTEES: SCIENTIFIC FOCUS AND SUB-FOCUS

Theme I Chemical physics, biological systems

- I.01 Polymers and Supramolecular Structures
- I.02 Water, aqueous solutions, polyelectrolytes, surfactants
- I.03 System of biological interest, Biophysics
- I.04 Colloids, nanostructures
- I.05 Gels, composite materials
- I.06 Other…

Theme II Crystallographic and magnetic structures

- II.01 Crystalline structures
- II.02 Phases transitions
- II.03 Magnetic Structures
- II.04 High pressures (on powders
- II.05 Other…

Theme III Magnetism: Single-crystal systems and thin layers

- III.01 Magnetic thin layers
- III.02 Spin density
- III.03 Systems with strong quantum correlations
- III.04 Extreme conditions (strong fields, high pressures)
- III.05 Magnetic nanosystems
- III.06 Other…

Theme IV Disordered Systems, nanostructured materials and materials

- IV.01 Liquid and amorphous structures
- IV.02 Dynamics of disordered systems
- IV.03 Thin film materials
- IV.04 Nanostructured materials, precipitation, cavities,…
- IV.05 Crystallographic textures
- IV.06 Strains and residual stresses
- IV.07 Other…

Theme V Excitations

- V.01 Magnons
- V.02 Supraconductivity
- V.03 Coupling spin-network
- V.04 Dynamics in frustrated systems
- V.05 Polarized neutrons with polarization analysis
- V.06 Phonons
- V.07 Other…

LLB 2013 Reviewing committees

LLB members	French users		European users	

COLLEGE 1: Chemical physics, biological systems

Organisers: J. Jestin, G. Fadda

F. Cousin	S. Lyonnard	CEA, Grenoble	F. Gabel	IBS, Grenoble
	F. Nallet [Pdt]	CRPP, Bordeaux		
	R Schweins‡	ILL, Grenoble		
	B. Deme*	ILL, Grenoble		
	Y. Tran	ESPCI, Paris		

COLLEGE 2: Crystallographic and magnetic structures

Organisers: F. Porcher, S. Petit

F. Damay	V. Paul Boncour	ICPME, Thiais	A. Daoud-Aladine	ISIS, UK
	S. Ravy	Soleil, St Aubin		
	P. Roussel	UCC, Villeneuve d'Ascq		

COLLEGE 3: Magnetism: Single-crystal systems and thin layers

Organisers: A. Bataille, F. Ott

G. André‡	T. Hauet	Université Nancy I	F. Palacio	Université Zaragoza, ES
A. Gukassov*	E. Ressouche	ILL, Grenoble	K. Temst [pdt]	Université Louvain, B

COLLEGE 4: Disordered Systems, nanostructured materials and materials

Organisers: P. Judenstein, V. Klosek

F. Audonnet	J. Henry [Pdt]	CEA, Saclay	K. Wierzbanowski	Cracovie, Pl
	L. Cormier	Universités Paris 6 et 7	M. Gonzalez	ILL, Grenoble

COLLEGE 5: Excitations

Organisers: J. Robert, Y. Sidis

J.-M. Mignot	M. Boehm‡ [pdt]	ILL, Grenoble	J. Hlinka	ASCR, Prague
	B. Fauqué*	ESPCI, Paris	D. Lamago	KIT, Allemagne
	M. d'Astuto*	IMPMC Jussieu, Paris	L. Paolasini	Univ. Edimburg, UK

‡ Only for spring session - * Only for automn session

Laboratoire Léon Brillouin
UMR12 CEA-CNRS
CEA Saclay, Bât. 563
F-91191 GIF-SUR-YVETTE Cedex
FRANCE

+33 (0)1 69 08 52 41
+33 (0)1 69 08 82 61
www-llb.cea.fr